Heat Transfer From a Spherical Surface By Jet Impingement:

An Experimental Study

by

Norman W. Schaeffler

Thesis submitted to the Faculty of the

Virginia Polytechnic Institute and State University

in partial fulfillment of the requirements for the degree of

Master of Science

in

Engineering Mechanics

APPROVED:

Demetri P. Telionis, Chairman	Mark S. Cramer
Dean T. Mook	Thomas E. Diller

December, 1988

Blacksburg, Virginia

Heat Transfer From a Spherical Surface By Jet Impingement:

An Experimental Study

by

Norman W. Schaeffler

Demetri P. Telionis, Chairman

Engineering Mechanics

(ABSTRACT)

Methods for the removal of heat from a sphere, via jet impingement by single and multiple jets was documented experimentally. Average heat transfer rates from a sphere maintained at constant temperature, by means of an internal electronic heater, and subjected to single or multiple jet impingements were obtained and related to the exit conditions of the impinging air jet(s) and to geometric parameters. The heat transfer rate was found to be insensitive to small changes in geometry. The heat transfer rate was found to increase with an increase in mass flow rate. The impingement of two jets was found not to be as efficient as a single jet using the same mass flow rate. Compressibility was found to decrease the heat transfer rate at high values of the Mach number. Attempts to increase the heat transfer rate by increasing the entrainment of the jet by acoustic or mechanical excitation or by the use of an elliptic orifice meet with no success. The decrease in velocity due to the increase in entrainment cancelled any benefit that was gained by increasing the entrainment of the jet.

Dedication

Dedicated to my Parents and Sister,

and to

Acknowledgements

The author wishes to express his gratitude to his committee chairman, Dr. Demetri P. Telionis for his guidance and support. This work would not have been possible if Dr. Telionis had not provided direction and inspiration to the author. Dr. Telionis has been both a mentor and a friend. Also the author wishes to express gratitude to Drs. Dean Mook, Mark Cramer, and Tom Diller for their serving on the author's graduate committee and for their constructive criticism concerning this work.

Special thanks is extended to , , and for their work with the models and the orifice plates and for their advice. Also thanks to Dr. Michael Ury and Charles Wood of Fusion Systems Corporation for their help and support.

Finally, special thanks to , , and for their help and constructive criticism concerning this work.

Table of Contents

List of Illustrations

1. Introduction and Literature Review

1.1 General Introduction

Of all the problems that an engineer or applied scientist can encounter while attempting to apply the principles of fluid mechanics to a given technology, turbulence is perhaps the most difficult. Turbulence has successfully evaded an adequate theoretical description from even the most talented minds of the Twentieth century. The physicist Werner Heisenberg once remarked that the problem of turbulence is just simply too difficult and turned his attention to quantum mechanics and nuclear physics [1]. With such a formidable barrier on the theoretical frontier, the importance of experimentation to document the characteristics of turbulent flows cannot be understated.

One of the areas where turbulence is an advantage is in heat and mass transfer. The extensive mixing found in turbulent flows enable them to carry

heat and/or mass from a surface or area of concentration far more efficiently than a similar laminar flow, which relies on molecular diffusion and convection for the transport of these properties. One of the most efficient uses of the turbulent advantage is the turbulent jet impinging upon a heated surface for the transfer of heat away from the surface. The rate at which the heat transfer takes place is a function of impingement process and the ratio of the area available for heat transfer to the area associated with the impingement process. If all the area of the surface is assumed to be involved in the impingement process, an average rate of heat transfer can be evaluated based on that area.

1.2 Theoretical Introduction

Once a heat transfer rate is known, it can be nondimensionalized into the Nusselt Number. The Nusselt Number is formed by the temperature difference between a body and its environment, the heat transfer rate, the thermal conductivity of the fluid and a characteristic length of the body, in the present investigation the diameter of the sphere. If the heat transfer rate is an average rate, then these values are combined in the average Nusselt number, which is defined as follows:

$$AvNu = \frac{\bar{h}D}{k} \qquad [1.1]$$

where $\bar{h}$ is the average film coefficient which is defined as

$$\bar{q} \equiv \bar{h}A(T_s - T_a) \qquad [1.2]$$

and T_s and T_a are the temperatures of the sphere and the environment, respectively, $\bar{q}$ is the average heat transfer rate, D is a characteristic length of the body, and A is the surface area available for heat transfer [2]. Thus an alternative definition of the average Nusselt number is given by

$$\text{AvNu} = \frac{\bar{q}D}{A(T_s - T_a)k}. \qquad [1.3]$$

The properties of the flow field associated with a turbulent jet contributes to the determination of the film coefficient and the observed heat transfer. Since the jet is turbulent, the impingement process and the boundary layers that are established on the surface are also turbulent. Thus the film coefficient is best described in terms of a statistically stationary value which should be related to the exit conditions of the jet.

A jet can be created by a pressure difference between two bodies of fluid separated by a wall. If an orifice, essentially a well contoured hole, is present, the fluid in the high pressure region will flow to the low pressure region, establishing a jet. This model of jet flow is often called the "leaking wall" [3]. Since the jet flow is established by a pressure difference and is initially laminar, the velocity of the jet can be determined by Bernoulli's equation, which when solved for velocity reads,

$$V_c = \sqrt{\frac{2\triangle P}{\rho}} \qquad [1.4]$$

where $\triangle P$ is the pressure difference across the wall, ρ is the density of the fluid, and V_c is the jet's velocity at the exit plane. This value of the velocity is accurate to about 2% across the entire exit plane and is known as the core velocity [4]. This approach is valid, if and only if the flow can be considered incompressible, i.e. the Mach number, defined as $M = \frac{V_c}{a}$, where a is the thermodynamic sound speed, is less than or equal to 0.3. For jets where compressibility has to be taken into account, the velocity can be determined by

$$\frac{P_o}{P} = (1 + \frac{(\gamma - 1)}{2} M^2)^{\gamma/(\gamma-1)} \qquad [1.5]$$

where γ is the ratio of specific heats of the fluid, P_o is the stagnation, i.e. the plenum, pressure, and P is the ambient pressure [5].

Since the jet is a free shear layer, the hydrodynamic properties of the jet are dominated by viscous forces and therefore the Reynolds number comes into play. The Reynolds number is defined as

$$Re = \frac{V_c d}{\nu} \qquad [1.6]$$

where d is the diameter of the jet, and ν is the kinematic viscosity of the fluid.

As a jet issues into the environment, the boundary layers between the swift moving jet and the stationary fluid environment grows towards the jet's centerline. The region of fluid trapped within the growing boundary layers is called the potential core and has the characteristics of the core velocity. This can be seen schematically in Fig. 1. Once the boundary layers close completely around the core, the flow is referred to as fully developed, quite similar to flow in a pipe. Generally before the flow becomes fully developed, turbulence appears in the outer edge of the boundary layers, and shortly thereafter the entire jet will, from that station forward, go turbulent.

It is important to note that turbulent jets have some interesting properties that are well documented experimentally. All turbulent jets, which are allowed to develop naturally, spread at a half angle of 13° [6] (See Fig. 1). This result is independent of the Reynolds number. What does change with the Reynolds number is the scale of the fully turbulent portion of the jet. The larger the Reynolds number, the smaller the scale of the turbulence [7]. Another interesting feature of jet flows, be they laminar or turbulent, is the fact that the momentum integrated along any plane perpendicular to the centerline of the jet is a constant and this constant is the same for all planes including the exit plane. The momentum integral is expressed as,

$$J = \int_{-\infty}^{\infty} \rho \bar{u}^2 dA = constant \qquad [1.7]$$

where $\bar{u}$ is the mean velocity as a function of position across the jet. Hence any attempt to spread the jet, by artificial means, to a half angle larger than 13° will entrain more mass but the momentum as expressed Equation [1.7] will have to remain constant, i.e. even though more mass is moving with the jet it will be moving at a lower mean velocity than in the natural case.

1.3 Literature Review

The cooling of a surface by a jet is not a new engineering device. For many decades, jets have been used in cooling glass, textiles, electronic components and in many other useful applications. But a detailed knowledge of the mechanisms of the heat transfer and the heat transfer rates that could be expected have, unfortunately, been restricted to the case of jet impingement cooling of a flat plate. The contributions of many investigators, notably Schauer and Eustis [8], Vlachopoulos and Tomich [9], and Diller and Striegl [10], have provided designers with ways of estimating heat transfer rates, while also providing researchers with valuable insight into the physical process of impingement heat transfer. Also, extensive work recently has been done on other configurations which relate to flat plate impingement as Refs. 11-13 attest.

But what of a geometry other than the flat plate? A geometry of just as much engineering importance, and the topic of this investigation, is that of a sphere. The cooling of a sphere by jet impingement has been relatively unexplored. Walts and London [14] examined the case of a jet inpinging on a sphere of a diameter only slightly larger than the diameter of the jet itself. These diameter ratios, sphere diameter to jet diameter ($\frac{D}{d}$), ranged from 1.66 to 3.10. Due to turbulent entrainment and spreading of the jet, at any station away from the orifice the sphere sees the jet as a turbulent stream on the same scale as its diameter. The experiments of Walts and London were obtained by heating the sphere to 100°F above the ambient. The temperature history of the cooling process was recorded, via a thermocouple and chart recorder, and the average film coefficent deduced.

The work of Walts and London concludes that the effect of target to orifice distance, nondimensionalized by the jet diameter, is to have the highest rates at the smallest distances, followed by a constant value, and then additional decay. The constant value was observed in the range of 3.0 to 4.5 nondimensional length units. Increasing the target size, i.e. the diameter of the sphere, increased the heat transfer for small distances and decreased the rate for increased distances.

But what of the case where the diameter of the sphere is much larger than the diameter if the jet impinging upon it. What of $\frac{D}{d} = 12$, 24, or 32? Investigations of ratios on this order are non-existent. It is therefore the goal of this

investigation to examine the heat transfer in these cases. In the present investigation, the sphere sees the jet as a disturbance about its stagnation point. The plan of attack was to heat a spherical model to a constant temperature by means of an electrical resistance heater contained in the model. While a thermocouple-based feedback loop holds the sphere at constant temperature, a jet impinges upon the model. The feedback loop reacts to an increase in cooling by increasing the voltage available to the heater and the loop reacts in a similar fashion to a decrease in cooling rate by decreasing the voltage. The average voltage required to hold the sphere at constant temperature, squared and divided by the electrical resistance of the heater is the electrical energy input into the model and dissipated into heat, or the average heat transfer rate. An energy balance indicates that this input must be balanced by the energy stored in the model, i.e. the temperature distribution within the structure of the model, and the energy loss by the transfer of heat out of the model to the environment. Once the ability to measure the average heat transfer is established the effect of the different geometric relationships and different dynamical configurations can be investigated.

Thus the average Nusselt number, in its simplest form, is proposed to be a function of

$$AvNu = f^{n}(Re, M, G) \qquad [1.8]$$

where G is the effect of geometrical parameters. It is the purpose of this investigation to document what this relationship is.

Once the functional form of Equation [1.8] is known, an important question remains. Can the flow field be changed in a way as to produce more heat transfer for given plenum pressure or given mass flow rate? If the jet could be spread, be made to entrain more ambient fluid, the area where the jet impinges upon the sphere, called the strike area, would be larger. This should be beneficial in increasing the rate of heat transfer. Several investigators have examined ways to increase the entrainment by using acoustic waves, elliptical orifices, and mechanical pulsing.

While the turbulence is first appearing within the boundary layers, waves of instability propagate on the surface of the jet just before the end of the potential core (see Fig.1). These waves and their effect on jet flow was the subject of an extensive experimental study by Crow and Champange [15]. These waves are of a single frequency which can be nondimensionalized into the Strouhal number. The Strouhal number is defined as

$$St = \frac{fd}{V_c} \qquad [1.8]$$

where f is the frequency of the wave structures. This Strouhal number will be referred to the natural Strouhal number, since it is based on the frequency of the natural structures. The natural Strouhal number of a jet is approximately equal to 0.40 over a large range of Reynolds numbers. If the jet is excited in some way, then another Strouhal number can be defined based on the frequency of the excitation. This Strouhal number will be refered to as the forced

Strouhal number and will be given the symbol St_f. Crow and Champange used hot wire anemometry and flow visualization to determine that a jet would break up in a more violent fashion, entraining more of the surrounding fluid if the jet was excited with by acoustic waves from a loudspeaker. A forced Strouhal number of 0.30 will produce the greatest effect; an entrainment increase of 32% over the unforced case.

A jet with a natural mechanism for increasing entrainment is the small-aspect-ratio elliptic jet, the characteristics of which were documented by Ho and Gutmark [16]. As the jet issues from the orifice, the jet retains the geometric orientation of the orifice. However, the minor axis of the jet, the shorter of the two axes, spreads faster than the major axis creating a diamond shaped cross section. The minor axis continues to spread at a faster rate than the major axis until the two axes have switched identity and the process begins again. During the axis-switching process, ambient fluid is entrained at a much higher rate, about 42%, than in a equivalent circular jet.

While the elliptical jet has a passive means of increasing the entrainment rate, the fully pulsed jet has an active means of accomplishing the same goal. Pulsing the flow, i.e. turning the flow completely on and off, at a forced Strouhal number much lower than the natural Strouhal number will produce a large increase in entrainment. Recall that spectra of unforced jets have a natural Strouhal numbers of approximately 0.40. Bremhorst reported a 180% increase in entrainment, utilizing a $St_f = 0.015$, over a jet with steady flow [17].

2.The Experimental Programme

2.1 Equipment and Facilities

2.1.1 The Models

Two spherical models were used in this study. Both were constructed of aluminum, one with a diameter of two inches and the other with a diameter of four inches. Schematics of these two models are shown in Fig.2. The models were mounted individually on teflon shafts in order to isolate them thermally from the rest of the test rig. The two models were heated in two different ways. The larger model had a 1-3/8 inch by 2-3/4 inch cylindrical section cut into the sphere which contained an oil bath. Into the oil bath an electrical resistance heater was placed. Connections for the heater were brought out of the model

through teflon shields in order to minimize conduction to the wires. The smaller model was heated by a solid cartridge type heater. The surface of the heater was in contact with the model, in contrast to the other model. Also the electrical resistances, which are important to the computation of the power dissipated, of the two heaters differed greatly. This implies that, for a given situation involving a fixed amount of heat loss, the voltage required to counteract this loss is very different for each model. Thus the recorded voltages for each model, while under the same thermal load, will be different. But, the calculated value for the power should be the same. Thus any unwanted behavior that one heater may have can be detected. form of heater or another.

Each of the models were instrumented with a thermocouple oriented in the model in such a way as to have the measuring volume as close to the surface as possible. The placement of the thermocouple relative to the placement of the heater was, in the smaller model, scaled down from the larger model so a similar temperature distribution could be assumed to be the same in both models.

The larger sphere was used to investigate the uniformity of the temperature distribution within the models. Two thermocouples were installed in the model. Thus when the model was heated to constant temperature, the temperature at two points within the interior could therefore be determined. The temperature was found to be practically constant within the structure, allowing the as-

sumption of an isothermal wall. Only the thermocouple in the long shaft shown in Fig. 2 was used in the heat transfer measurements.

2.1.2 Description of the Experimental Rig

A special rig was designed and constructed to provide mountings for both the sphere and the jet source and allow the two to translate relative to each other. A plenum was constructed by capping a section of steel pipe with two aluminum plates. Different top plates were machined to provide the orifice diameters necessary for the experiment. The orifices were machined in such a way as to avoid vena contracta, a phenomenon of jet flow shown schematically in Fig. 3. An orifice of diameter d will produce a jet of diameter d only if the entrance to the orifice is bell shaped (See Fig. 3a). If the orifice is simply drilled straight through, the fluid is unable to turn the sharp corner and the effective jet diameter, d_e, which is less than d and very difficult to measure (See Fig. 3b). A photograph of the orifice plates and the spherical models is shown in Fig. 4. The plates were held in place by threaded rods.

The plenum contained instrumentation to provide temperature and pressure data, via a thermocouple and manometer respectively. A honeycomb was placed in the plenum in order to reduce the turbulence inherent in the compressed air supply. Also, a loudspeaker was installed in the plenum to provide

the acoustic excitation necessary for one phase of the experiment. The plenum was bolted to a movable bridge which moved vertically by means of a threaded rod. The position of the plenum relative to the sphere was measured by a calibrated dial indicator. A schematic sketch of this hardware is displayed in Fig. 5 and a photograph is shown in Fig. 6. The traverse allowed movement in the X and Y direction. This, in conjunction with the movable bridge, allowed the sphere and the jet to be placed in a variety of geometric relationships, especially positions where the axis of the jet and the axis of the sphere are not co-linear. The traverse was in turn mounted to the stationary bridge.

2.1.3 Instrumentation

The thermocouple within each of the models measure the temperature of the aluminum close to the outside surface of the model. This output is sent to an Eurotherm temperature controller, as shown schematically in Fig. 7. The controller adjusts the power delivered to the heater within the model in order to keep the temperature at the measuring point of the thermocouple constant. This is accomplished by the two modules within the controller. The first module has as input the thermocouple leads. The temperature that the thermocouple indicates is compared to the set temperature that the user has entered, via a set of keys, into the module. If the measured temperature and the set temperature are not the same the first module send an signal to the

second module to increase or decrease the power to the heater depending on if the measured temperature is too low or too high. The power being delivered to the heater from the second module is varied by chopping an 120 Volt AC signal, removing parts of the waveform in order to achieve the desired power. On the average the waveform resembles an isolated triangle wave with peaks of 120 Volts and a period of 60 Hz. This is shown schematically in Fig. 8. The controller is very sensitive to the values of its setup parameters. The variations of the measured heat fluxes could be as large as 20% if the controller was setup in a less than optimum fashion. However, if a large number of samples are taken the result will become statistically independent.

In order to arrive at a statistically stationary value for the average power, the voltage was sampled over a large number of periods. This data was acquired using two distinct methods. In the first method the output of the controller was attenuated and used as input to an integrated circuit, which provided a DC output proportional to the RMS value of the original signal. This DC signal was in turn sampled by a Digital Minc-11 data acquisition computer at a very low sampling rate, 0.123 Hz. In the second acquisition method the output of the controller, after attenuation, was sampled directly by an IBM-PC via an Data Translation 2805 A/D board. The signal was sampled at a rate of 6000 Hz for one second then the data was reduced and the process repeated. In each method the first and last sample in the time record was separated by a period of about ten minutes. This long period of time was found to be necessary in order for the average to become statistically stationary. Both of the

programs, containing both acquisition control and data reduction are listed in Appendix A.

As outlined in the introduction, the core velocity of the jet is intimately tied to the plemum pressure. In order to measure this pressure, two manometers were used. The primary manometer was an 80 inch water filled manometer. For higher pressures, a mercury manometer with 80 inches of travel was used. The plenum pressure was controlled by the use of a pressure controller on the compressed air line that supplied the experimental rig.

In order to measure the velocity profiles of the jet, a hot wire anemometer was used. Frequency spectra of the hot wire signal at certain positions in the flow were also measured. This was accomplished using a Dantec hot wire anemometer, a Dantec Anemometer Controller unit and a Hewlett Packard (HP) Digital Signal Analyser. The hot wire anemometer was a Dantec P15 0.5 micron wire. The P15 is a boundary layer type of probe. The calibration for velocity measurements were conducted using the core velocity of the jet at low speeds to avoid compressibility effects. The velocity versus voltage curve was then fit by a fourth order polynomial. The IBM-PC equipped with its Data Translation DT-2805 Analog to Digital converter was used for the data acquisition. The data was sampled at a rate of 1000 Hz for a period of 5 seconds, converted into velocity and averaged. For the spectral analysis the HP Digital Signal Analyser was run in 150 sample averaging autocorrelation mode. The

signal was considered by the analyser as random and the total bandwidth was from 0 to 10,000 Hertz with a bandwidth bin of 100 Hertz.

2.1.4 Description of Wind Tunnel Facility

The wind tunnel testing to determine the heat transfer rates for full stream cooling were conducted in the VPI-ESM wind tunnel. The VPI-ESM wind tunnel is an open circuit variable speed tunnel, and is shown schematically in Fig. 9. The tunnel was constructed to provide basic research support for the laboratory and is capable of a speed range of 5 to 15 m/s in its present configuration. This velocity was measured by a pitot-static tube connected to a six inch inclined manometer. The contraction ratio after the settling chamber is 5.2. The test section is 51 by 51 by 125 cm. The maximum turbulent intensity is 1.25% [18].

2.2 Experimental Procedure

The experimental procedure is essentially the same regardless of the specific effect being investigated. Once the temperature controller stabilizes the temperature at its pre-set value under whatever thermal load present, be it a single jet impingement, multiple jet impingement or full stream cooling, the

data acquisition can begin. For experimental runs using the wind tunnel the velocity of the tunnel was entered into the data acquisition program, for runs involving the jet impingments the plenum pressure was recorded. This was done mainly for bookkeeping purposes within the data files. The programs used were responsible for both the data acquisition and the data reduction. Therefore while the program is running, data may be being acquired of it may be being reduced. After each was completed the average Nusselt number was computed and stored in the data file.

The data acquisition program for the Minc involved a single analog to digital conversion. A sample of 400 voltages each separated by 1.45 seconds was acquired. These voltages correspond to the instantaneous value of the RMS voltage of the controller as determined by the integrated circuit discussed earlier. When the IBM-PC was being used to acquire the data, the voltage from the controller was sampled directly, after attenuation. A 6000 point sample is taken, this is a 100 point resolution per period for 60 periods, and the RMS value of this sample is found by the computer and the result stored. This process is repeated 100 times yielding 100 RMS values of voltage.

In each case the recorded RMS values were then averaged to arrive at a value for the average voltage. This value was then squared and divided by the resistance of the heater. This is the average heat loss, $\bar{q}$. To calculate the average Nusselt number a modification of Equ. [1.3] was used. Substituting into

Equ. [1.3], the equation for the total surface area of a sphere yields after rearrangement,

$$AvNu = \frac{\bar{q}}{\pi D(T_s - T_j)k} \qquad [2.1]$$

T_j is the temperature indicated on the thermocouple display for the plenum as mentioned in the Instrumentation section.

2.3 Comparisons with Earlier Work

To provide confidence in the experimental method it is necessary to compare results from the current work to data of other investigators. A well documented phenomenon related to the present investigation is the cooling of a sphere by a free stream. There are three well accepted expressions for this, two which are of an experimental nature and one which is an analytic solution. One of the experimental correlations is attributed to McAdams [19] and is:

$$AvNu = 0.37Re_D^{0.6}. \qquad [2.2]$$

The experimental correlation attributed to Cary [19] is

$$AvNu = 0.27Re_D^{0.56} \qquad [2.3]$$

and the analytical expression attributed to Johnstone [20] is

$$AvNu = 0.714\sqrt{\frac{\mu c\, Re_D}{k}} \qquad [2.3]$$

where c is the specific heat of the cooling fluid. This expression was derived from the Boussinesq relation for the heat transfer from a flat plate and ideal flow solution for flow over a sphere. Note that the two correlations and the analytical solution are all functions of Reynolds number based on the diameter of the sphere. These expressions and the data from the present investigation are plotted in Fig. 10. The two experimental correlations are separated by a large distance while the analytic expression and the data from the present study lie in between. The correlation of Mc Adams is higher than the rest due to the large turbulent intensity in the wind tunnel used. Within the range of Reynolds numbers examined in this investagation, the relationship between average Nusselt number and Reynolds number was found to be, for $19{,}500<Re<38{,}000$,

$$AvNu = 0.002209Re_D + 55.560 \qquad [2.4]$$

In addition to the effect of full stream cooling, the characteristics of the jets which were used in the impingment process were documented. The velocity profiles of one of the jets is displayed in Fig 11. The decay of the centerline velocity can be seen in Fig. 12 contrasted to the data of Petersen and Samet [20]. The two sets of data agree very well.

3. Jet Impingement Heat Transfer

What kinds of parameters are important to the jet impingement heat transfer from a sphere? What are the relative roles of geometry and dynamics? Are there any optimum configurations or combination of parameters? It is the goal of this investigation to learn how all these pieces fit together to form the whole picture and how an understanding of the pieces can be used to the advantage of an engineer. In this section what was learned about jet impingement heat transfer will be examined.

3.1 Geometry

Similitude is one of the cornerstones of fluid mechanics. The idea that two similar objects, which can have very different length scales, can exhibit similar behavior is the basic premise of all experimentation. The field equations of

fluid mechanics, i.e. the Navier-Stokes and the Energy equations, when nondimensionalized provide the dynamic similarity parameters. Two, which play an important role in this investigation, are the Mach number and the Reynolds number. In addition to dynamic similitude, geometric similitude is also important. In the present investigation, it appears intuitive that the distance from the orifice to the sphere or the orientation of the jet axis with respect to the axis of the sphere will be important geometrical parameters. These distances are defined as H, the distance from the orifice to the plane tangent to the sphere, and x, the perpendicular distance from the axis of the jet to the axis of the sphere, $x=0$ being the axisymmetric case. For the purposes of this experiment, axis of the sphere was defined as the axis which is perpendicular to the tangent plane of the sphere, the same tangent plane that parallel to the plane of the orifice. These distances are shown schematically in Fig. 13. The two distances are nondimensionalized by dividing H by d, the jet diameter, and by dividing x by D, the sphere diameter. These two geometrical ratios coupled with the ratio of the jet diameter to the sphere diameter $(\frac{D}{d})$ complete the geometrical picture.

Experiments were conducted to determine what effect, if any, changing these distances has on the amount of heat transfered from the sphere. If a jet flow is established at constant Reynolds number and H is increased, the heat transfer rate will remain essentially constant as long as H is greater than 3 jet diameters but smaller than 14 jet diameters. For values smaller than 3 jet diameters the heat transfer rate will begin to decline. As H becomes larger than

14 jet diameters the heat transfer will begin to fall off in a linear fashion. This data is plotted in Fig. 14 for a small range of H and Fig. 15 for a larger range of H. The fact that the heat transfer rate remains constant for the range of 3 to 14 jet diameters indicates that small changes in the strike area, the area on the sphere where the jet impinges, does not change the heat transfer at all. This may be due to the fact that in the range of $\frac{D}{d}$ investagated, recall that this ratio ranged from 12 to 32, the strike area is very small compared to the total surface area of the sphere. In order to gain an appreciation for how these two areas compare, Fig. 16 presents a shadowgraph of the impingement process. The jet diameter is 0.167 inches, and the sphere diameter is 2.0 inches, yielding the smallest $\frac{D}{d}$ with a value of 12. H is equal to 1.0 inches, for a $\frac{H}{d}$ =6.0. The shadowgraph was produced by using carbon dioxide to pressurize the plenum. This provided the index of refraction change necessary to make the jet visible to the shadowgraph technique.

When the axis of the sphere is moved with respect the axis of the jet impinging upon it at constant Reynolds number, the heat transfer remains constant to a value of half the sphere diameter. As the axes become separated by more than half a sphere diameter, the heat transfer begins to drop off as the square root of the separation. This is shown in Fig. 17. The constant value of average Nusselt number for small x may be due to the same reason as the constant value of average Nusselt number for the reported range of H. When the axis of the jet corresponds to the same line as the axis of the sphere the strike area is essentially a plane, due to the relative size of the area of the

sphere to the strike area. But as x becomes larger the curvature of the sphere becomes increasingly apparent and this has a negative effect on the heat transfer.

The effect of the final geometric ratio, $\frac{D}{d}$, proved very difficult to examine. At first the effect of $\frac{D}{d}$ was thought to be captured in the Reynolds number and the geometric distance $\frac{H}{d}$. It was felt that the jet diameter controlled the behavior of the jet only on a scale local to the orifice and that this effect would be adequately captured in the Reynolds number. This proved not to be the case. The discussion of the effect of $\frac{D}{d}$ will be postponed until after discussion of the effect of a changing Reynolds number.

3.2 Dynamics

As noted earlier two dynamic similitude parameters are of importance in this investigation; the Mach number and the Reynolds number. Since the Mach number is the ratio of the core velocity of the jet to the thermodynamic sound speed, the diameter of the jet is independent of the Mach number. However, the Reynolds number is not independent of jet diameter. Thus varying the Mach number while keeping the Reynolds number constant will require the diameter of the jet to change. The effect of the Reynolds number can be investigated independently of the Mach number if the core velocity is kept low

so that the Mach number is less than 0.3. This will keep the effect of compressibility small.

If all of the geometric parameters are fixed, sweeping the Reynolds number through a range of values corresponds essentially to changing the mass flow rate. In flat plate jet impingement heat transfer the average Nusselt number is related to the Reynolds number as $AvNu = C\,Re^m$ where m ranges from $0.50 < m < 0.80$ [3] and C is a constant. In the present study the Reynolds number linearly correlates with the average Nusselt number. This data is shown in Fig. 18. A linear fit to the data yields, with an excellent correlation coefficient

$$AvNu = 0.0092281Re + 96.8201 \qquad \frac{D}{d} = 24. \qquad [3.1]$$

If a jet of different diameter, and thus different $\frac{D}{d}$, is tested, the same Reynolds number will produce a different average Nusselt number. There are four different curves in Fig. 19 for four different $\frac{D}{d}$. One of the curves is the same curve discussed earlier, namely the $\frac{D}{d}=24$. The correlations for the other three curves are:

$$AvNu = 0.0134294Re + 20.1056 \qquad \frac{D}{d} = 32, \qquad [3.2]$$

$$AvNu = 0.0082246Re + 120.7227 \qquad \frac{D}{d} = 16, \qquad [3.4]$$

and

$$\text{AvNu} = 0.0087981\text{Re} + 197.5394 \qquad \frac{D}{d} = 12. \qquad [3.3]$$

These correlations suggest that the relationship between average Nusselt number and the Reynolds number is linear of the form

$$\text{AvNu} = A\text{Re} + B \qquad [3.5]$$

where $A = A(\frac{D}{d})$ and $B = B(\frac{D}{d})$. For the range of $\frac{D}{d}$ examined, the following correlations are suggested for A and B. For $12 \leq \frac{D}{d} \leq 32$,

$$A = 0.1537 - 0.00084\frac{D}{d} + 0.00002(\frac{D}{d})^2 \qquad [3.6]$$

$$B = 17.5988\frac{D}{d} - 0.49340(\frac{D}{d})^2 - 38.6304 \qquad [3.7]$$

The use of these correlations will correctly capture the effect of $\frac{D}{d}$.

Since the ability of the Reynolds number to capture the influence of jet size on the heat transfer was not as strong as originally thought, the ability of the average Nusselt number to capture correctly the heat transfer effect was checked. Increasing the temperature of the sphere and repeating the Reynolds number sweep for a known jet diameter and geometric configuration should yield the same values for the average Nusselt number. This is indeed the case as the data shown in Fig. 20 attests. The sphere temperature was raised from

60° C to 80° C and the same value of the average Nusselt number was found. Thus the average Nusselt number correctly captures the heat transfer effect.

Lying somewhere between a dynamic effect and a geometric effect is the use of two jets to cool the sphere. This is both a case of geometry and dynamics because using two jets doubles the mass flow rate and the spacing between the jets can be varied. The distance between the centerline of the jets is defined as e and is nondimensionalized by dividing by D. The geometry is shown in Fig. 21. The effect of varying the quantity e is a rise in heat transfer until the maximum is reached at a value of $\frac{e}{D} = 0.60$. The heat transfer then begins to decrease. This data is shown in Fig. 22. The value plotted as $\frac{e}{D} = 0.0$ corresponds to the heat transfer for a single jet with half the mass flow rate of the two jet case. It is interesting to note that this value is identical the value at $\frac{e}{D} = 0.15$ which corresponds to two jets and therefore twice the mass flow rate. Thus the use of two jets offers a very modest increase in heat transfer over the single jet case. A quick review of the Reynolds number sweep indicates that a higher heat transfer rate can be obtained by using a single jet running at twice the speed, and thus the same mass flow rate of two jets, than can be obtained using two jets separated by some distance.

The final dynamic effect is the effect of compressibility or the effect of the Mach number. If the physical dimensions of a given geometrical setup were all reduced by a factor of two, a nondimensional measurement made on the larger geometry should have the same value as the same nondimensional

measurement made on the smaller geometry. The laws of similtude guarantee that this is indeed the case if the two systems are, in fact, one hundred percent dynamically and geometrically similar. But in the present study, the Mach number is not dependent on the geometry. Thus the smaller geometry, in order to match the jet Reynolds number of the larger geometry, will have an associated jet Mach number twice that of the larger geometry. Thus the two systems are not one hundred percent geometrically and dynamically similar. The effect of this difference can be seen in Fig. 23. At low Mach numbers, i.e. Mach numbers less than 0.3, there is no difference in the two geometries. The two curves are identical. However, as the Mach number increases, the curve for the small geometry begins to deviate from the curve for the larger geometry. For the purpose of comparison, the endpoint of the curve for the larger geometry is, $M=0.5$ while the endpoint for the curve for the smaller geometry is, $M=0.75$. From the curves it appears that compressibility tends to decrease the heat transfer. This can be seen in Fig. 24 where lines of constant Reynolds number are shown as functions of the Mach number and the average Nusselt number. In order to provide a correction for the effect of compressibility consider the following. If Equation [3.1], which is the proper correlation for this value of $\frac{D}{d}$, is plotted versus the data for the smaller geometry then where the two deviate from one another is where compressibility needs to be taken into account. This data is shown in Fig. 25. Recall that the correlation expressed in Equation [3.1] was derived using only data that could be considered in the incompressible regime. The region where the two curves begin to deviate from

one another corresponds to a Mach number of about 0.55. Thus for $M \geq 0.55$, the following correction is suggested

$$AvNu = CAvNu_o. \qquad [3.8]$$

where $AvNu_o$ is the value of the average Nusselt number as computed using Equations [3.5] - [3.7] and C is defined as

$$C = 1.4423 - 1.11902M + 0.64127M^2 \qquad [3.9]$$

This completes the investigation into the effect of the various dynamical and geometrical parameters on the heat transfer, i.e. the average Nusselt number. Now ways of modifying the flow field as to increase the heat transfer while not increasing the mass flow rate will be examined.

3.3 Flow Field Excitation

As mentioned in the Introduction there are several ways to increase the entrainment of a turbulent jet over the amount of natural entrainment. Elliptical jets, acoustic excitation, and mechanical pulsing are all well documented routes to an increase in entrainment. It is a hypothesis of this investigation that an increase in entrainment will produce an increase in heat transfer over a natural jet with the same amount of mass flow rate at the jet exit.

The effect of an elliptically shaped orifice was examined first. Since the axis switching associated with this type of jet evolves as a function of distance along the centerline, two different positions of the sphere in space were tested. The results of these experiments are plotted in Fig. 26. The extra entrainment of the elliptic jet has no effect on the amount of heat transfer experienced.

A second attempt at an increase in heat transfer by increasing the entrainment was made by examining acoustic excitation. A loudspeaker was located in the plenum to provide the needed excitation. Before the experiments were conducted, the natural spectra of the jet was investigated to see if the results would be similar to the work of other researchers. The spectra are shown in Figs. 27-35 for different Reynolds numbers. When the frequencies are reduced to natural Strouhal numbers all fall around a value of 0.40 which is in agreement with the work of other researchers [15,20]. The variation of natural Strouhal number with Reynolds number is plotted in Fig. 36. Experiments to determine if the heat transfer could be increased by acoustic excitation were conducted at $St_f = 0.4$, $St_f = 0.8$, and $St_f = 0.3$, note that these forced Strouhal numbers are based on the frequency of the acoustic excitation. Also the velocity profile of the jet in its excited state was measured at a $\frac{H}{d} = 4.0$ and a $St_f = 0.3$. This data is compared to similar data by Crow and Champagne [15] in Fig. 36. As in the case of the elliptical jet, the heat transfer rate for all the cases of excitation failed to increase over the natural case. This can be seen in the data plotted in Fig. 37.

The final attempt at an increase in heat transfer via an entrainment increase was the mechanically pulsed jet. The jet was pulsed by rotating a circular disk with ten equally spaced holes. Both holes and solid sections of the disk were equally spaced so that there was equal time with the flow on and with it off. The rotational speed of the disk was determined by a strobe light. In order to arrive at the suggested Strouhal number of 0.015 [16], the disk was rotated at 45 Hz resulting in a pulsing frequency of 450 Hz and a forcing Strouhal number of 0.0151. Since the compressed air supply which provided air to the experimental rig provided a constant mass flow rate of air, the pressure in the plenum would rise and fall with increasing and decreasing orifice area. Thus keeping the total mass flow rate the same as in the case of the non-pulsed jet. Yet again there was no increase in heat transfer rate, as shown in Fig. 38.

From the above it appears that the hypothesis that an increase in entrainment will produce an increase in heat transfer is incorrect. The fact that the momentum in a jet is a constant implies that the more mass entrained, the lower the mean velocity the entrained fluid must have, compared to the natural case. This decrease of average velocity must counteract the beneficial effect of a larger area that additional entrainment provides.

4. Discussion and Recommendations

This study had two goals: (1) to document the effect of geometrical and dynamical parameters on jet impingement heat transfer from a spherical surface, and (2) to attempt to increase the heat transfer rate over the natural jet impingement case by increasing the entrainment of the jet. Addressing the first goal it was found there is a wide range of geometrical parameters in which a change in geometry produces no change in the rate of heat transfer. This was attributed to the large values of $\frac{D}{d}$ examined. A large value of $\frac{D}{d}$ means the sphere is of a much larger diameter than the jet diameter, enabling changes in geometry not to influence the interaction of the sphere and the jet. Of all the geometric effects studied, it is the diameter ratio, $\frac{D}{d}$, That had the most influence in changing the heat transfer rate.

Changing dynamical parameters had a larger effect on the heat transfer rate. Increasing the Reynolds number of the jet increases the heat transfer. This is interpreted to mean that the rate of heat transfer increases with mass

flow rate. Compressibility was found to play a role in reducing the rate of heat transfer as the Mach number grew towards unity.

The second goal of the study was actually a working hypothesis. Working on the interpetation of the data obtained earlier which indicates higher heat transfer for higher mass flow rates, it was thought that an increase in the heat transfer rate could be brought about by an increase in jet entrainment. This is based on the fact that the more ambient fluid a turbulent jet entrains, the more fluid mass acquires some non-zero velocity. This was thought to be beneficial because it would increase the strike area on the sphere, essentially making a small jet appear, to the sphere, as a large jet. However, this entrainment increase occurs under the constraint that the momentum integrated across any perpendicular plane must be a constant. This constant is determined based on the initial velocity profile of the jet. Therefore allowing more fluid mass to acquire non-zero velocity, by increasing the entrainment, actually decreases the mass flow rate. This reduction in mass flow rate, and thus the heat transfer rate, cancels any increase in heat transfer rate that may come about through an increase in strike area. This was shown experimentally to be the case. As a recommendation for further study, a jet which entrains less fluid than a natural jet is the best candidate for a modified flow field solution to higher heat transfer rate. The search for a method to arrive at less entrainment for a turbulent jet is outside the scope of this study.

Summary of Results

A. Geometry

1. The effect of increasing the distance between the orifice and the sphere has little effect on the heat transfer rate, as long as the distance is not too large or too small. As long as $3 \leq \frac{H}{d} \leq 14$ is the case. This is attributed to the fact that the strike area does not change appreciably over a range of different distances and the velocity of the jet does not decay appreciably either.

2. The effect of increasing the perpendicular distance between the axis of the jet and the axis of the sphere does not change the heat transfer until the distance exceeds a quarter of the sphere diameter. This can be attributed to same reasons as in 1. As long as the jet impinges near the axis of the sphere the strike area is essentially plane with a 90° impingement angle. However, as the angle of impingement becomes less than 90° the rate of heat transfer decreases.

3. Of all the geometrical ratios, the ratio of sphere to jet diameter, $\frac{D}{d}$, proved the most important. Increasing the jet diameter relative to the diameter of the sphere increased the rate of heat transfer for a constant Reynolds number. Changing the diameter can also help avoid some unwanted effects, such as the effect of compressibility.

B. Dynamics

1. As the Reynolds number of the jet impinging upon the sphere increases, the heat transfer increases. There is a linear dependence of the average Nusselt number on the Reynolds number. The increase in heat transfer with increasing Reynolds number indicates that the rate of heat transfer that can be expected has a strong dependence on the mass flow rate.

2. As the Mach number increases, the rate of heat transfer is effected. The effect of compressibility results in a decrease in the rate of heat transfer from the amount which would be expected if flow were incompressible. This is probably due to heating of the jet due to its high speed.

3. If two jets are used, the rate of heat transfer will be larger than if just one jet was used. However this increase is not as high as the amount of heat transfer that can be removed by a single jet with the same mass flow rate as the two jet case. Thus the use of two jets is not recommended.

C. Modification of the Flow Field

1. The hypothesis that an increase in heat transfer rate can be brought about by increasing the entrainment of the jet was shown not to be correct. The increase in area due to entrainment is paid for with a decrease in impingement

velocity, thus cancelling any increase in heat transfer rate that may have come about by an increase in strike area.

Recommendations

The interesting question, which this study tried to answer in part, "Is there any way for an engineer to increase the heat transfer from a spherical surface over the rates associated with natural jet inpingement?", is far from being answered completely. In addition to the previous recommendation, the use of supersonic nozzles offers some interesting possibilities. An overexpanded supersonic nozzle suffers a large increase in area which may be beneficial enough to outweigh the negative effect of compressibility. Another area of possible interest is an examination of the local values of the heat transfer rate on the sphere. This would allow an investigator to find areas where the rate of heat transfer is critically low and devise a way to remedy this local weakness in order to increase the overall cooling.

With the conclusion of this study a great deal of evidence has been compiled on the subject of jet impingement cooling of spherical surfaces. This information would be valuable in the development of a numerical scheme capable of capturing the effects of all the different phenomena examined. Any numerical scheme will be plagued with the common problems associated with

the calculation of turbulent flows, e.g. the problem of closure and uncertainty with the boundary conditions just to name two. However, such a numerical scheme, together with the results of this study, will provide engineers with valuable tools for solving similar problems in applied heat transfer.

5. References

1. Simpson, R. L., *Introduction to Turbulence Shear Flow*, Lecture VPI&SU 1988
2. Holman, J.P., *Heat Transfer* New York, McGraw-Hill, 1986.
3. Diller, T. E. and Telionis, D. T., *Jet Impingment Heat Transfer*, to appear.
4. Rajaratnam, N., *Turbulent Jets*, Oxford, Elsevier Scientific Publishing Company, 1976.
5. Anderson, J. D., *Modern Compressible Flow*, New York, McGraw-Hill, 1982.
6. White, F., *Viscous Fluid Flow* , New York, McGraw Hill, 1974.
7. *Turbulence* National Committee on Fluid Mechanics Flims, 1968
8. Schauer, J. J. and Eustis, R. H., " The Flow Development and Heat Transfer Characteristics of Plane Turbulent Impinging Jets", Stanford University Department of Mechanical Engineering, Technical Report No. 3, 1963.
9. Valachopoulos, J., and Tomich, J. F., "Heat Transfer from a Turbulent Hot Air Jet Impinging Normally on a Flat Plate", *Canadian Journal Of Chemical Engineering*, Vol. 49, 1971, pp. 462-466.
10. Diller, T. E. and Striegl, S. A., "An Analysis of the Thermal Effect on Jet Impingement Heat Transfer", *Journal of Heat Transfer*, Vol. 54, 1982.
11. Hollworth, B. R., and Wilson, S. I., "Entrainment Effects on Impingement Heat Transfer: Part I - Measurements of Heated Jet Velocity And Temperature Distributions and Recovery Temperatures on Target Surface", *Journal of Heat Transfer*, Vol. 106, 1984,pp. 767-803.
12. Hollworth, B. R., and Wilson, S. I., "Entrainment Effects on Impingement Heat Transfer: Part II - Local Heat Transfer Measurements", *Journal of Heat Transfer*, Vol. 107, 1985,pp. 910-915.

13. Golstein, R. J., Behbahani, A. I. and Heppelmann, K. K., "Streamwise Distribution of the Recovery Factor and the Local Heat Transfer Coefficient to an Impinging Circular Air Jet", *International Journal of Heat and Mass Transfer*, Vol. 20, 1986, pp. 1227-1235.
14. Waltz, D. R. and London, A. L., "Spot Cooling And Heating Of Surfaces With High Velocity Impinging Air Jets", Stanford University Department of Mechanical Engineering, Tecnical Report No. 61, 1964.
15. Crow, S. C. and Champagne, F. H., "Orderly Structure in Jet Turbulence", *Journal of Fluid Mechanics*, Vol. 48, 1971, pp. 547-549.
16. Ho, C. and Gutmark, E., "Vortex Induction and Mass Entrainment in a Small-Aspect-Ratio Elliptic Jet", *Journal of Fluid Mechanics*, Vol. 179, 1987, pp. 383-405.
17. Bremholst, K., "Unsteady Subsonic Turbulent Jets", *Recent Developments in Theoretical and Experimental Fluid Mechanics*, Berlin, Springer Verlag, 1979.
18. Seider, G. "The Design, Construction, and Calibration Of a Low Speed Wind Tunnel", Report filed for Dr. D.P.Telionis on behalf of the VPI-ESM Fluid Mechanics Laboratory, 1984.
19. Chang, P., *Seperation of Flow*, Oxford, Pergamon Press, 1966.
20. Johnstone, H., "Heat Transfer to Clouds Of Falling Particles", *Americian Institute of Chemical Engineers Transactions*, Vol.37, 1941, pp. 95-133.
21. Petersen, R. A. and Samet, M. M., "On the Perfered Mode of Jet Instability", *Journal of Fluid Mechanics*, to appear

6. Figures

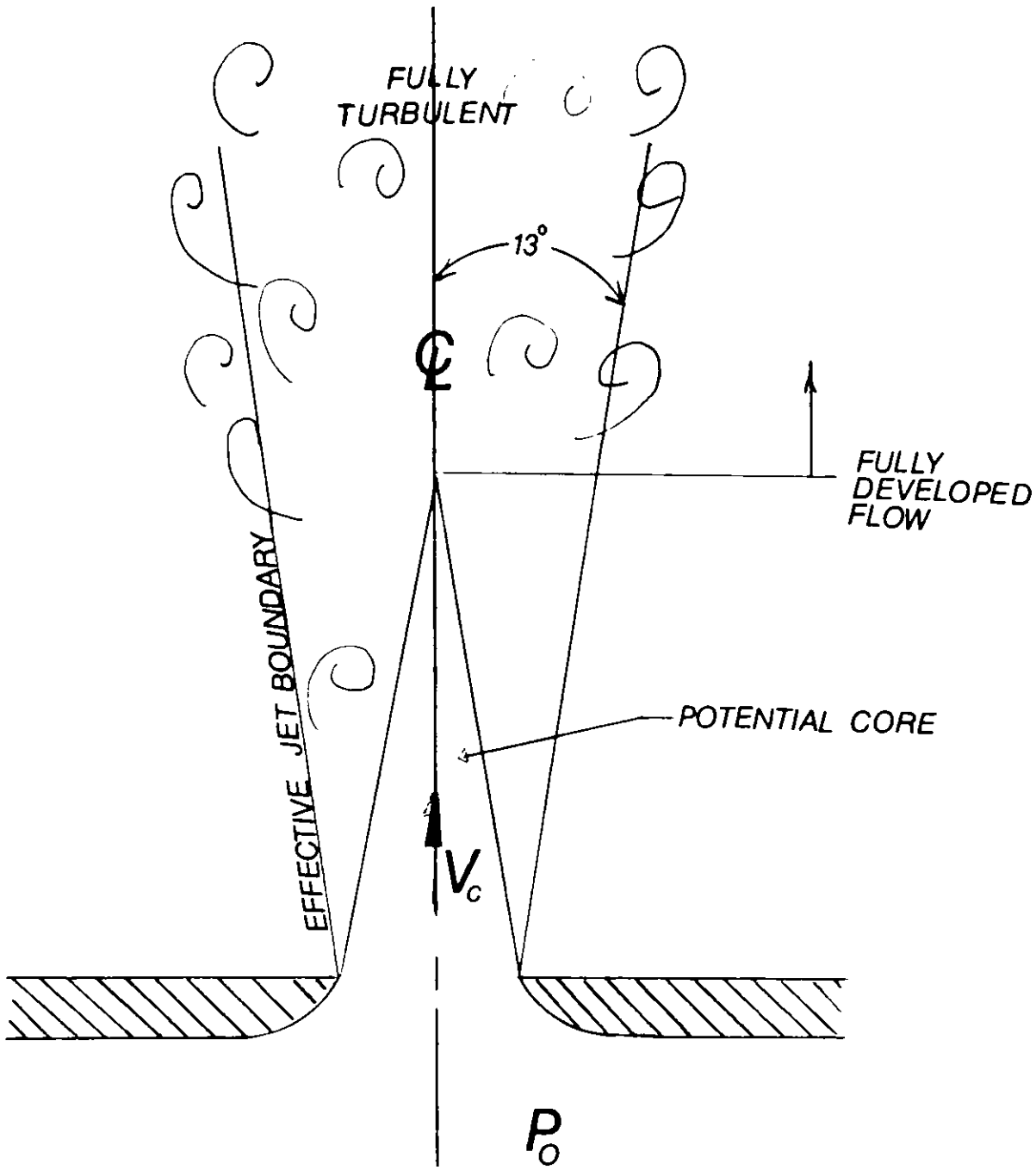

Figure 1. Regions in jet flow.

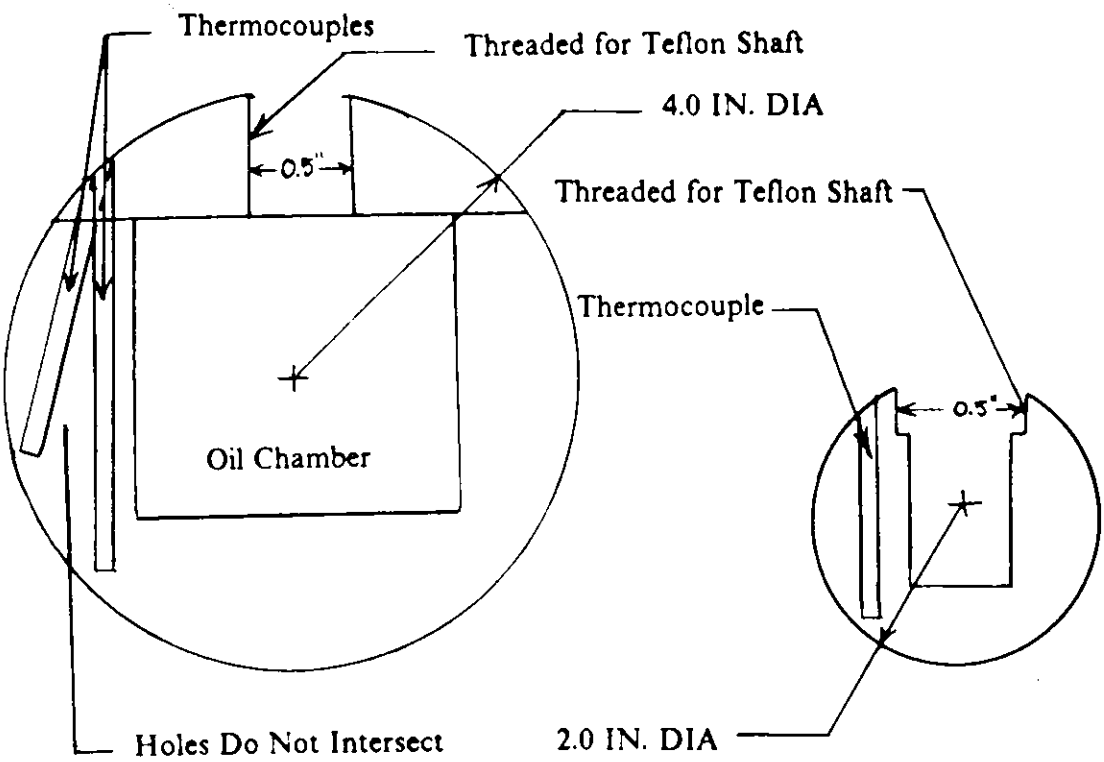

Figure 2. Schematic of the two models used in the study.

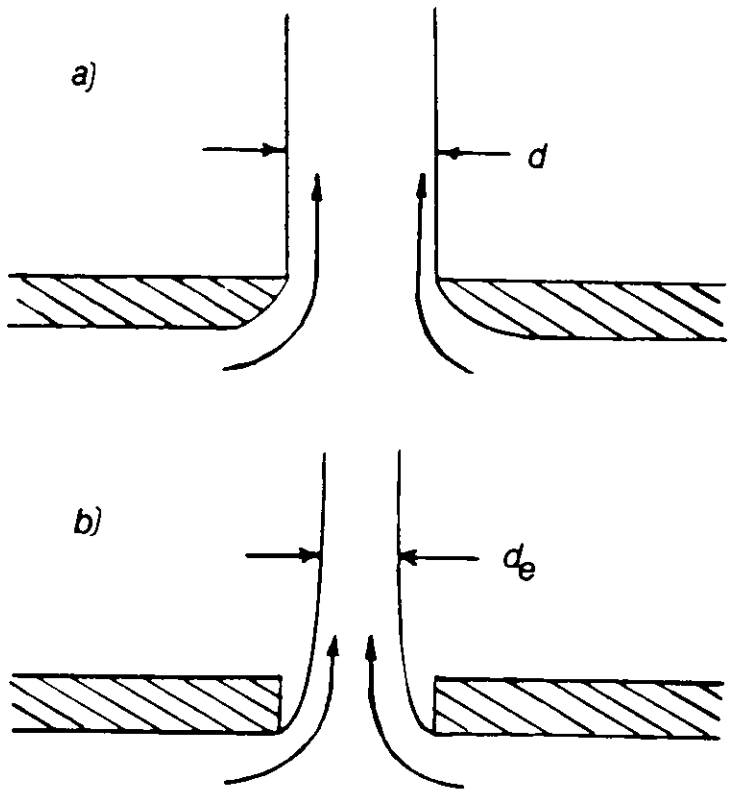

Figure 3. The effect of vena contracta.

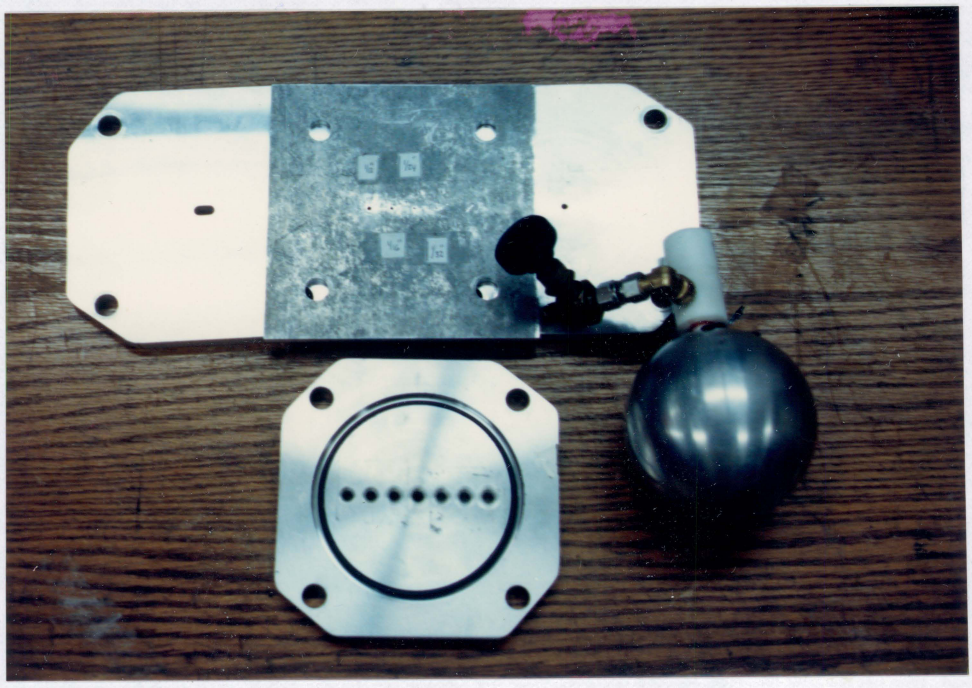

Figure 4. Photograph of some of the orifice plates and models.

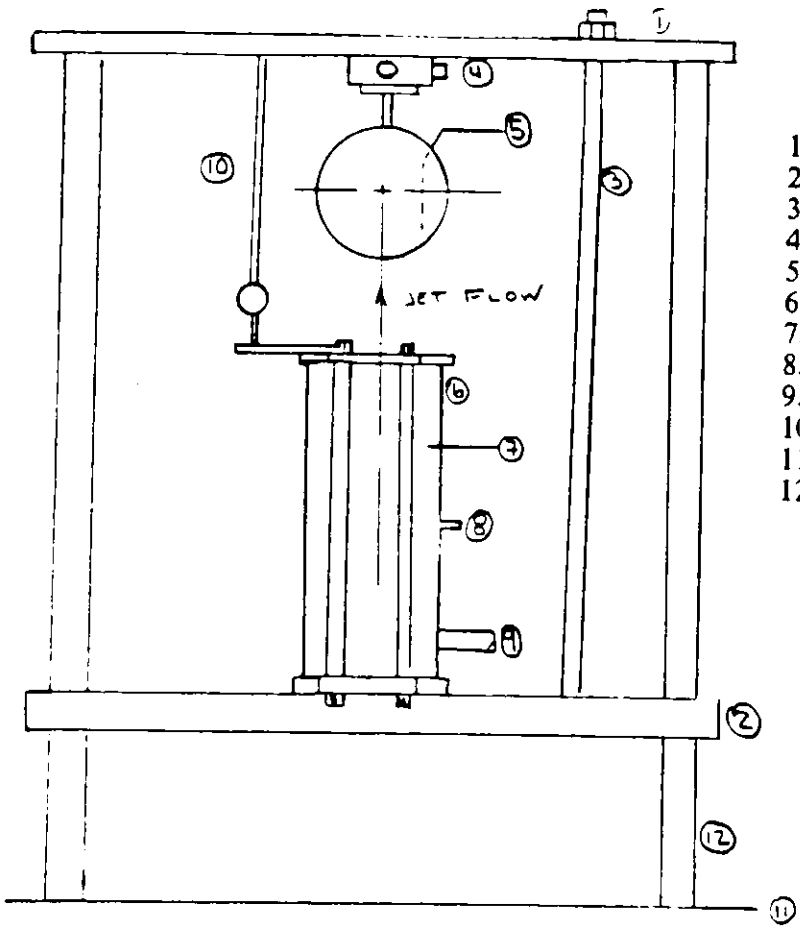

1. Stationary Bridge
2. Movable Bridge
3. Threaded Rod
4. X-Y Traverse
5. Thermocouple 1
6. Plenum
7. Thermocouple 2
8. Manometer Tap
9. Air Supply
10. Dial Indicator
11. Base
12. Support

Figure 5. Schematic of the experimental rig.

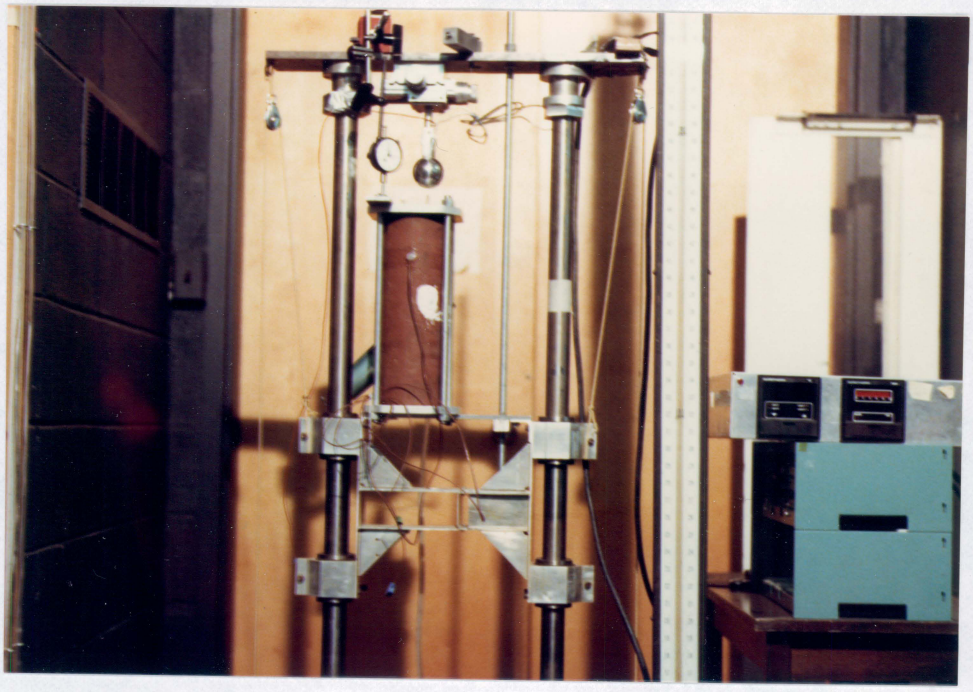

Figure 6. Photograph of the experimental rig.

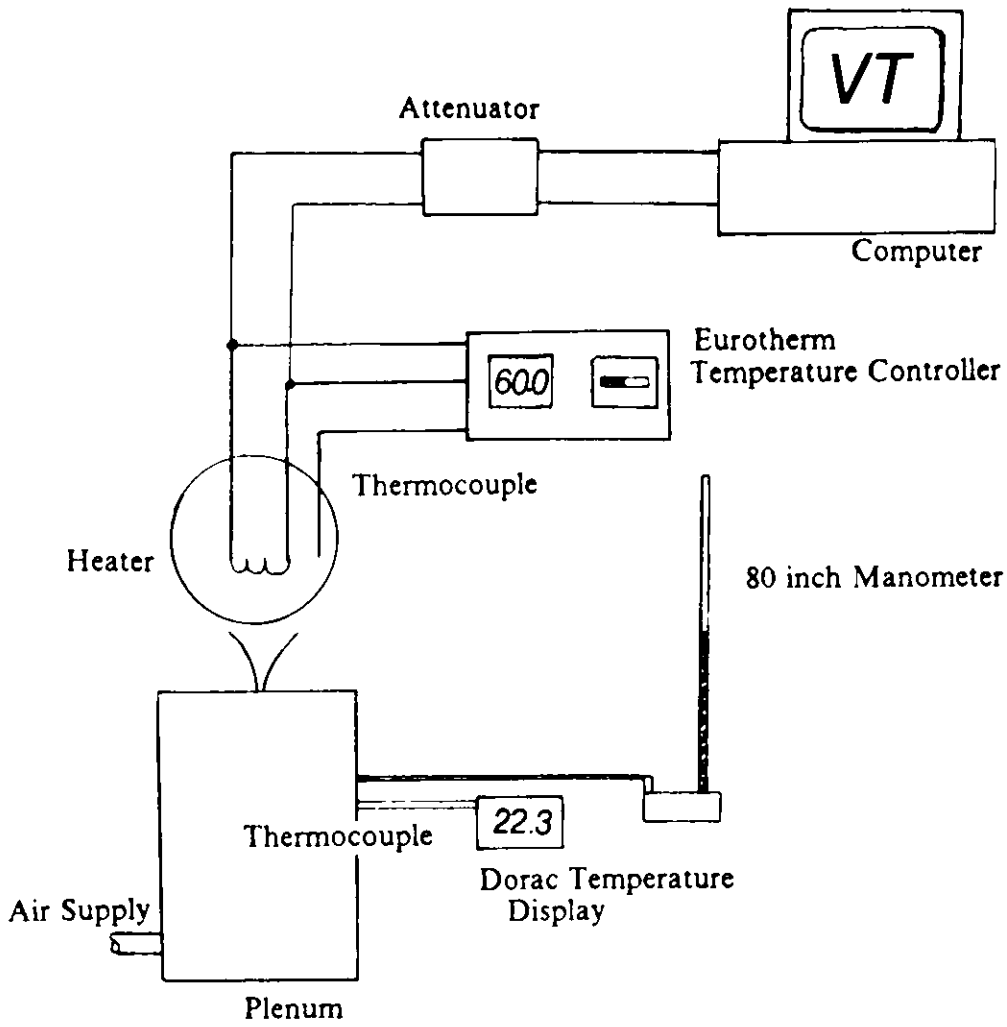

Figure 7. Schematic of the instrumentation setup.

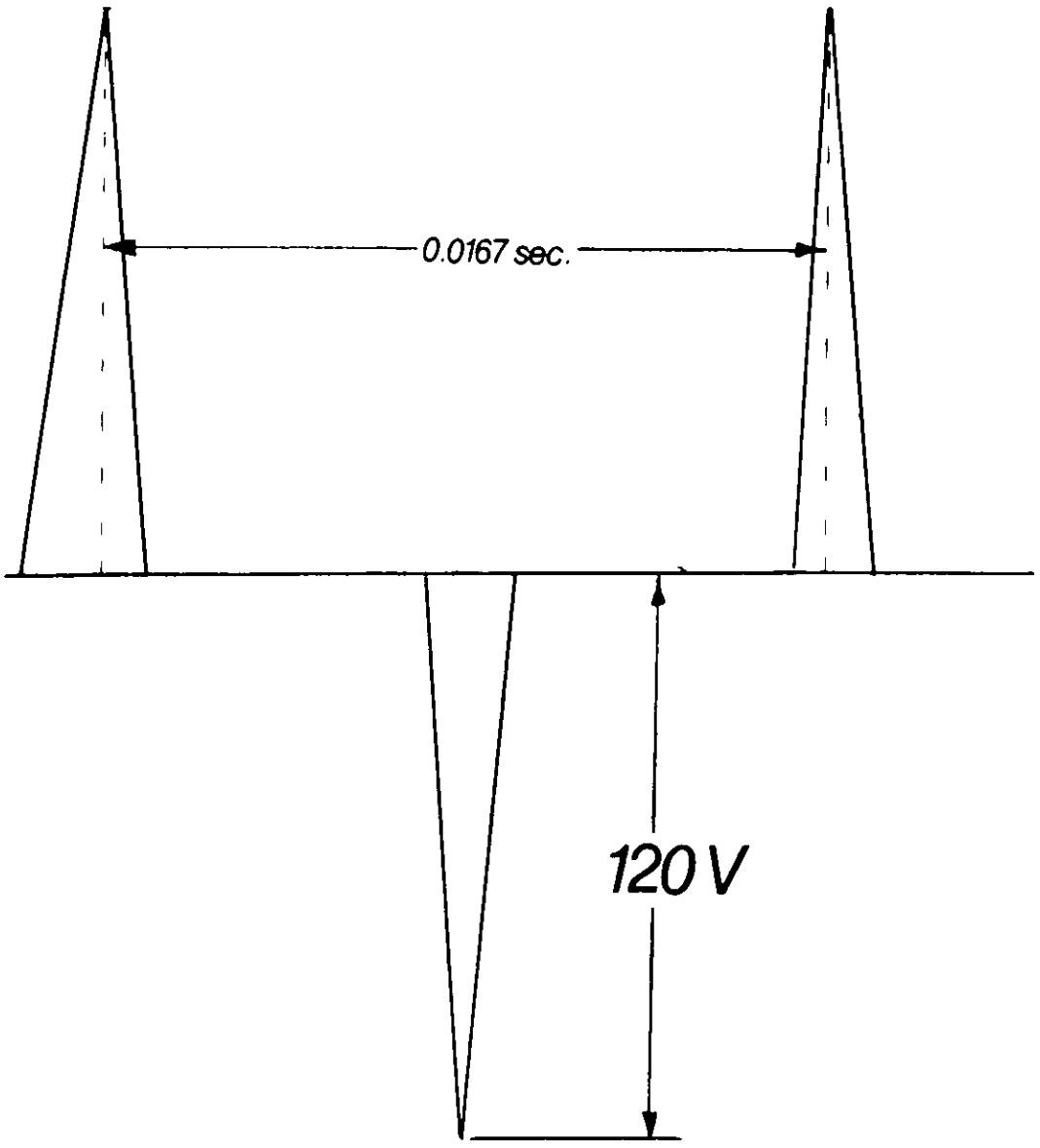

Figure 8. Schematic of measured waveform.

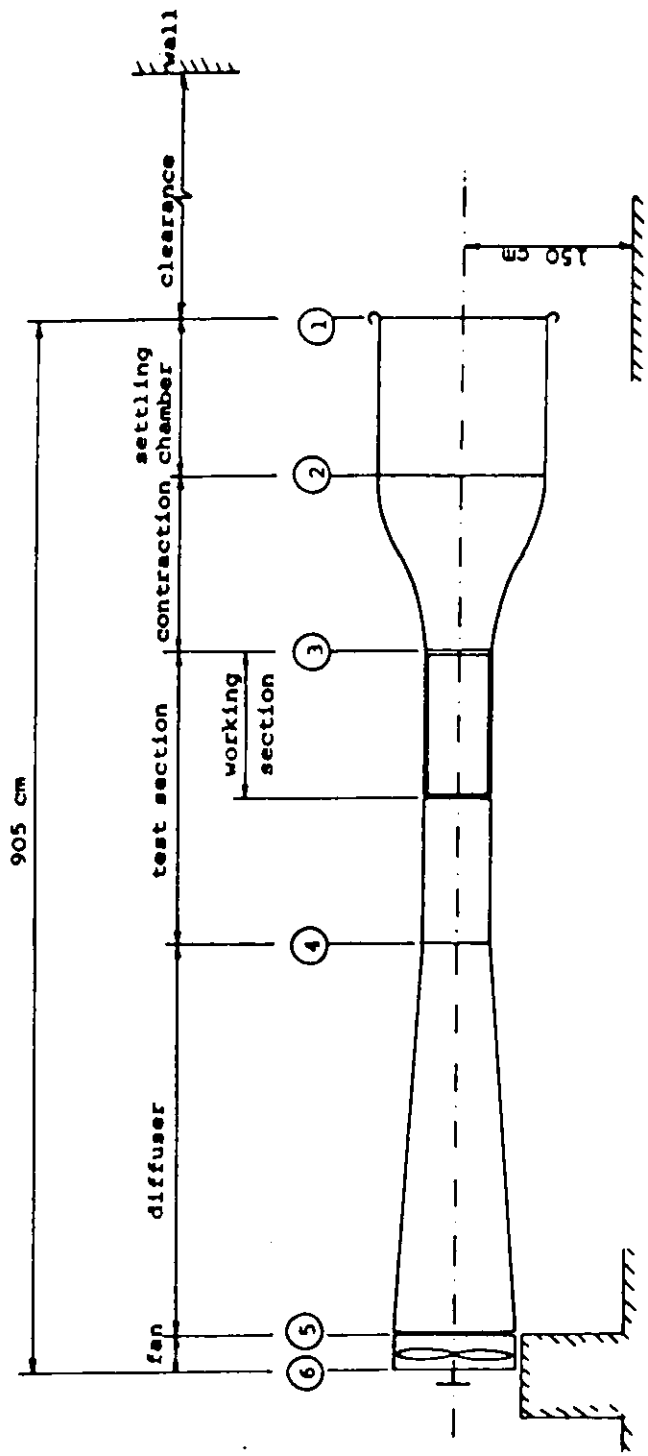

Figure 9. Schematic of the VPI-ESM Low Speed Wind Tunnel from [18].

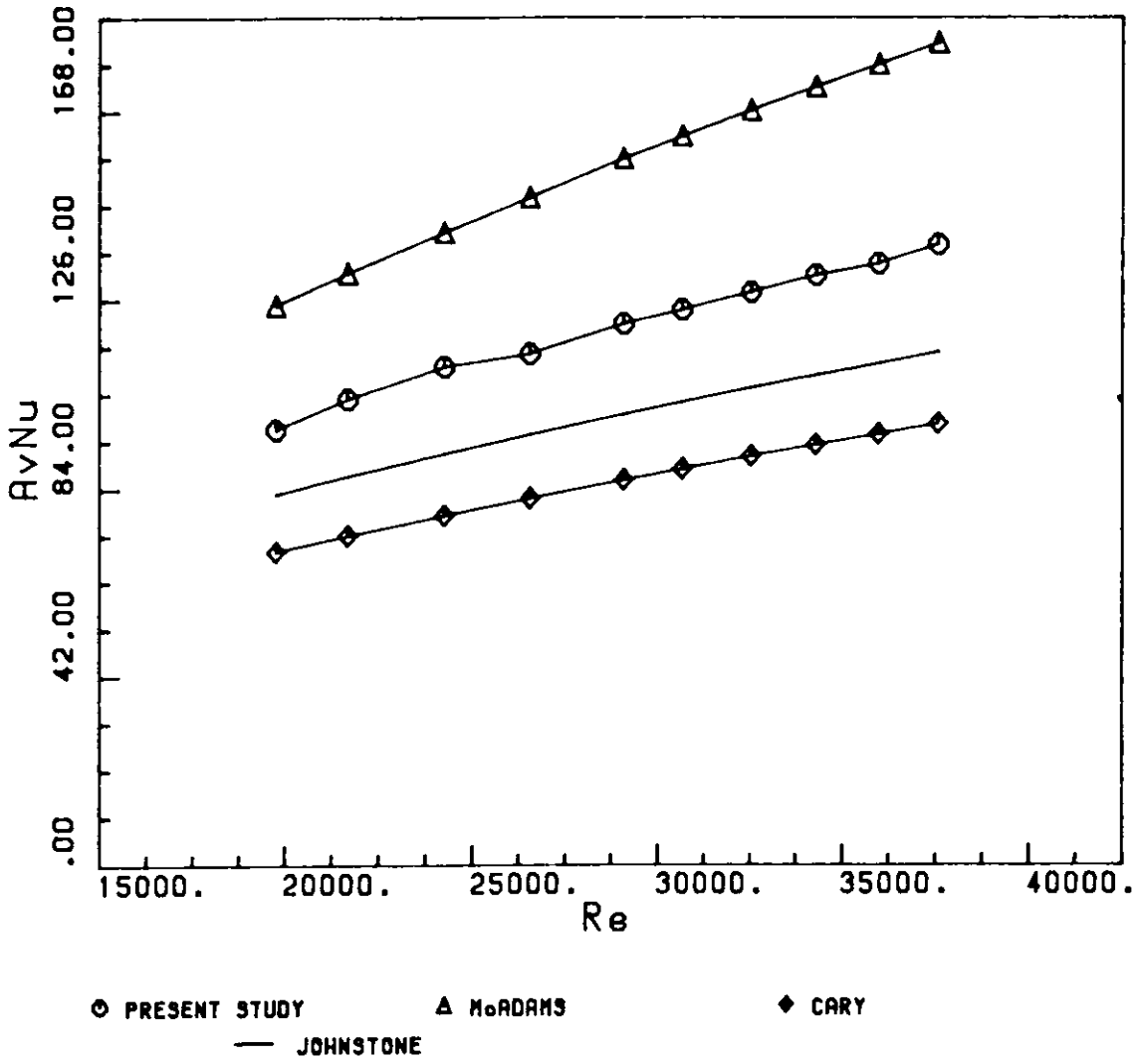

Figure 10. The effect of free stream cooling.

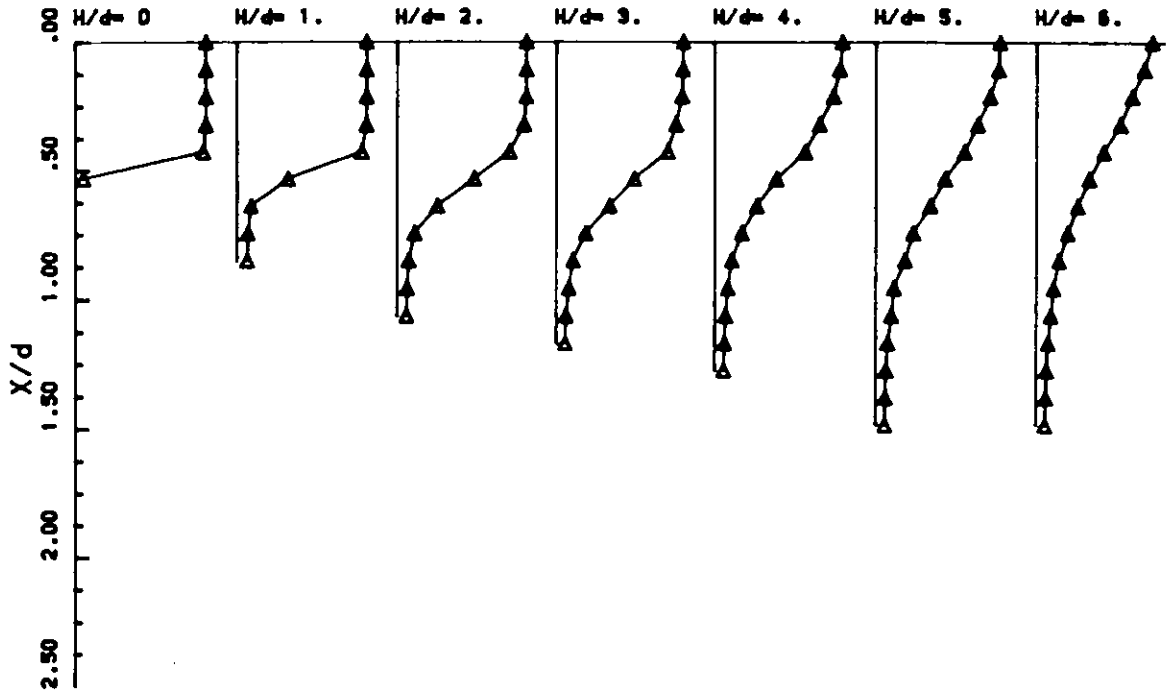

Figure 11. Velocity profiles for a unexcited jet close to the orifice.

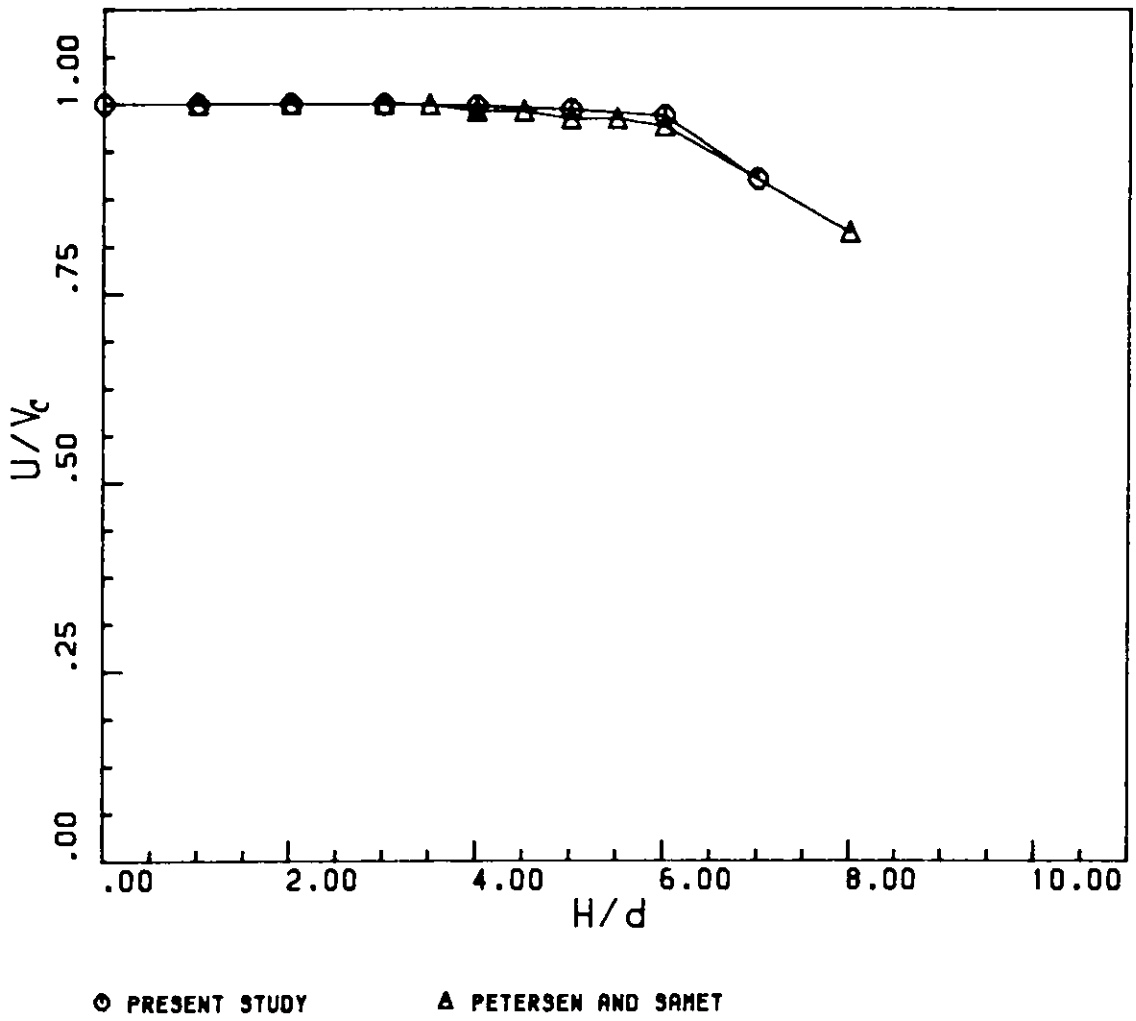

Figure 12. The decay of the centerline velocity in an unexcited jet.

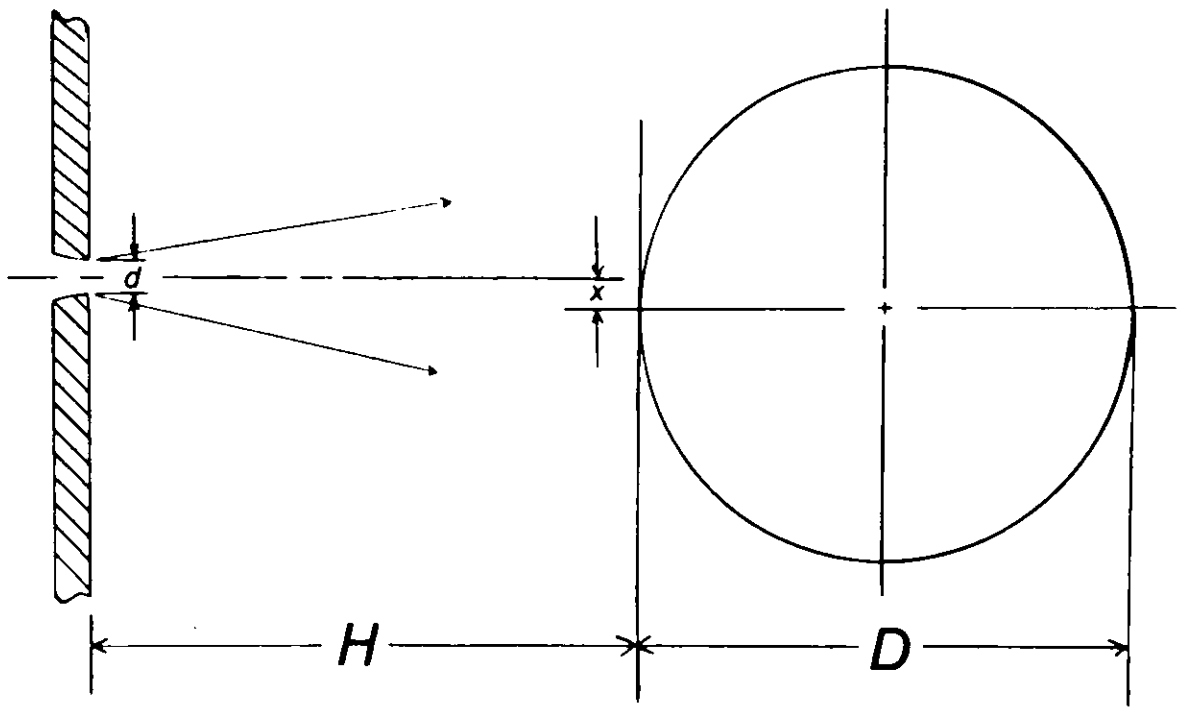

Figure 13. The geometrical distances used in this study.

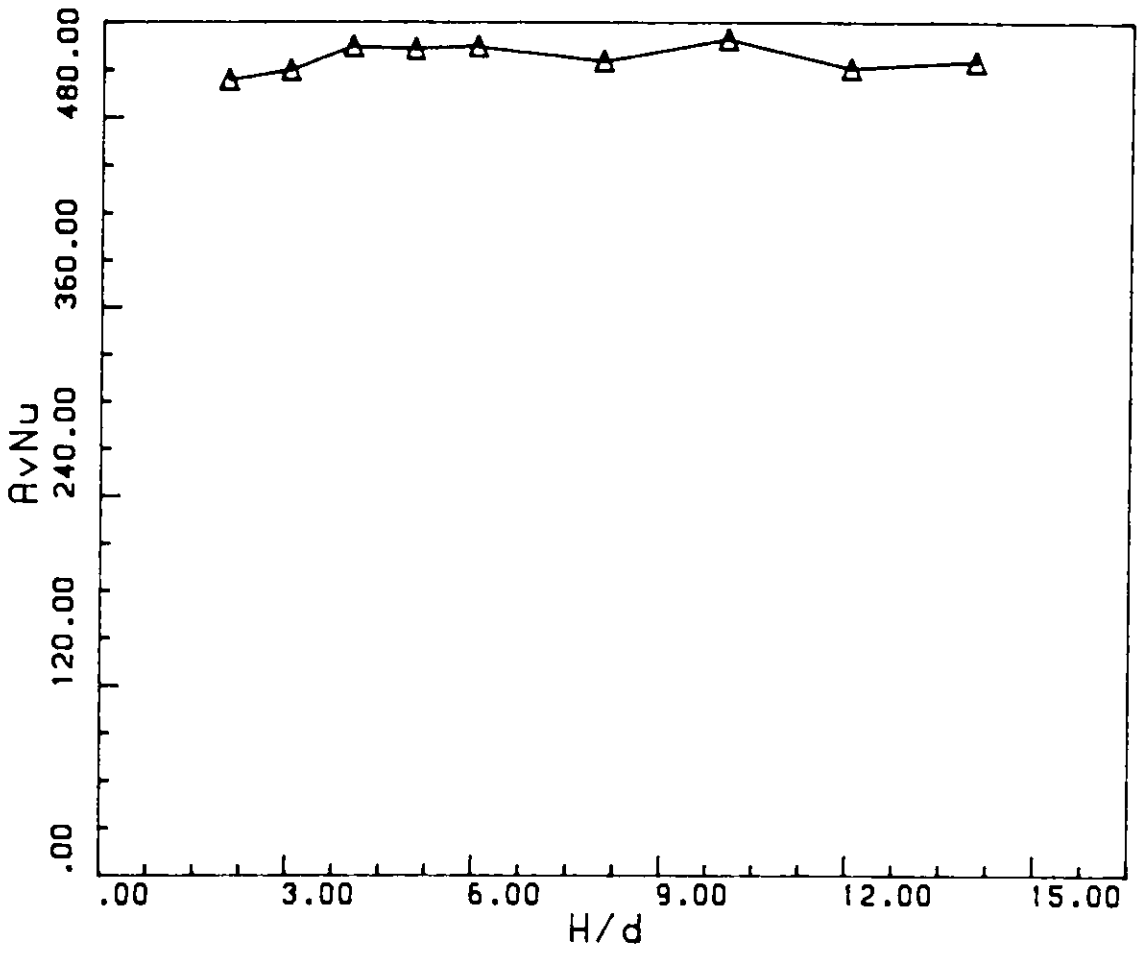

Figure 14. The effect of small values of $\frac{H}{d}$.

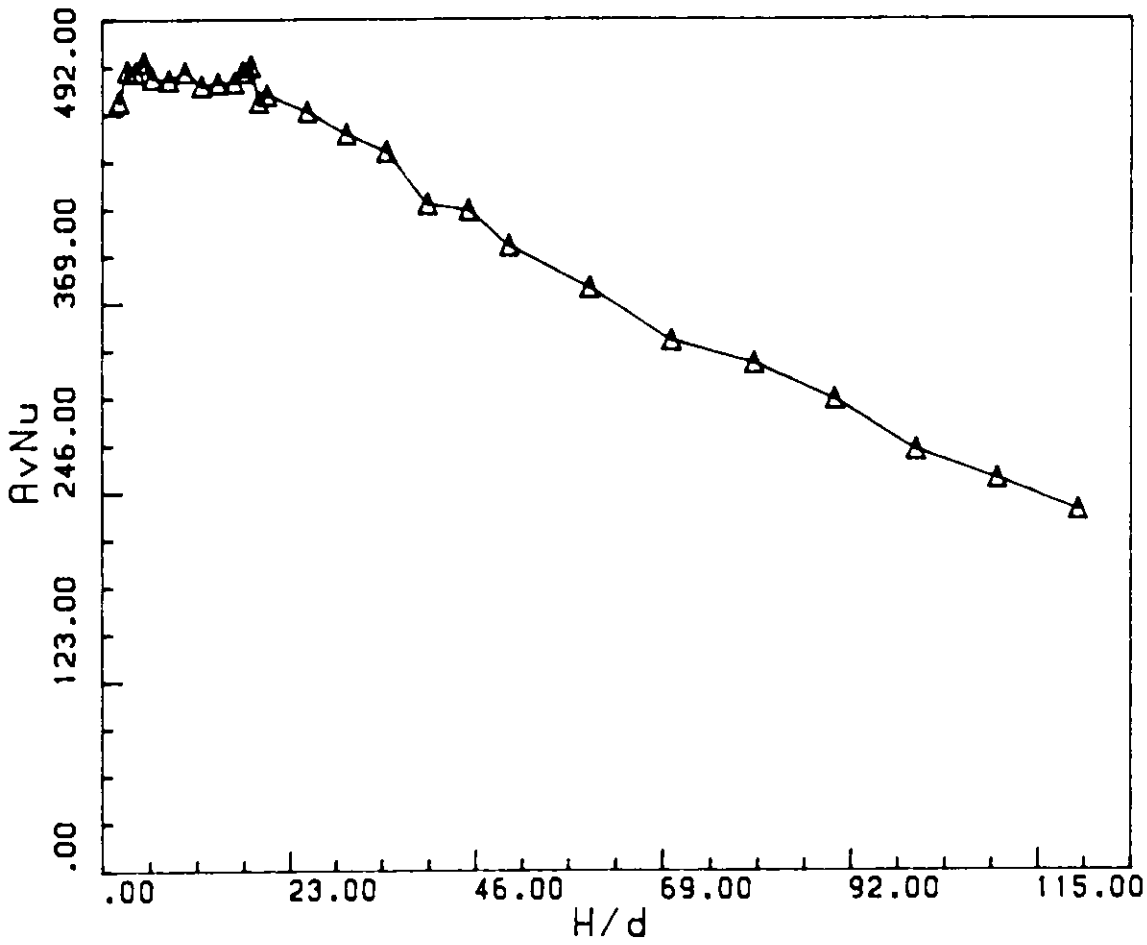

Figure 15. The effect of large values of $\frac{H}{d}$.

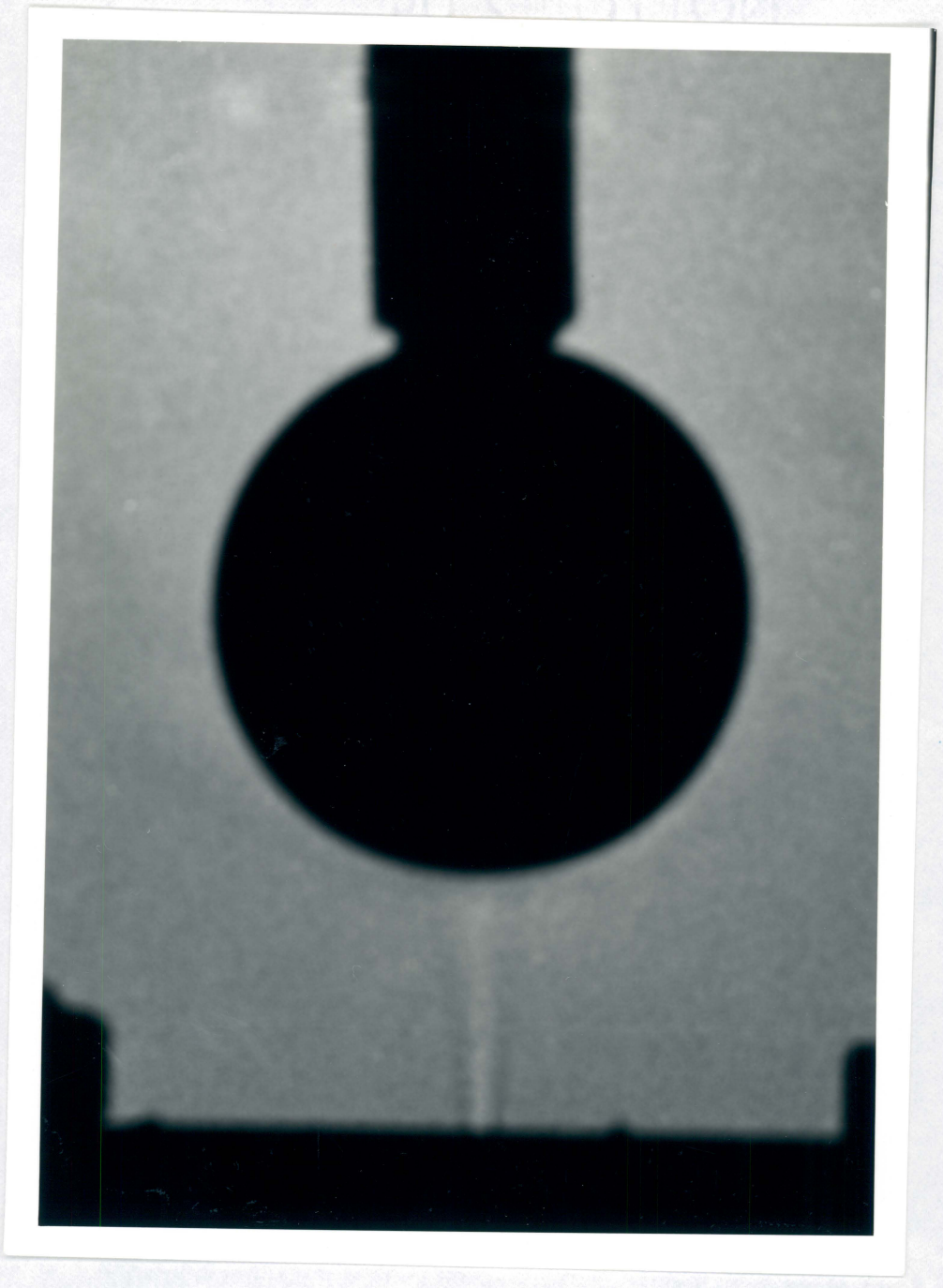

Figure 16. Shadowgraph of the impingement process.

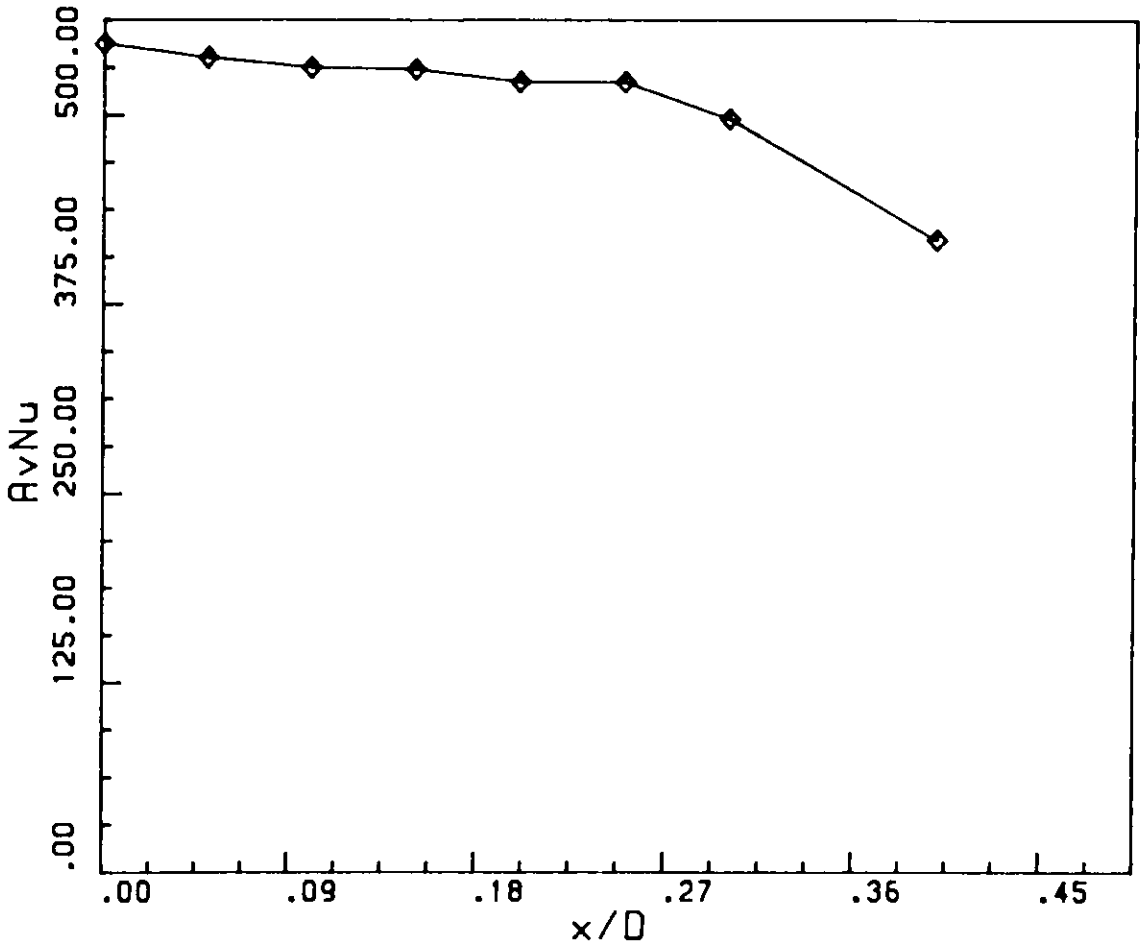

Figure 17. The effect of $\frac{x}{D}$

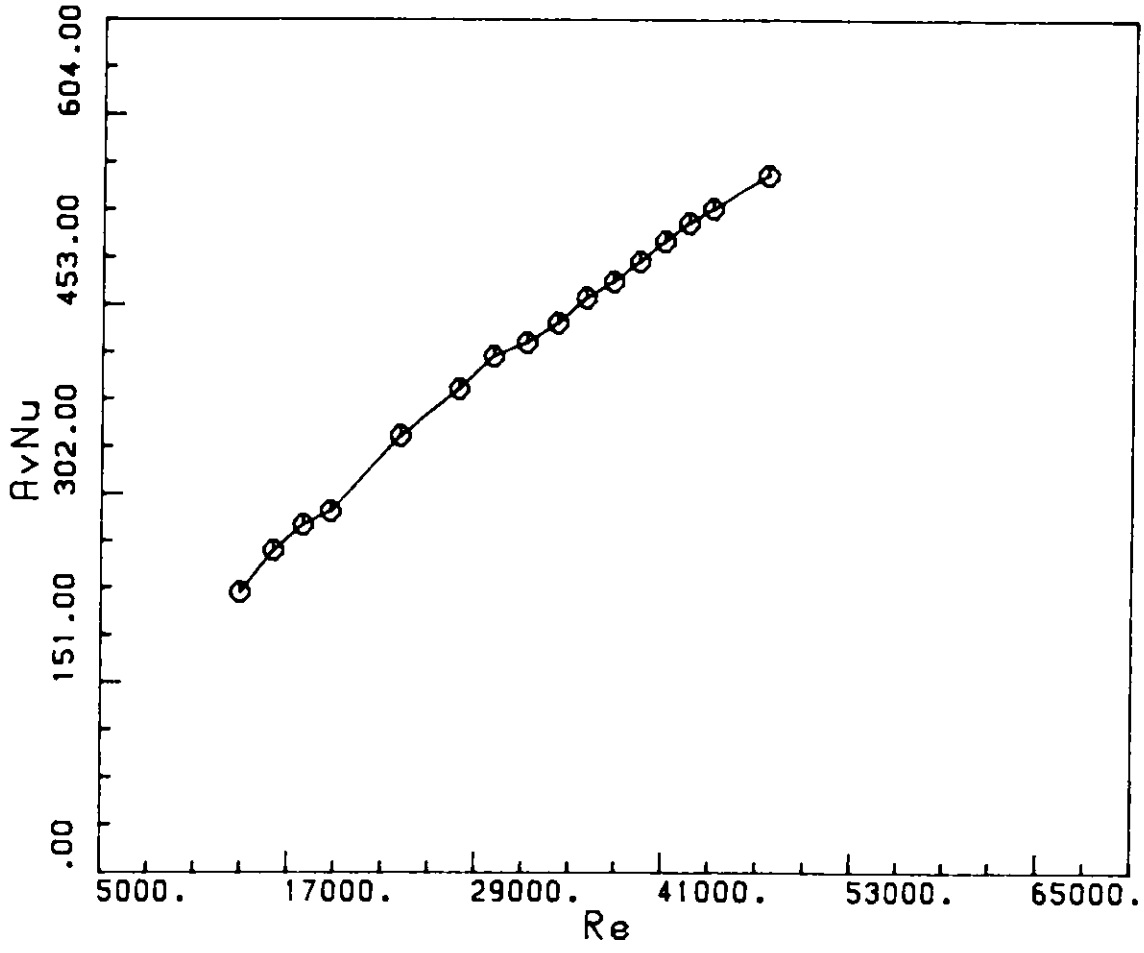

Figure 18. The Average Nusselt number as a function of Reynolds number.

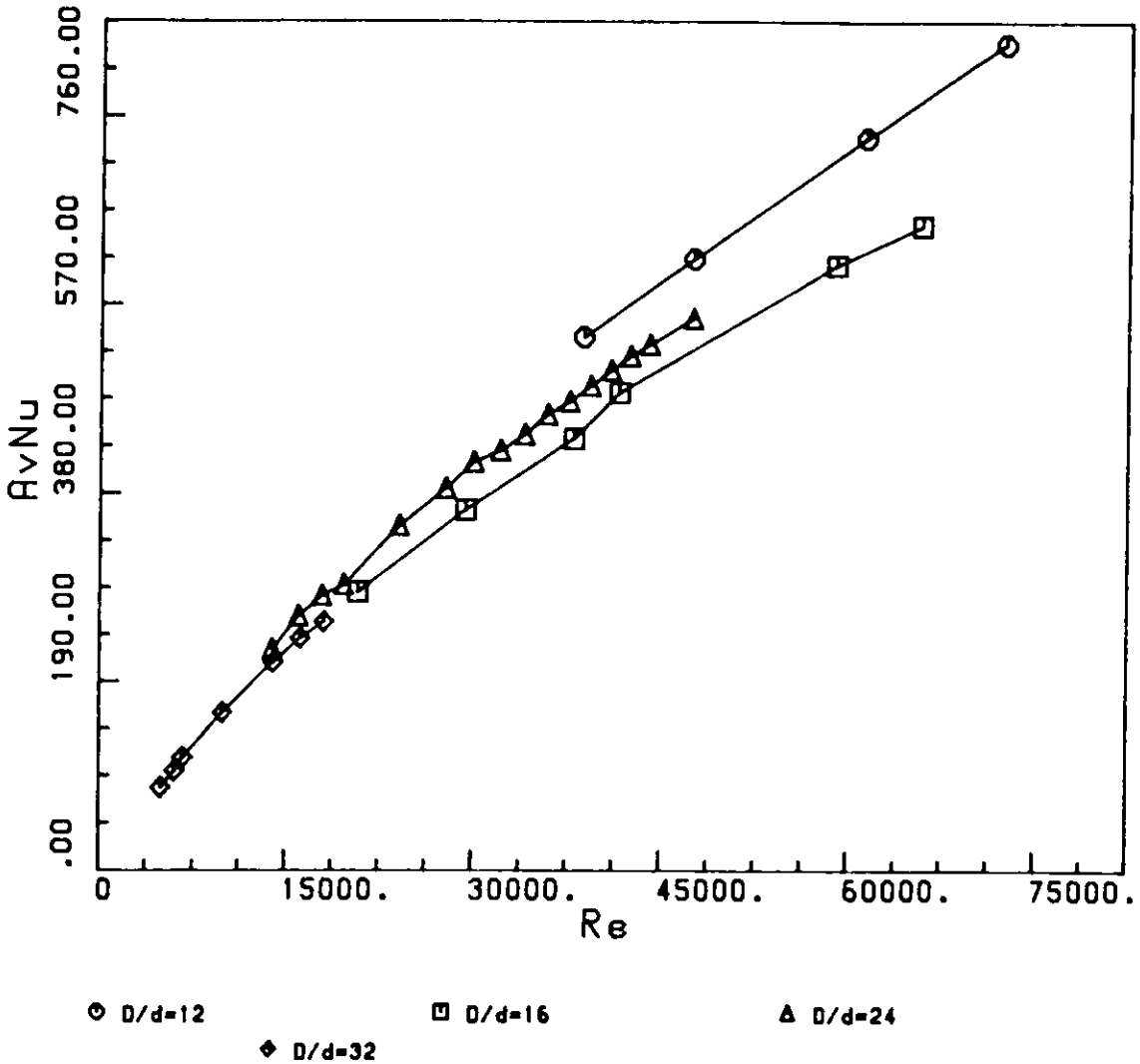

Figure 19. Average Nusselt number as a function of Reynolds number for different values of $\frac{D}{d}$.

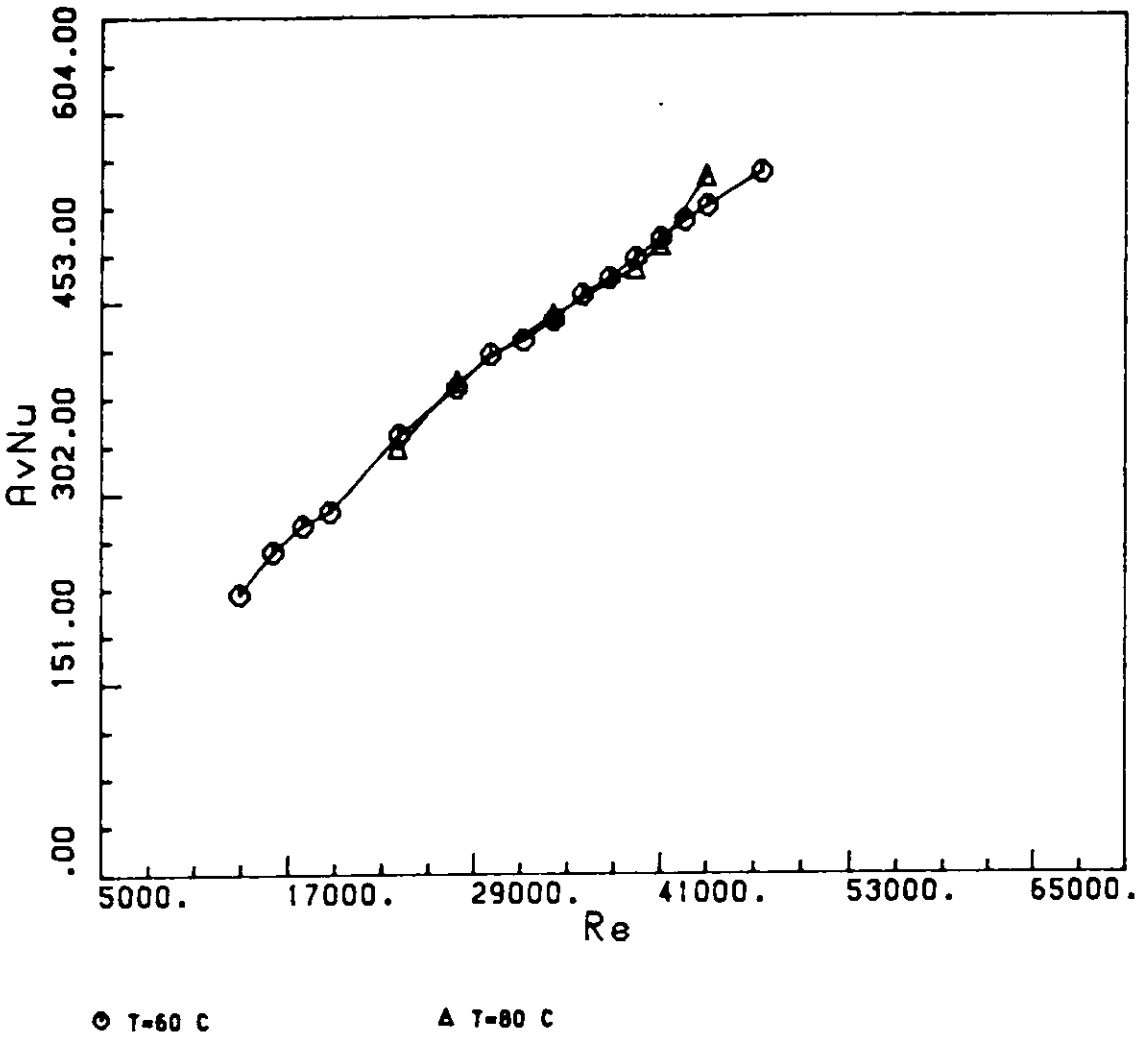

Figure 20. Average Nusselt number as a function of Reynolds number for different sphere temperatures.

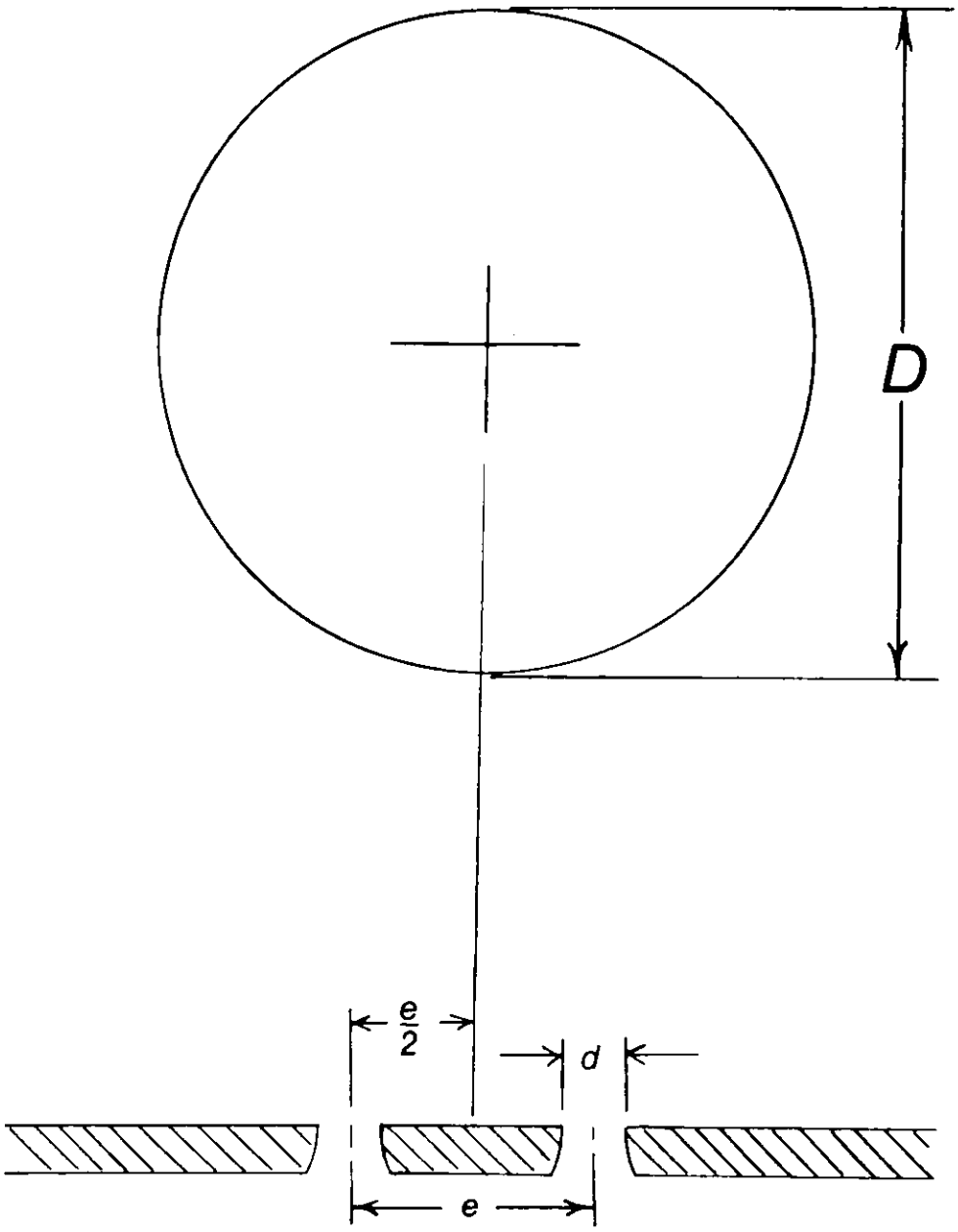

Figure 21. The definition sketch for $\frac{e}{D}$.

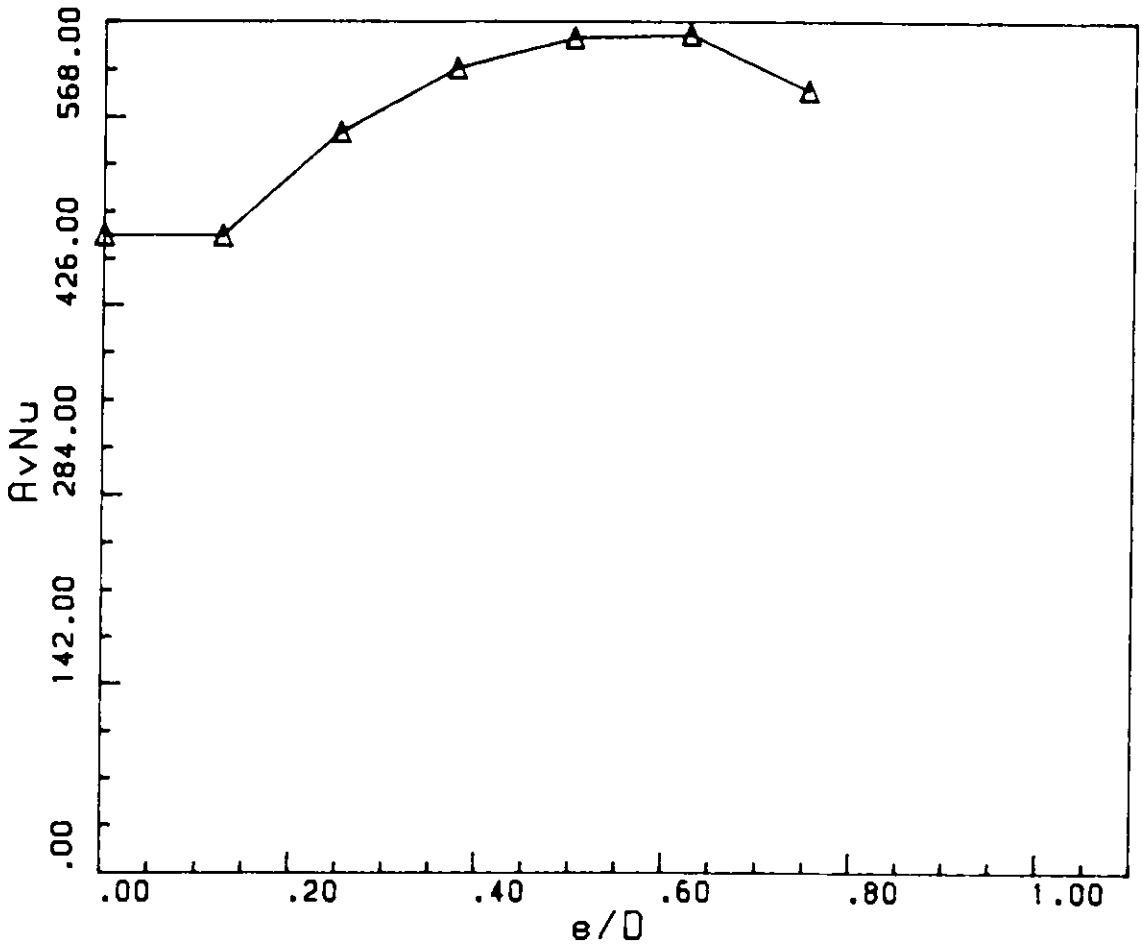

Figure 22. The effect of $\frac{e}{D}$

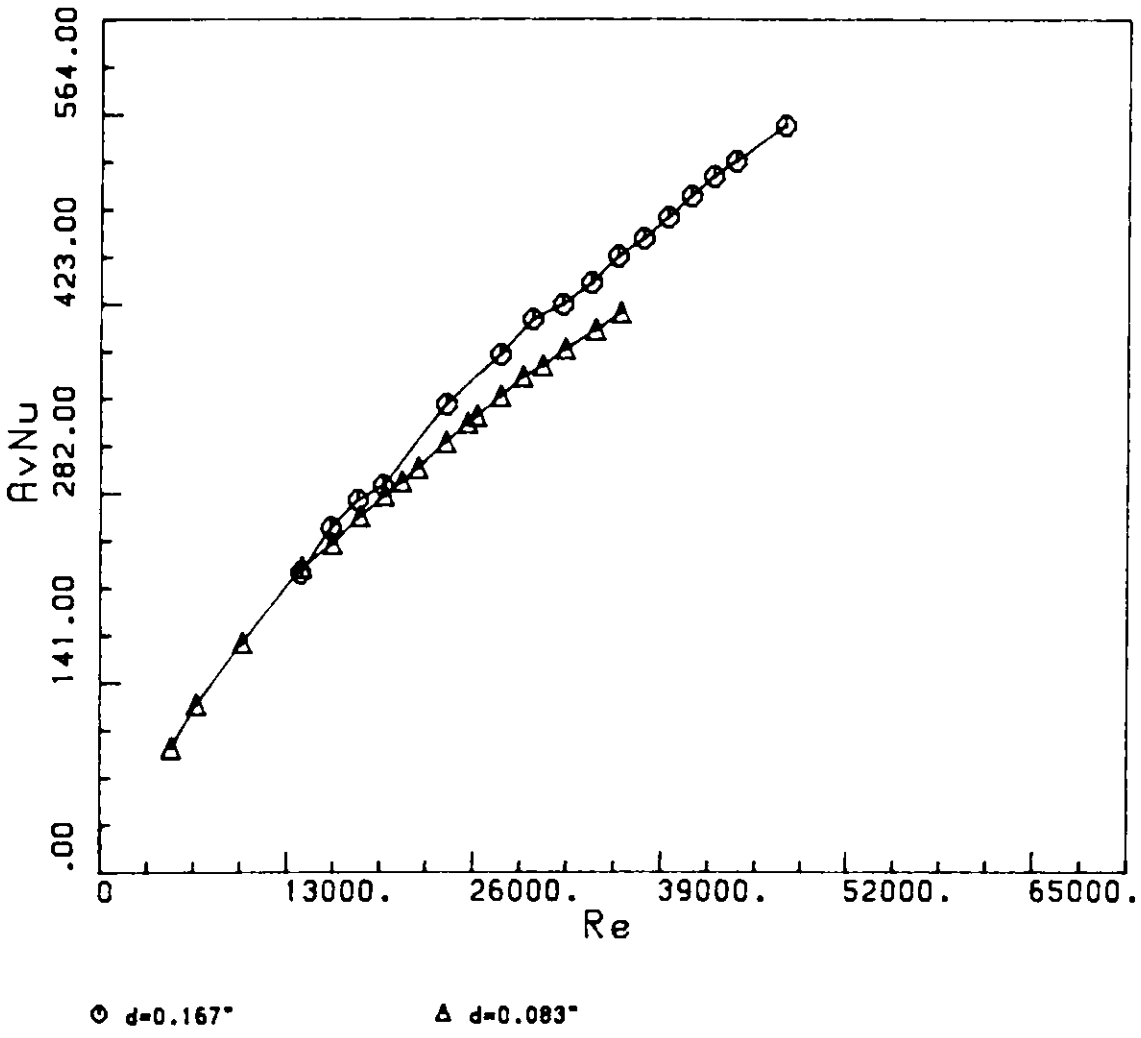

Figure 23. Evidence of a Mach number effect.

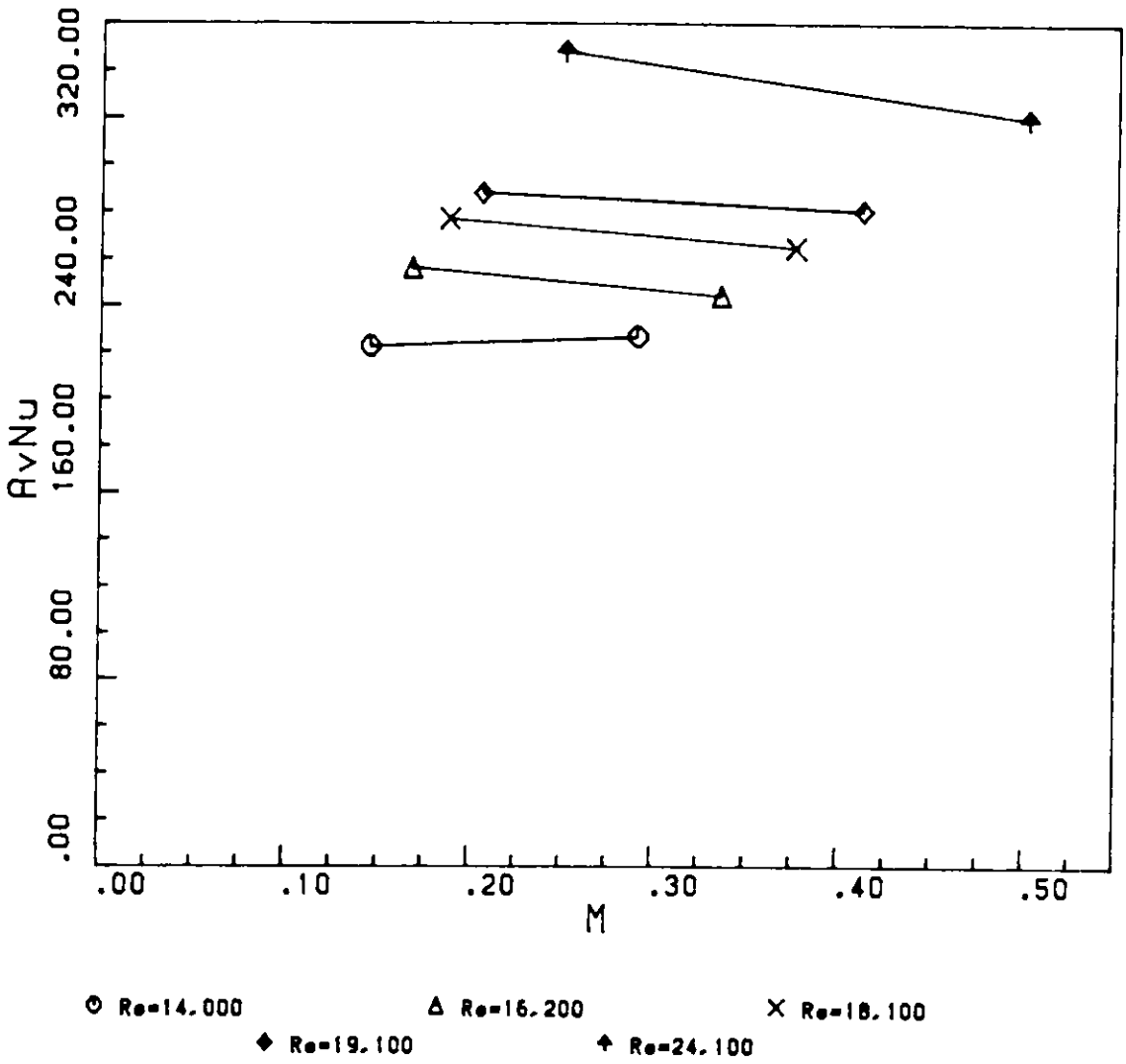

Figure 24. The average Nusselt number as a function of Mach number for lines of constant Reynolds number.

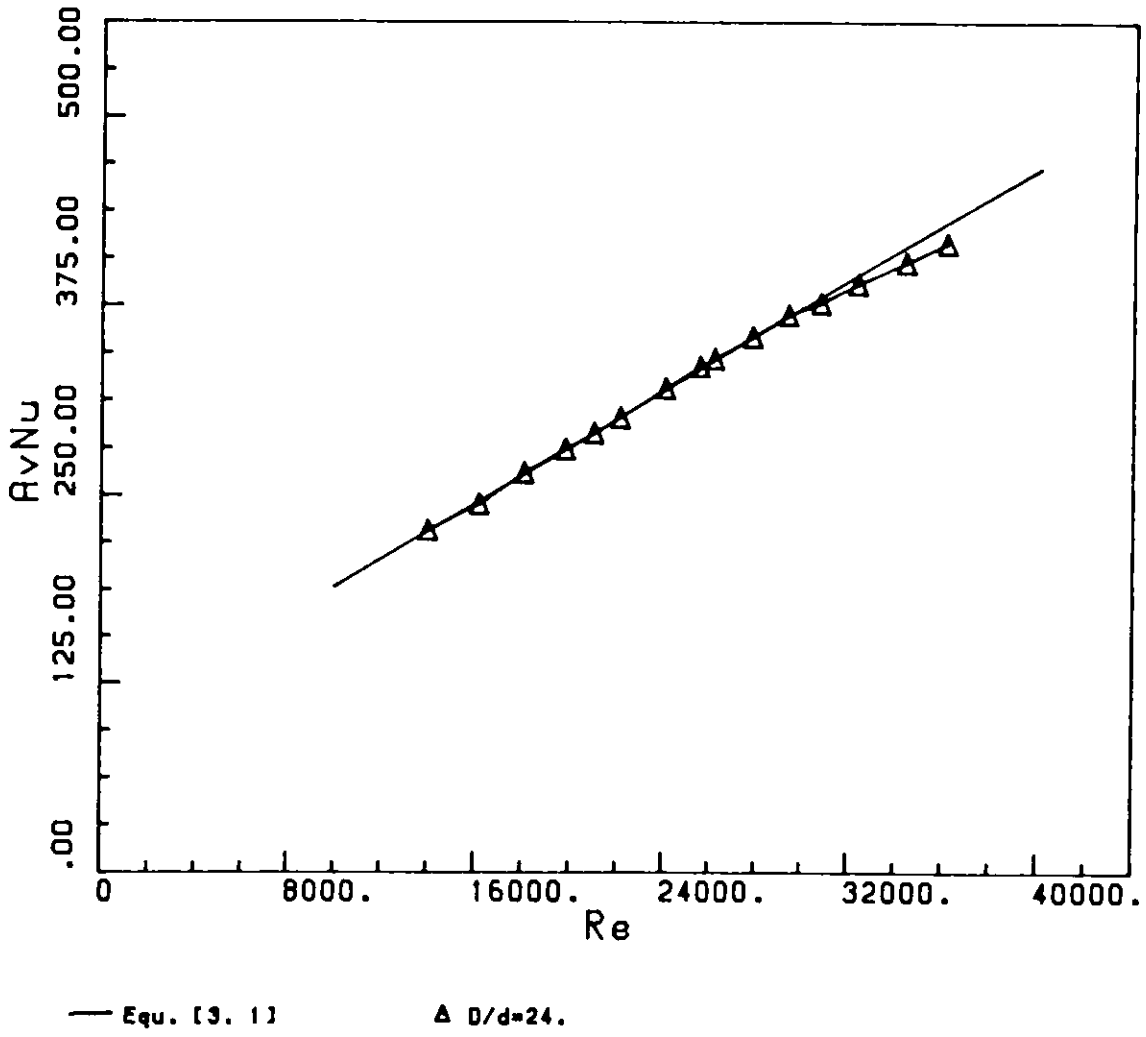

Figure 25. Comparison of Equation [3.1] and data for $\frac{D}{d} = 24$.

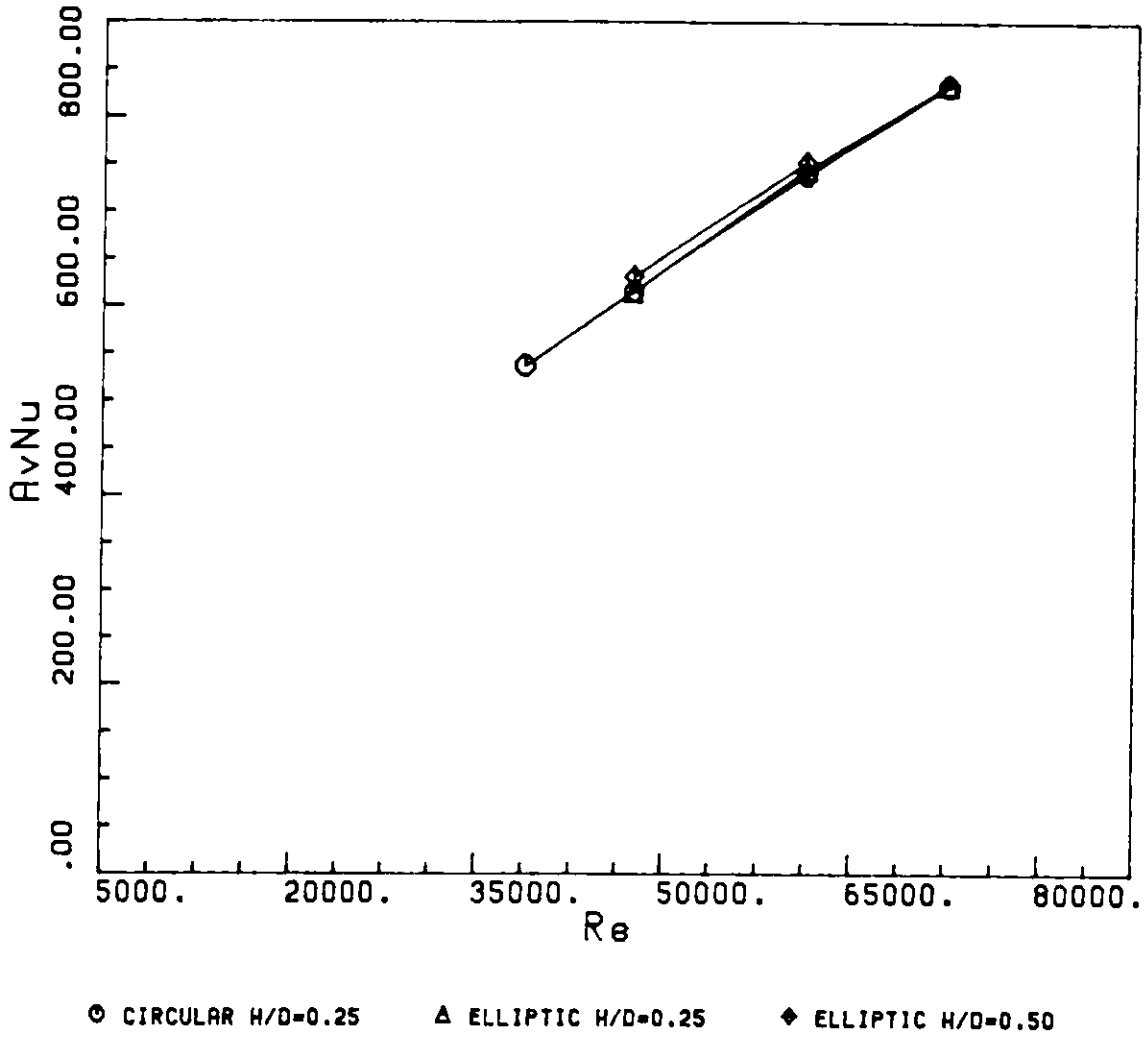

Figure 26. The effect of an elliptic orifice.

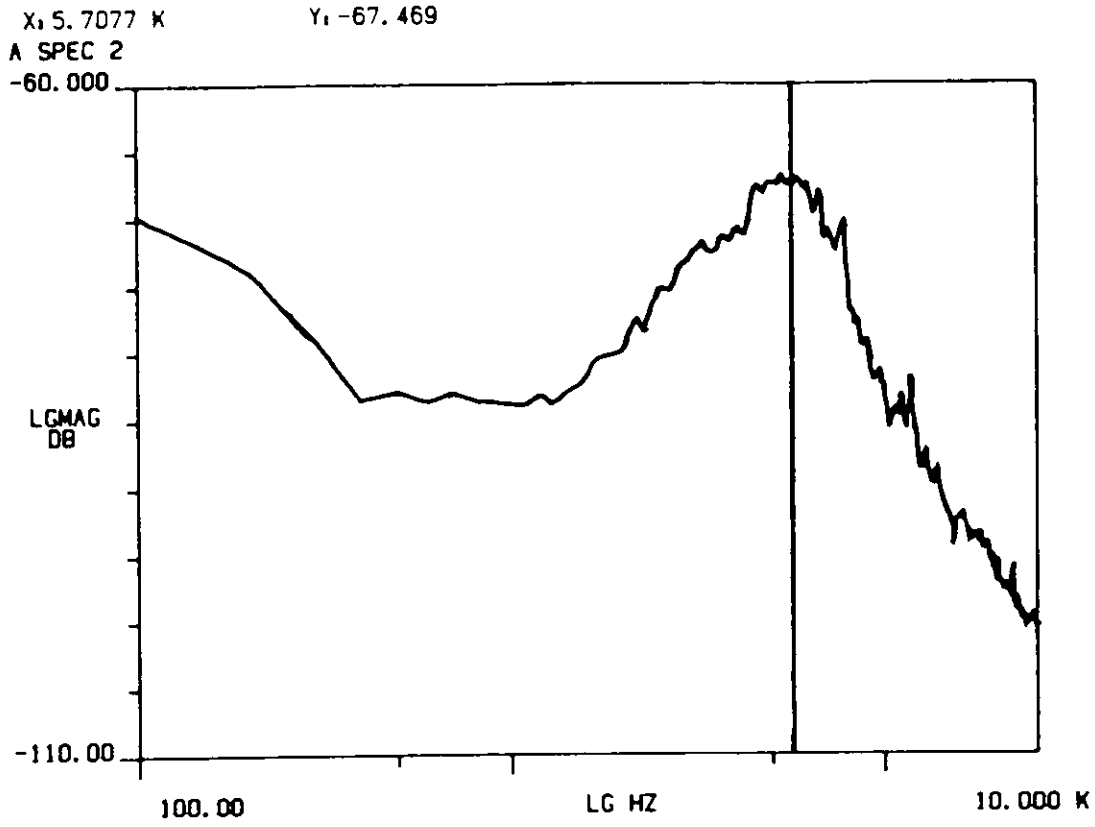

Figure 27. Spectra for a natural jet at Reynolds number of 12,800.

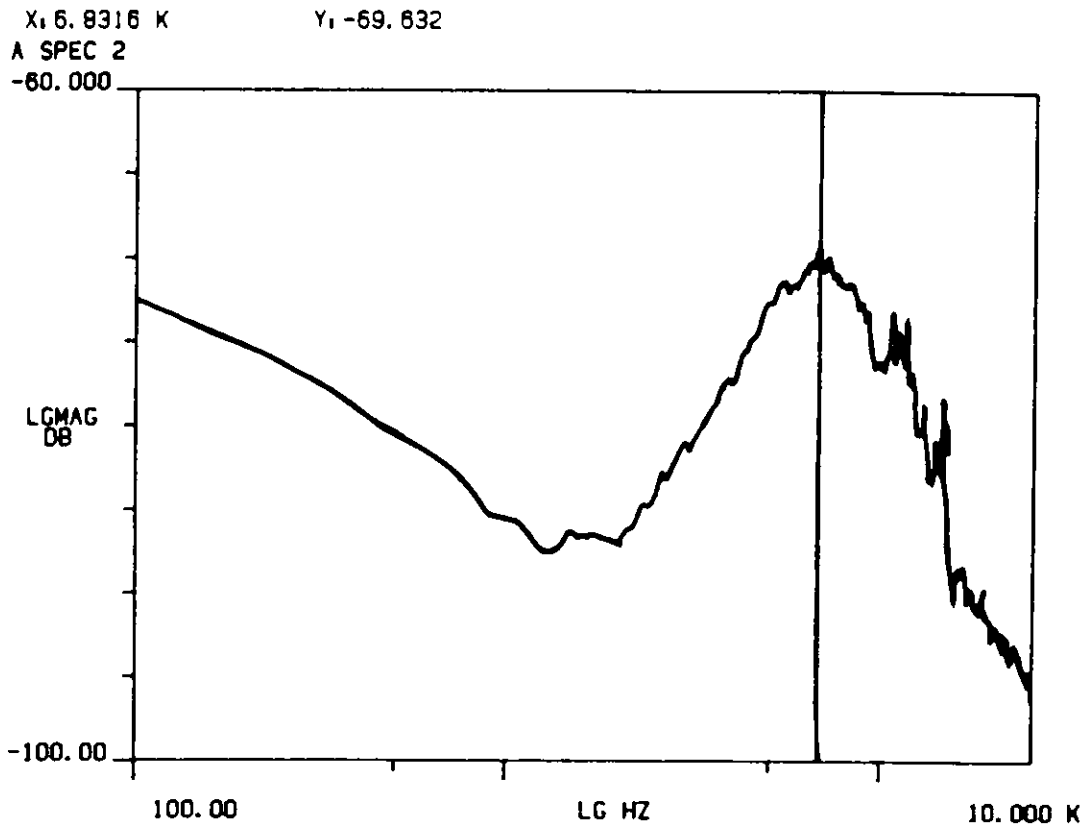

Figure 28. Spectra for a natural jet at Reynolds number of 18,000.

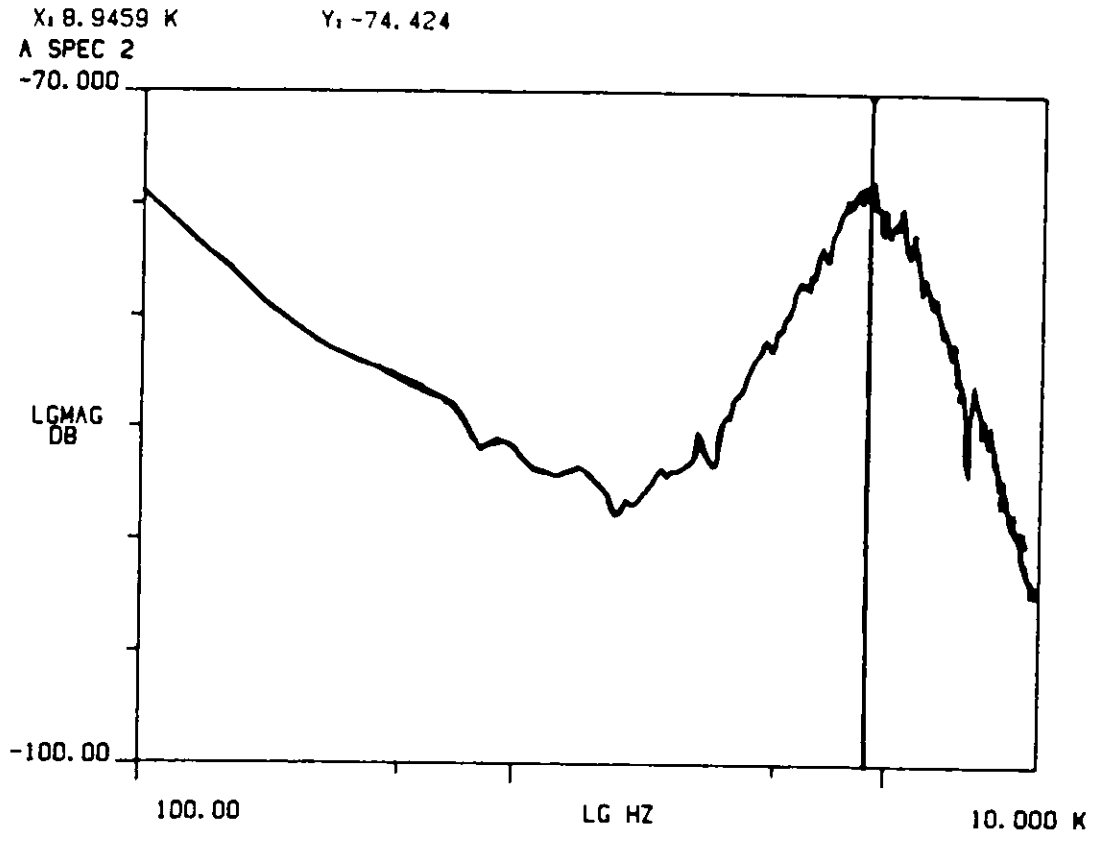

Figure 29. Spectra for a natural jet at Reynolds number of 25,570.

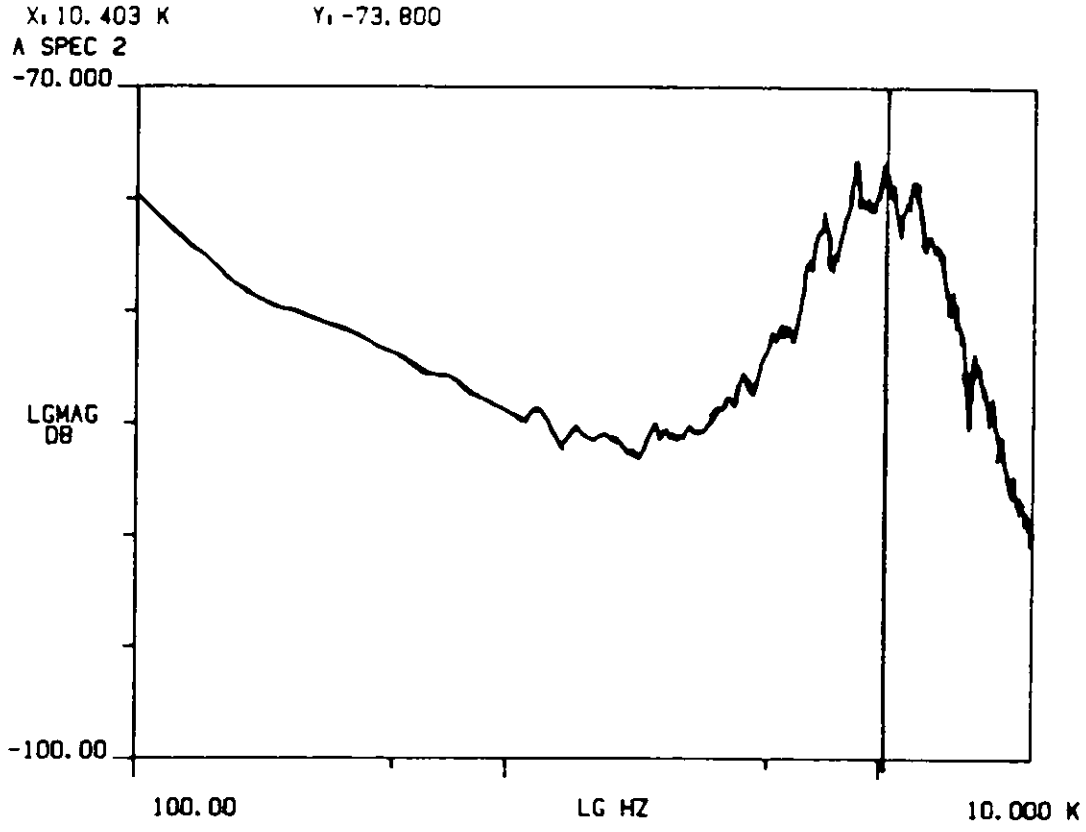

Figure 30. Spectra for a natural jet at Reynolds number of 31,230.

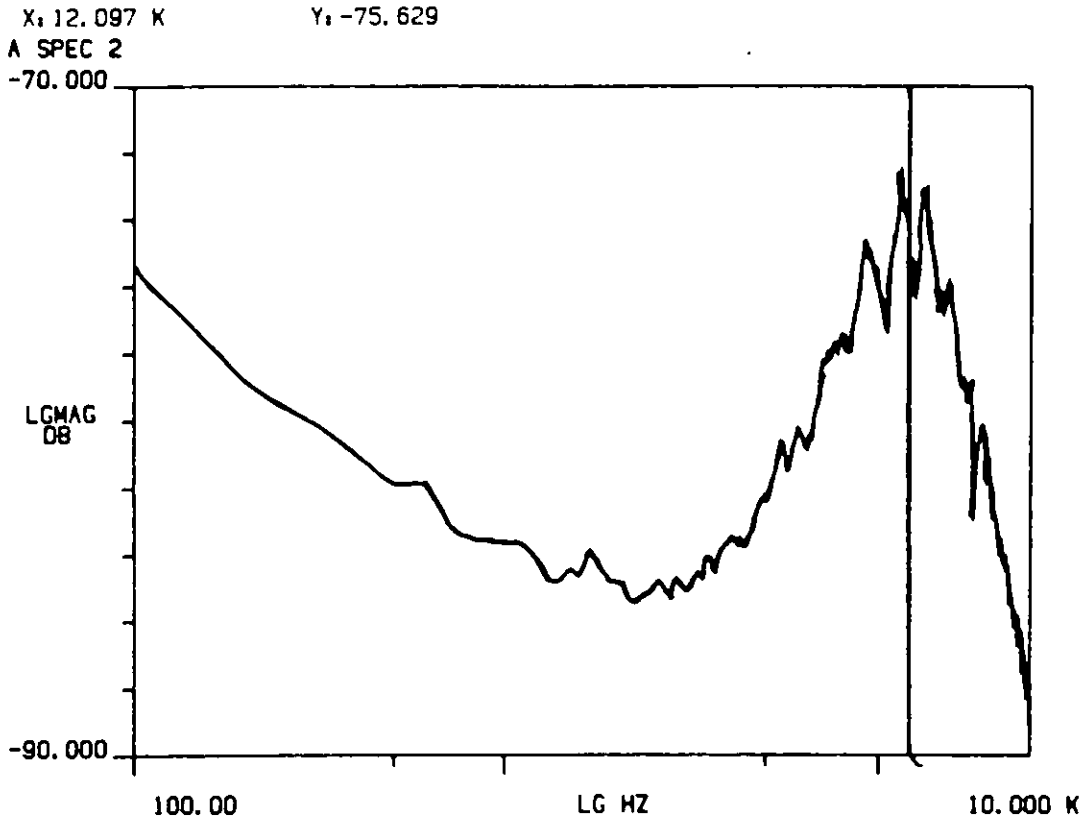

Figure 31. Spectra for a natural jet at Reynolds number of 35,600.

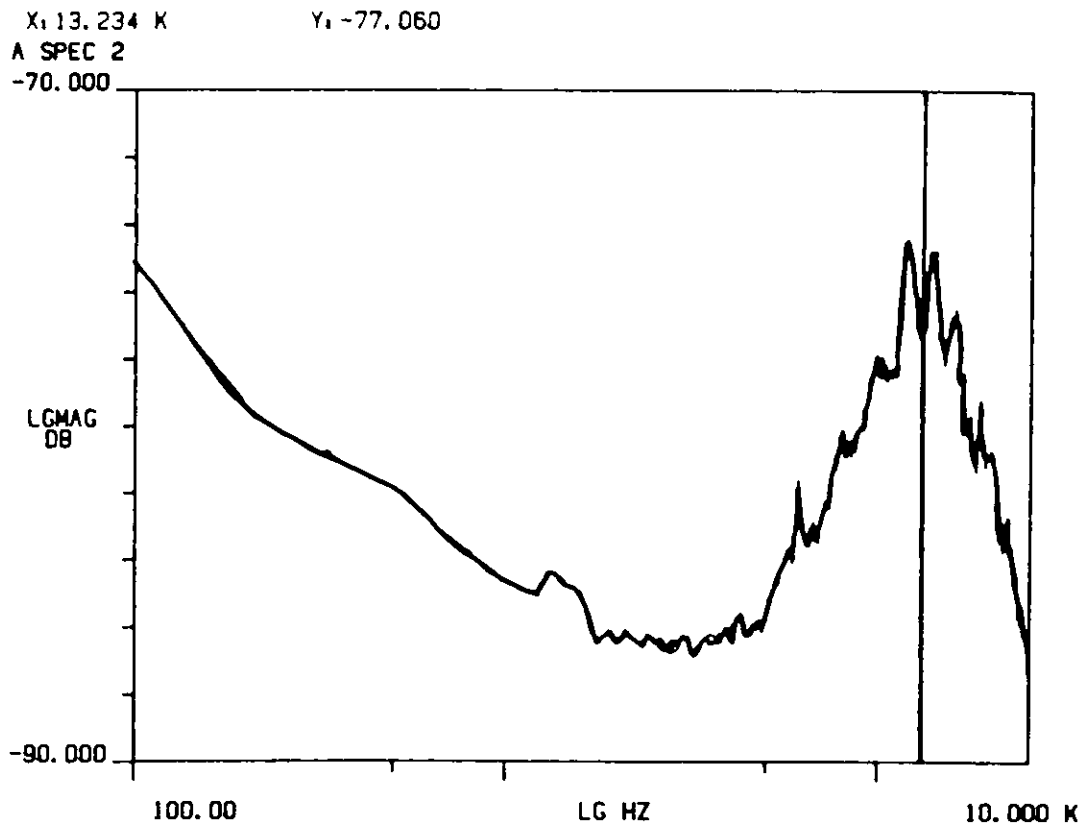

Figure 32. Spectra for a natural jet at Reynolds number of 39,500.

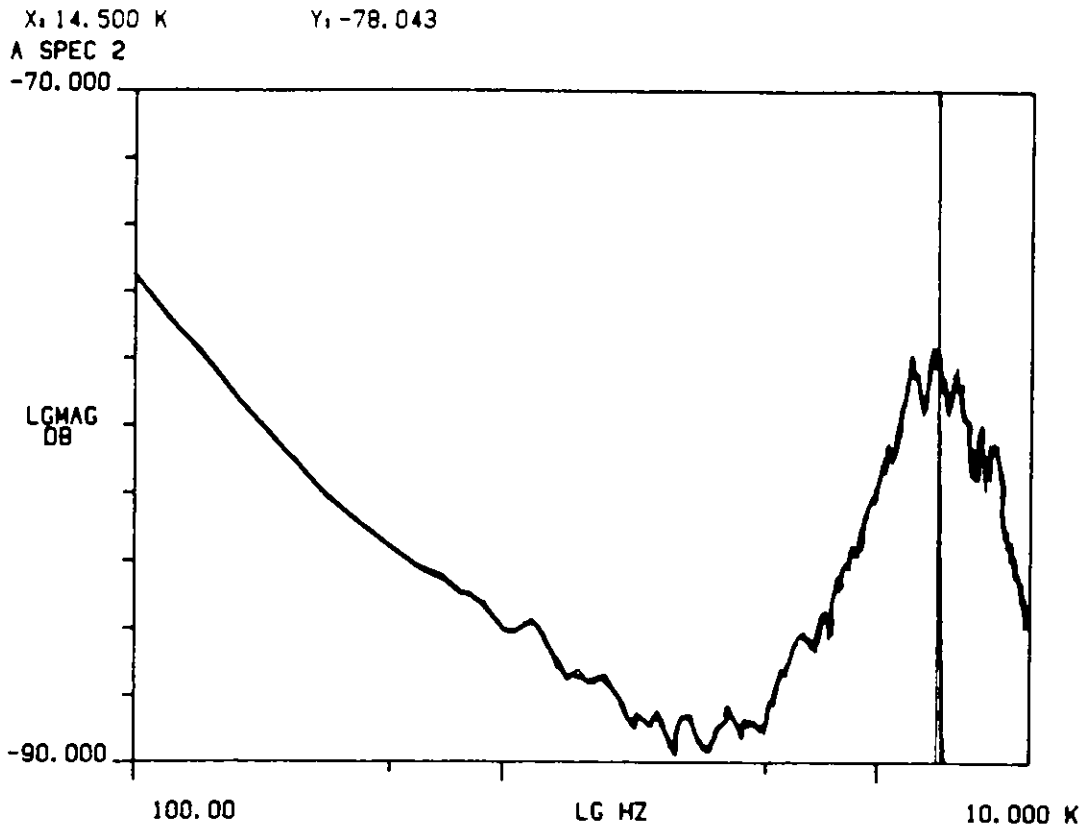

Figure 33. Spectra for a natural jet at Reynolds number of 42,722.

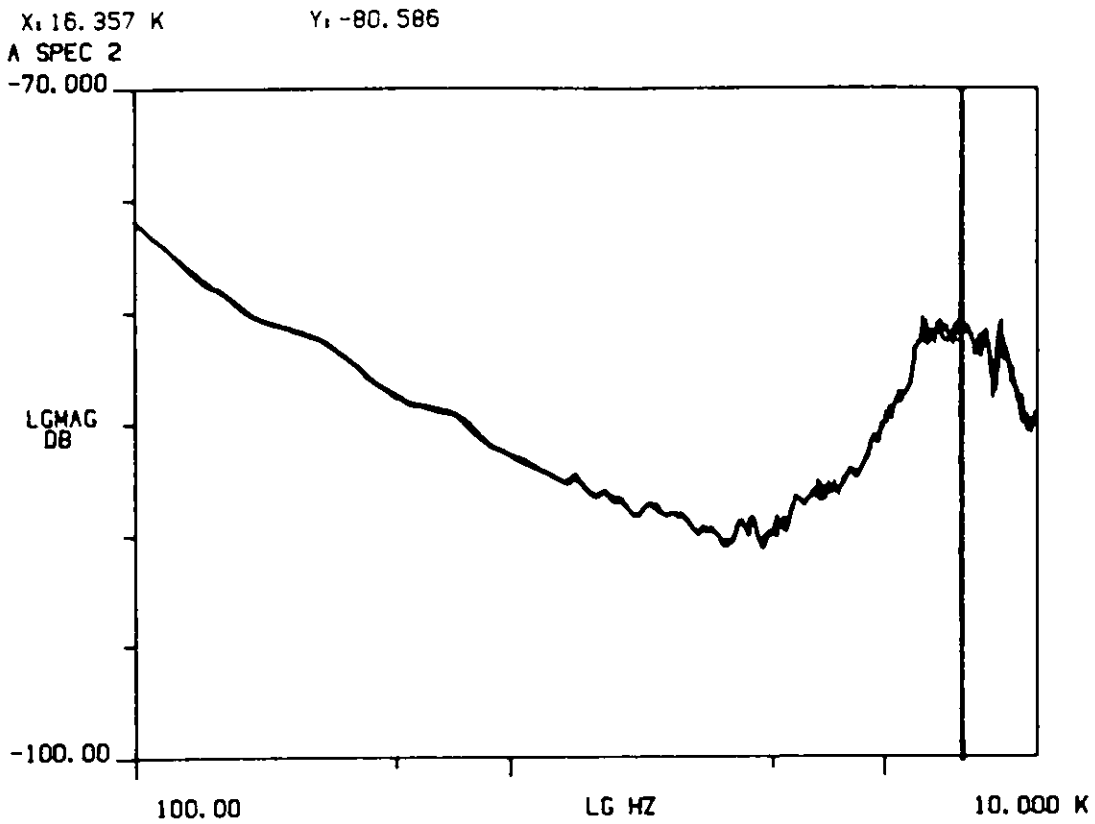

Figure 34. Spectra for a natural jet at Reynolds number of 45,000.

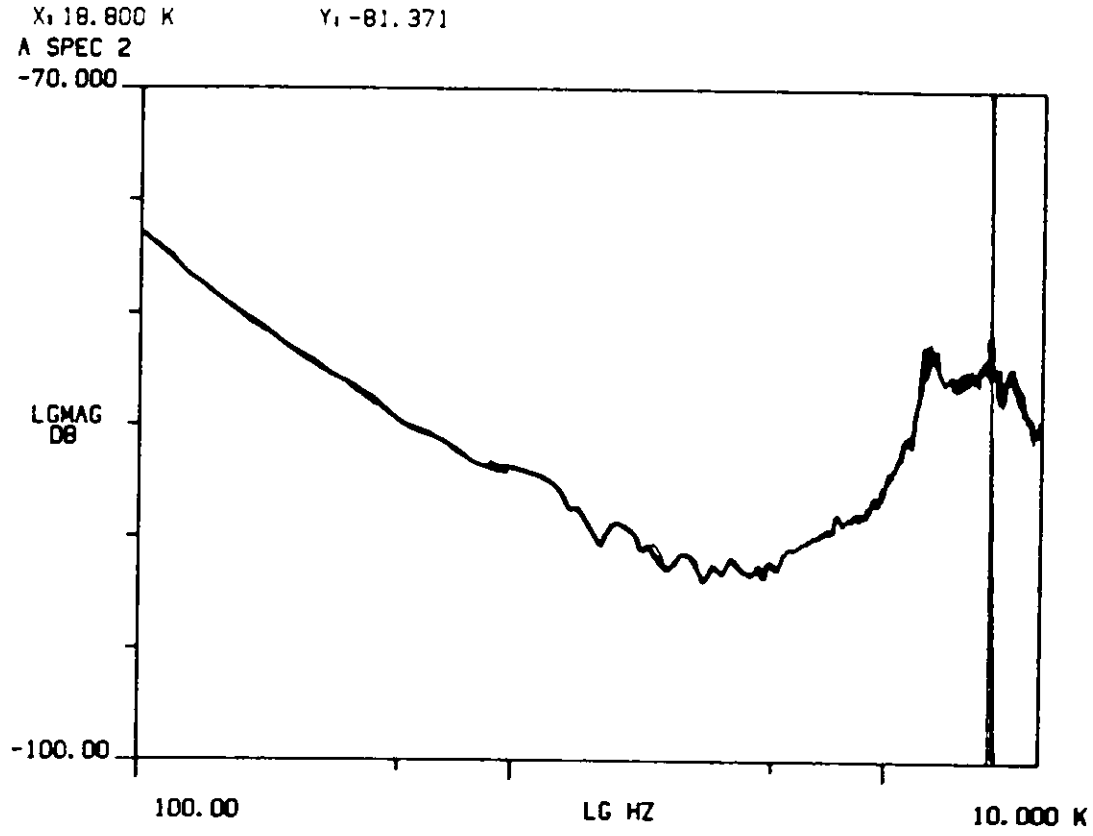

Figure 35. Spectra for a natural jet at Reynolds number of 48,500.

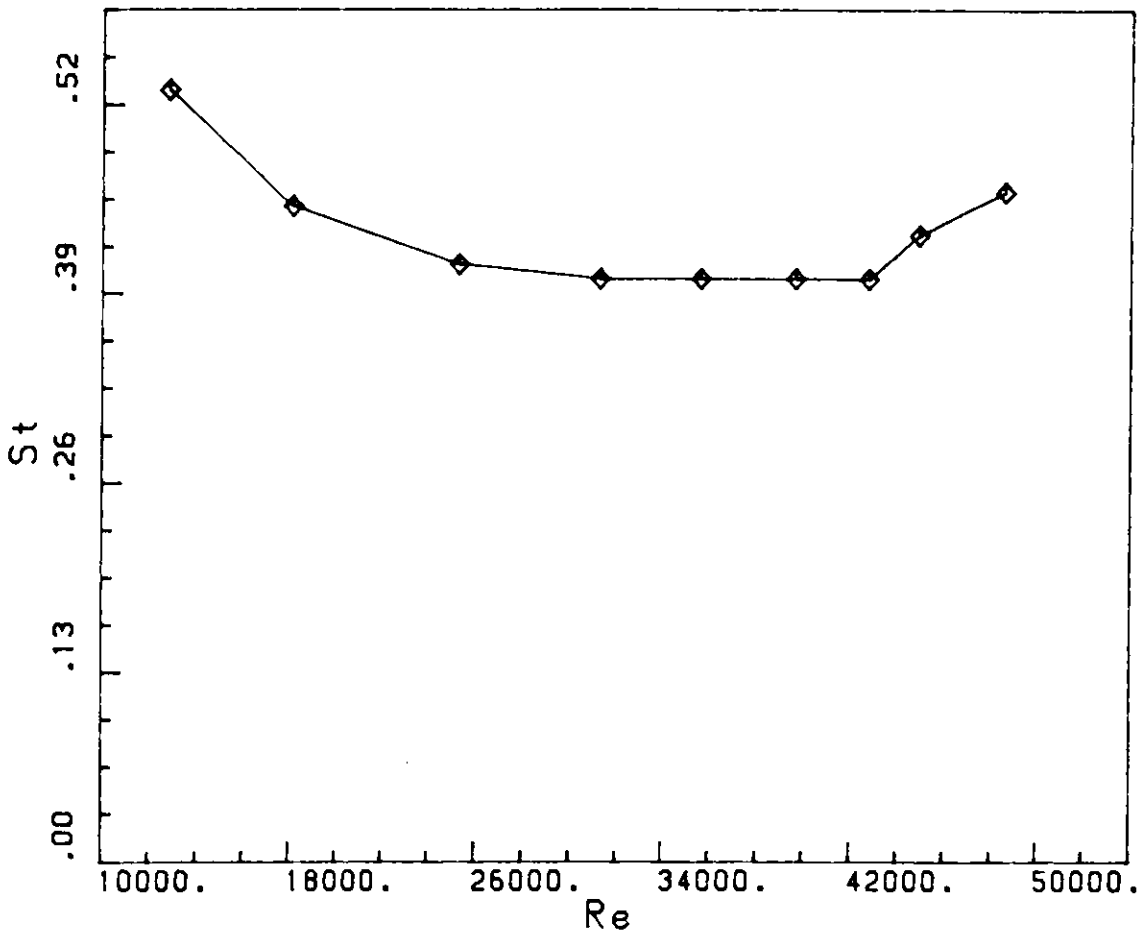

Figure 36. The natural Strouhal number as a function of the Reynolds number

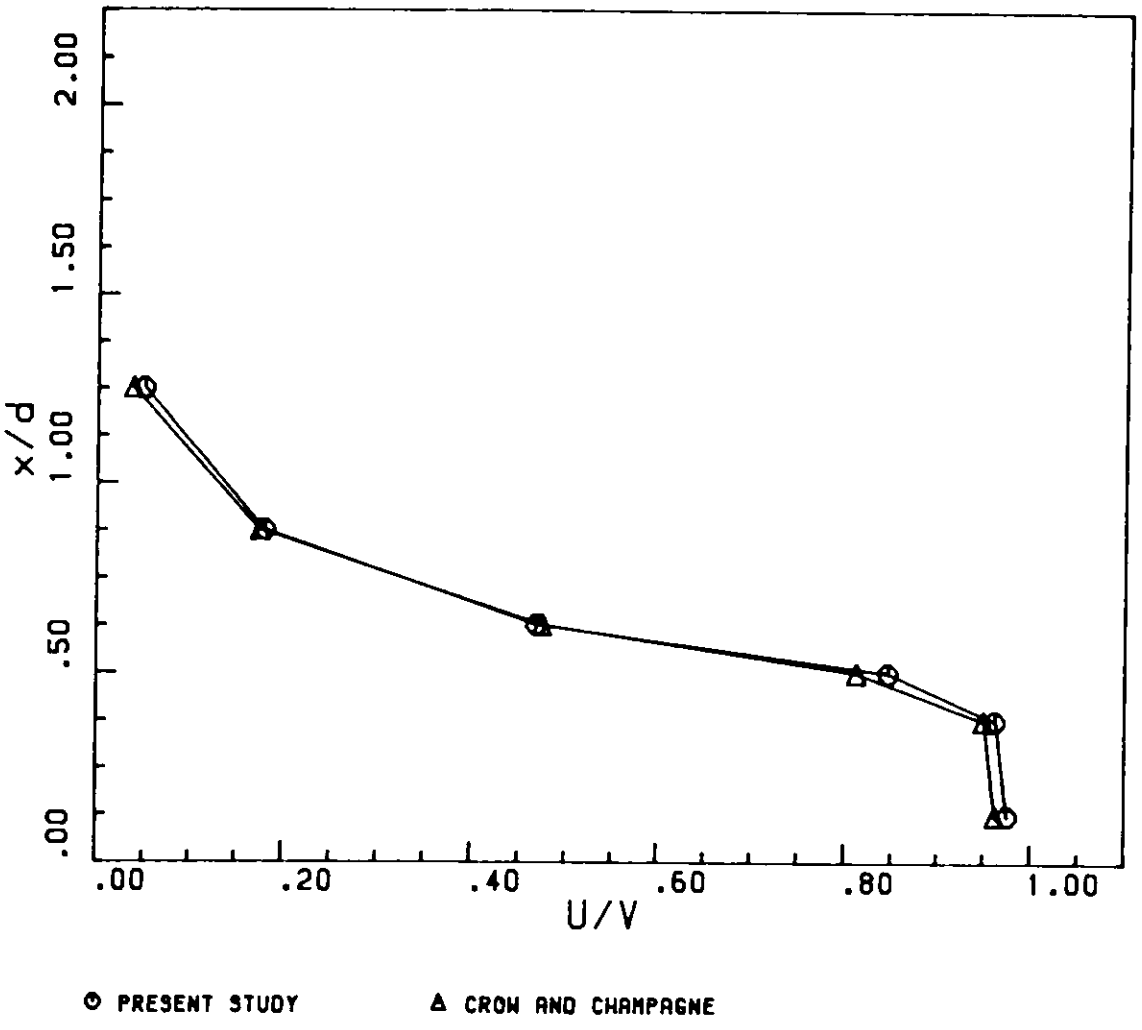

Figure 37. Velocity profiles of an excited jet at $\frac{H}{d}$ of 4.0

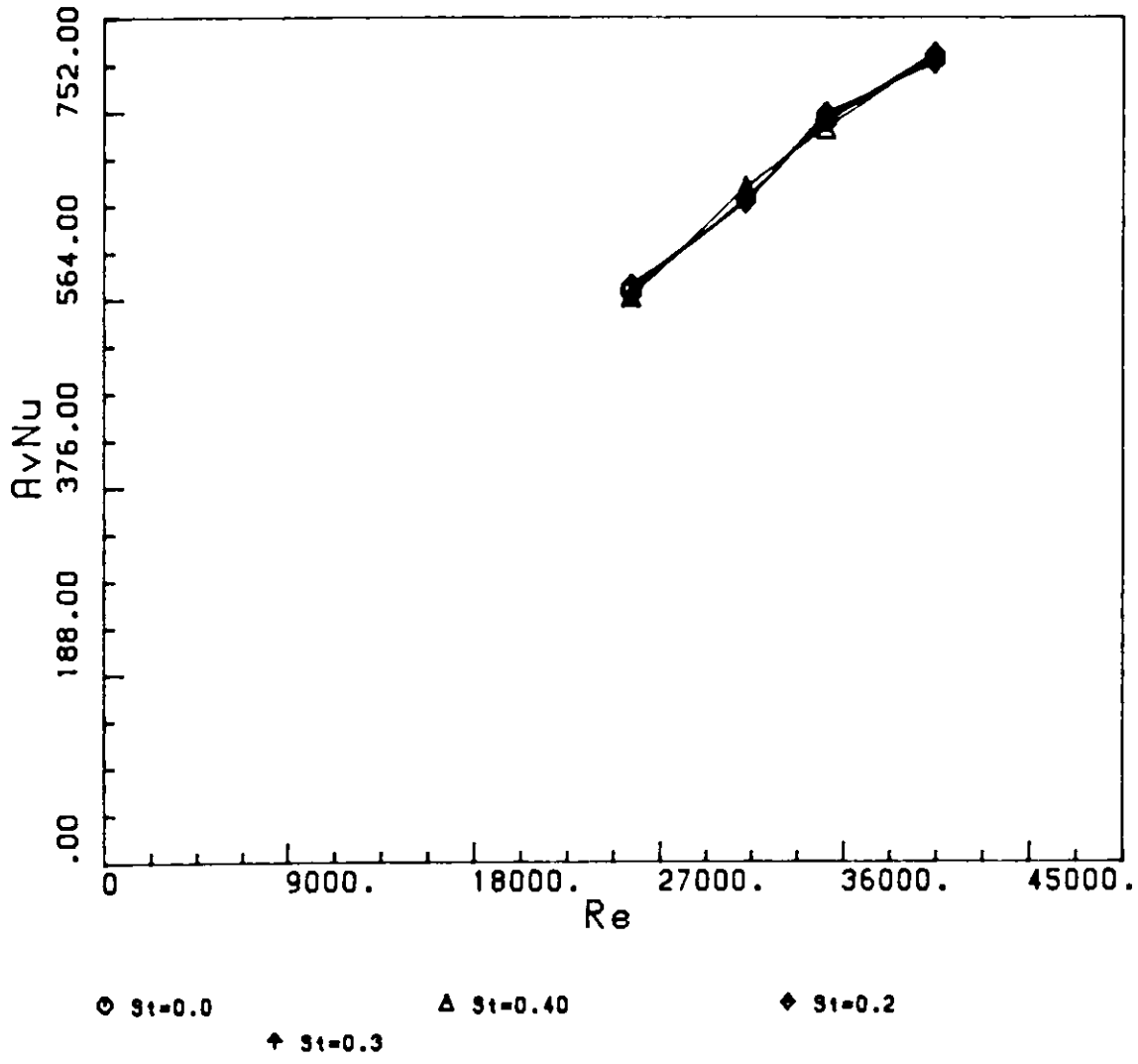

Figure 38. The effect of acoustic excitation on heat transfer rate.

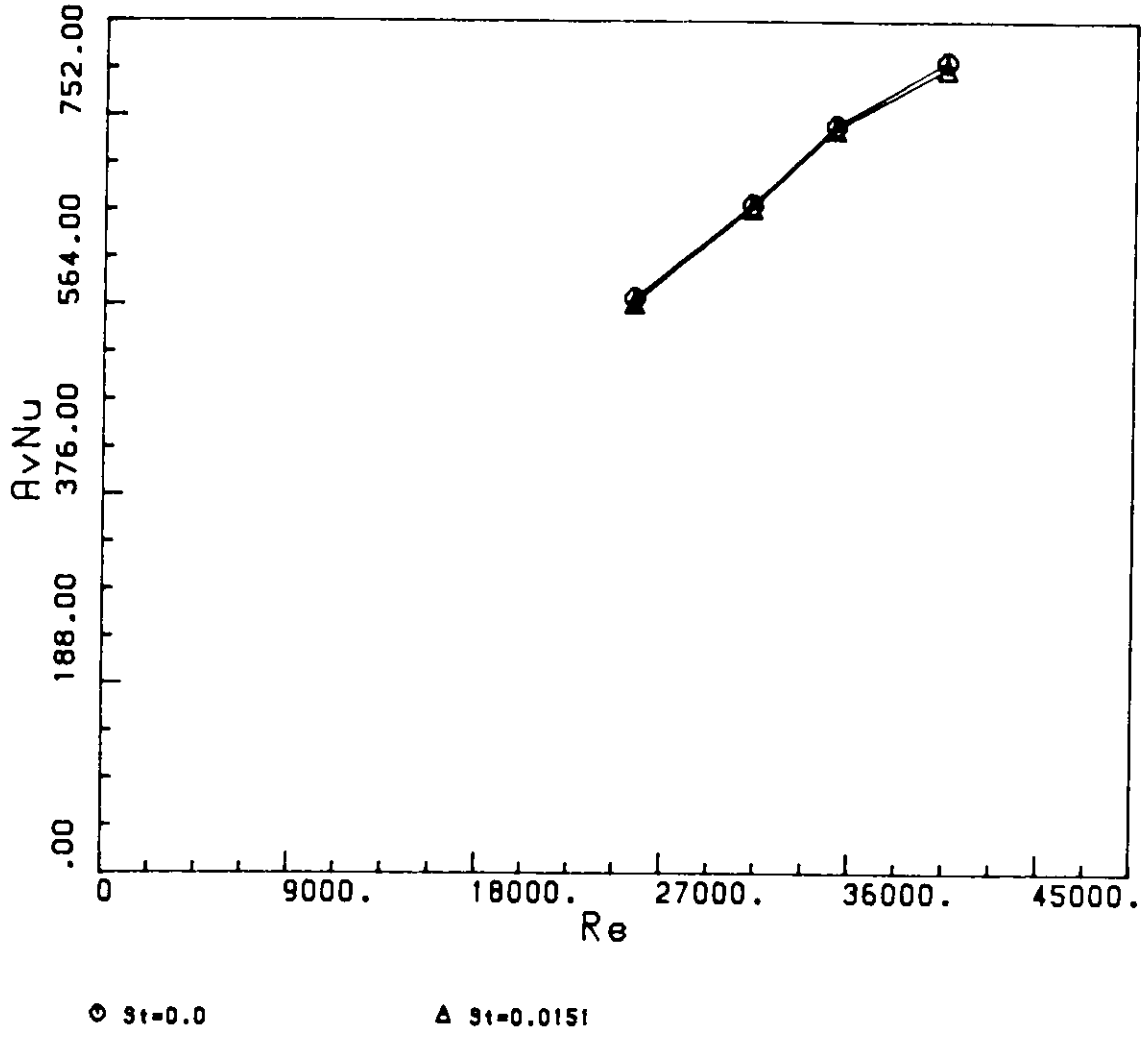

Figure 39. The effect of mechanical excitation on heat transfer rate.

Appendix A. Data Acqusition and Reduction Programs

A1. Data Acqusition and Reduction Program for IBM-PC

```
$NOFLOATCALLS
$STORAGE:2
$DEBUG
C THIS PROGRAM AND THE ASSOCIATED METACOMMANDS IS DESIGNED
C SPECIFICALLY FOR USE WITH THE 8087 MATH COPROCESSOR
    PROGRAM FUSION
    IMPLICIT DOUBLE PRECISION(A-H,O-Z)
    DIMENSION XAVG(4),YAVG(4)
    INTEGER*2 IVOLT(6000)
    INTEGER*4 ISUMSQ,CDIVD
C
C  PCLERRS.FOR – PCLAB FORTRAN error definition file
```

```
C provided by Data Translation Inc.
C
      PARAMETER ( EOUTTMO   = 7 )
C                   user timeout exceeded on output
      PARAMETER ( EINPTMO   = 6 )
C                   user timeout exceeded on input
      PARAMETER ( EDMABSY   = 5 )
C                   DMA channel currently busy
      PARAMETER ( E2FAST    = 4 )
C                   board clocked too fast
      PARAMETER ( ENORMAL   = 0 )
C                   normal completion, no error
      PARAMETER ( ENOPCL    = -1 )
C                   device driver PCL not found
      PARAMETER ( EMANYFIL  = -2 )
C                   too many files open
      PARAMETER ( EGATING   = -4 )
C                 ILLEGAL gating source for clock routines
      PARAMETER ( ENOTFUNC  = -5 )
C                   board not capable of requested function
      PARAMETER ( EDMAFREE  = -6 )
C                   DMA not currently in use
      PARAMETER ( EDMAASN   = -7 )
C                   DMA channel not assigned to unit
      PARAMETER ( EILLSBX   = -8 )
C               ILLEGAL iSBX SLOT, CHIP SELECT OR CHANNEL
      PARAMETER ( EGAIN     = -10 )
C                   illegal gain specification
```

```
      PARAMETER ( EDMABND   = -13 )
C                     DMA buffer crosses 64K boundary
      PARAMETER ( EILLFUN     = -15 )
C                     illegal function call
      PARAMETER ( ETIMING     = -19 )
C                     illegal timing source value
      PARAMETER ( EHIFREQ     = -22 )
C                     requested frequency too high
      PARAMETER ( ELOFREQ     = -23 )
C                     requested frequency too low
      PARAMETER ( ESMALLP     = -24 )
C                     requested period too small
      PARAMETER ( ELARGEP     = -25 )
C                     requested period too large
      PARAMETER ( ECLKDIV     = -26 )
C                     illegal clock divider
      PARAMETER ( EPORT       = -27 )
C                     illegal digital port
      PARAMETER ( ECLKTIM     = -28 )
C               ILlegal clock period or clock frequency
C                     period or freq. too small or too large
      PARAMETER ( ECHANNL     = -29 )
C                     illegal channel number
      PARAMETER ( EDACSEL     = -30 )
C                     illegal DAC select
      PARAMETER ( EBOARD      = -31 )
C                     illegal board number
      PARAMETER ( ESTARTC     = -32 )
```

```
C                   illegal start channel
      PARAMETER ( ENODIN      = -33 )
C                   DIO port enabled for output
      PARAMETER ( ENODOUT     = -34 )
C                   DIO port enabled for input
      PARAMETER ( ETYPE       = -35 )
C             ILlegal thermocouple type. Must be ASCII
C                   of (B, E, J, K, R, S, or T)
      PARAMETER ( EOVTAB      = -36 )
C             SPecified voltage in routines XDTV or XMT
C                   is not in thermocouple type range
      PARAMETER ( EOTTAB      = -37 )
C             TEMPerature specified is not in thermocouple
C                   type range.
      PARAMETER ( ECJC  = -38 )
C             COMPensated voltage (DT707-T channel zero)
C             IS OUT OF LINEAR RANGE (0 TO 40 DEGS. C)
      PARAMETER ( EINIDAC     = -42 )
C                   DAC not initialized
      PARAMETER ( EINIADC     = -43 )
C                   ADC not initialized
      PARAMETER ( EINPUT      = -44 )
C                   board timeout on input
      PARAMETER ( EOUTPUT     = -45 )
C                   board timeout on output
      PARAMETER ( EREADY      = -46 )
C                   board timeout on ready
      PARAMETER ( EILIV  = -49 )
```

```
C               VOLTage value in routine XATV is not between
C               CURrent board's negative full scale and
C                    positive full scale
      PARAMETER ( PCUNEXP    = -100 )
C                    unexpected error
C
C  end of PCLERRS.FOR
C
      CHARACTER*10  FILENAME
      REAL*4 NOC,LSB,PRMS(402),X(402)
      SUMSQT=0.0
      RMST=0.0
      M=0
      WRITE(*,*) 'NUMBER OF SAMPLE GROUPS?   (MAXIMUM IS 402) '
      READ(*,*) IMAX
      WRITE(*,*) 'JET TEMPERATURE ( SPHERE TEMPERATURE IS ASSUMED TO BE
     $60 C)'
      READ(*,*) TJ
      WRITE(2,*)
      WRITE(2,*) TJ
C     WRITE(*,*) 'REQUESTED FREQUENCY?'
C     READ(*,*) RFREQ
      SUMSQ=0
      TS=60.0
      RES=114.29
      INUM=IMAX*5+2
      AK=0.0273
      DIA=2.0*2.54/100.
```

```
PI = 3.14592654
NUMVAL = 6000
HIGHV = 10.0
VLOW = -10.0
RANGE = HIGHV-VLOW
NOC = 4096.
LSB = RANGE/NOC
ITIME = 0
ISTART = 0
IEND = 0
IGAIN = 1
ISCANL = (IEND + 1)-ISTART
NSCANS = (NUMVAL/ISCANL)-1
IGAIN = 1
SCALSB = LSB/IGAIN
SCALOW = VLOW/IGAIN
RFREQ = 6000.
CDIVD = (800000./RFREQ)
CALL XSCD(CDIVD)
CALL XSA(ITIME,ISTART,IEND,IGAIN)
DO 10 I = 1,IMAX
CALL XDSC
CALL XAS(6000,IVOLT(1))
CALL XESC
SUMSQ = 0.0
RMS = 0.0
ISUMSQ = 0
DO 40 JJ = 1,6000
```

```
      VOLT = IVOLT(JJ)*SCALSB + SCALOW
      SUMSQ = SUMSQ + VOLT*VOLT
   40 CONTINUE
      RMS = SQRT(SUMSQ/6000.)*230.913
      WRITE(*,5) I,RMS
      PRMS(I) = RMS
      RMST = RMST + RMS
   30 CONTINUE
   10 CONTINUE
      AVRMS = RMST/(IMAX)
      DO 11 I = 1,IMAX,2
   11 WRITE(2,9) PRMS(I),PRMS(I + 1)
      WRITE(*,6) AVRMS
      AVNU = (AVRMS**2)/(RES*(TS-TJ)*AK*PI*DIA)
      WRITE(*,7) AVNU
      WRITE(2,8) AVRMS,AVNU
      WRITE(*,*) ' DO YOU WANT TO SEE THE RMS VALUES PLOTTED?'
      READ(*,*) ANS
      IF(ANS.NE.1) GO TO 999
      DO 50 I = 1,IMAX
   50 X(I) = REAL(I)
      CALL PLOTS(0,0,0)
      CALL PLOT(.5,.5,-3)
      CALL SCALE(X,6.0,IMAX,1)
      CALL SCALE(PRMS,3.0,IMAX,1)
      CALL AXIS(0.,0.,'NUMBER',-6,6.0,0.,X(IMAX + 1),X(IMAX + 2))
      CALL AXIS(0.,0.,'RMS',3,3.0,90.,PRMS(IMAX + 1),PRMS(IMAX + 2))
      CALL LINE(X,PRMS,IMAX,1,0,0)
```

```
      YAVG(1) = AVRMS
      YAVG(2) = YAVG(1)
      XAVG(1) = 1.0
      XAVG(2) = FLOAT(IMAX)
      XAVG(3) = X(IMAX + 1)
      XAVG(4) = X(IMAX + 2)
      YAVG(3) = PRMS(IMAX + 1)
      YAVG(4) = PRMS(IMAX + 2)
      CALL LINE(XAVG,YAVG,2,1,0,0)
      WRITE(*,*) 'AVNU = = ',AVNU
      WRITE(*,*) 'TO CLEAR SCREEN TYPE 1'
      READ(*,*) ANS
      CALL SETIBM(2)
    5 FORMAT(5X,I3,3X,F8.4)
    6 FORMAT(5X,'AVRMS = = ',F8.4)
    7 FORMAT(5X,'AVNU  = = ',F8.4)
    8 FORMAT(5X,F10.6,3X,F10.6)
    9 FORMAT(5X,F10.6,5X,F10.6)
  999 STOP
      END
```

A2. Data Acquision and Reduction Program for the Digital Minc-11

```
      PROGRAM DATA
      INTEGER*2 INFO(40),IBUF(1924,1),IGINFO(30),FNAME(15)
      REAL*4 V(812,3),X11(812)
      TYPE 100 100    FORMAT('$INPUT H OVER D = = > ')
      ACCEPT *,HD
      TYPE 101
101   FORMAT('$INPUT REYNOLDS NUMBER = = > ')
      ACCEPT *,RE
      TYPE 102
102   FORMAT('$INPUT SURFACE TEMPERATURE = = > ')
      ACCEPT *,TS
      TYPE 103
103   FORMAT('$INPUT JET TEMPERATURE = = > ')
      ACCEPT *,TJ
      TYPE 107
107   FORMAT('$ENTER BEGINING CHANNEL NUMBER = = > ')
      ACCEPT *,IFIRST
      TYPE 108
108   FORMAT('$ENTER TIME BETWEEN DATA POINTS IN SEC = = > ')
      ACCEPT *,TBD
      TYPE 109
109   FORMAT('$ENTER NUMBER OF DATA POINTS = = > ')
      ACCEPT *,NP
```

```
      TBD = 1.75
      NP = 400
      TS = 60.0
      DO 122 I = 1,NP
      X11(I) = I*TBD
      DO 122 J = 1,3
122   V(I,J) = 0.
      TYPE 111
111   FORMAT('$ENTER FILESPEC OF DATA FILE = = > ')
      CALL GETSTR(5,FNAME,14,EFLG)
      OPEN (NAME = FNAME,TYPE = 'NEW',UNIT = 10)
      CALL XRATE(TBD,IRATE,IPRE)
      CALL CLOCKA(IRATE,IPRE,IND)
      IF(IND.EQ.0) STOP 'CLOCKA ERROR'
        TYPE 36
36      FORMAT('$START OF DATA ACQUISITION')
        MP = 3*NP
C     START A/D CONVERSION WITH EXTERNAL TRIGGER
40      FORMAT(I5)
        SUM1 = 0.
        SUM2 = 0.
        SUM3 = 0.
        SUMSQ1 = 0.
        SUMSQ2 = 0.
        SUMSQ3 = 0.
        CALL SETIBF(INFO,IND,,IBUF(1,1))
        CALL RLSBUF(INFO,IND,0)
        CALL ADSWP(INFO,MP,1,0,,,,IFIRST,3)
```

```
C     WAIT FOR BUFFER OR CARRIAGE RETURN. IF BUFFER BECOMES
C     AVAILABLE, SAVE THE DATA.
      WRITE(7,40) K
      CALL IWTBUF(INFO,,IBUFN,IND)
      IF(ITTINR().GE.0) GO TO 510
      DO 16 I = 1,NP
      V1 = ((IBUF(I*3-2,IBUFN + 1).AND.'7777)-2048)*.0025
      V(I,1) = V1
      V2 = ((IBUF(I*3-1,IBUFN + 1).AND.'7777)-2048)*.0025
      V(I,2) = V2
      V3 = ((IBUF(I*3,IBUFN + 1).AND.'7777)-2048)*.0025
      V(I,3) = V3
      SUM1 = SUM1 + V1
      SUM2 = SUM2 + V2
      SUM3 = SUM3 + V3
      SUMSQ1 = SUMSQ1 + V1*V1
      SUMSQ2 = SUMSQ2 + V2*V2
      SUMSQ3 = SUMSQ3 + V3*V3 16        CONTINUE
      V1MEAN = SUM1/FLOAT(NP)
      V2MEAN = SUM2/FLOAT(NP)
      V3MEAN = SUM3/FLOAT(NP)
      WRITE(10,702) V1MEAN,V2MEAN,V3MEAN
702    FORMAT(3F10.5)
      DSUM1 = 0.
      DSUM2 = 0.
      DSUM3 = 0.
      DO 801 I = 1,NP
      DSUM1 = DSUM1 + (V1MEAN-V(I,1))**2
```

```
        DSUM2 = DSUM2 + (V2MEAN-V(I,2))**2
801       DSUM3 = DSUM3 + (V3MEAN-V(I,3))**2
        WRITE(10,701) (V(I,1),I = 10,NP,10)
        WRITE(10,701) (V(I,2),I = 10,NP,10)
        WRITE(10,701) (V(I,3),I = 10,NP,10)
701       FORMAT(8F8.4)
        DRMS1 = DSUM1/FLOAT(NP)
        DRMS2 = DSUM2/FLOAT(NP)
        DRMS3 = DSUM3/FLOAT(NP)
        WRITE(10,702) DRMS1,DRMS2,DRMS3
         TYPE 601
601     FORMAT('$PLOT PROFILES? 1 FOR YES, 0 FOR NO = = > ')
       ACCEPT *,NPLOT
       IF(NPLOT.NE.1) GO TO 226
C    PLOT PROFILES ON SCREEN (CHANNELS 0 AND 1)
       CALL GRINIT(IGINFO)
       CALL GRREGN(IGINFO,0,1)
       CALL GRAPHS(IGINFO,,X11,V(1,1),NP,,0)
       CALL GRREGN(IGINFO,1,2)
       CALL GRAPHS(IGINFO,,X11,V(1,2),NP,,1)
C DELAY FOR ABOUT 5 SEC
       DO 225 I1 = 1,60
       DO 225 I2 = 1,60
       DO 225 I3 = 1,60
  225  CONTINUE
C ERASE THE SCREEN
       CALL VTCLR
226     RS1 = SQRT(SUMSQ1/FLOAT(NP))
```

```
      RS2 = SQRT(SUMSQ2/FLOAT(NP))
      RS3 = SQRT(SUMSQ3/FLOAT(NP))
200    CONTINUE
      WRITE(10,702) RS1,RS2,RS3
      RES = 4.95
      AK = 0.0273
      DIA = 0.1
      PI = 3.141592654
      AVNU = 400.*V1MEAN**2/(RES*(TS-TJ)*AK*PI*DIA)
      WRITE(10,511) HD,RE,V1MEAN,TS,TJ,RES,AK,AVNU
      WRITE(7,511) HD,RE,V1MEAN,TS,TJ,RES,AK,AVNU
511    FORMAT(7F8.4,F10.4)
510    CALL STPSWP(INFO,,IND)
      CLOSE(UNIT = 10)
      STOP
      END
```

Appendix B. The Fluctuation of the Energy Loss under Different Conditions

In order to give the reader a taste of the dimensional flavor of this study, the following data is presented. Each graph represents the time record of the energy loss, in Watts, during a particular thermal load. Figures 40-51 show how the controller reacts to not being setup in the most optimum fashion. Figures 52-66 show somewhat better behavior.

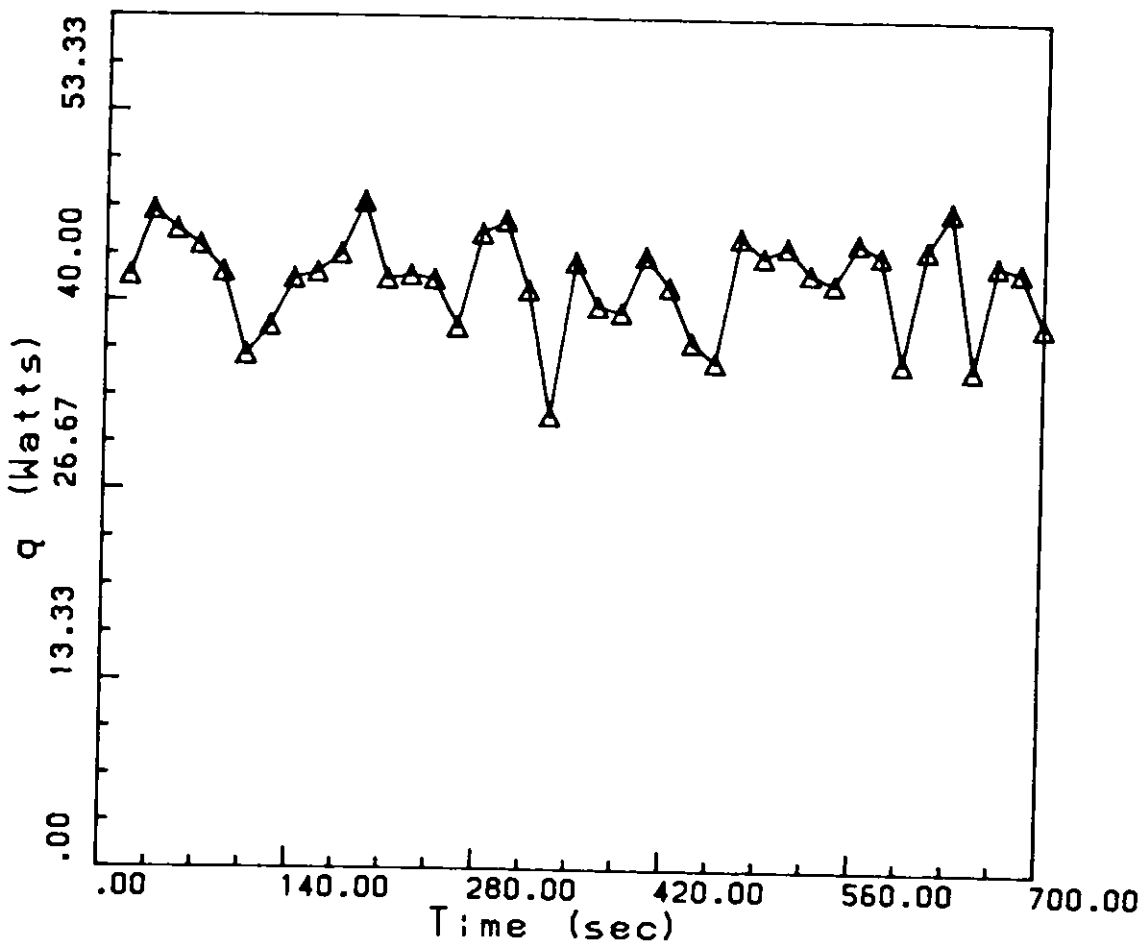

Figure 40. Time record of energy loss. Single jet impingement $\frac{D}{d}=24$ Re = 43,900

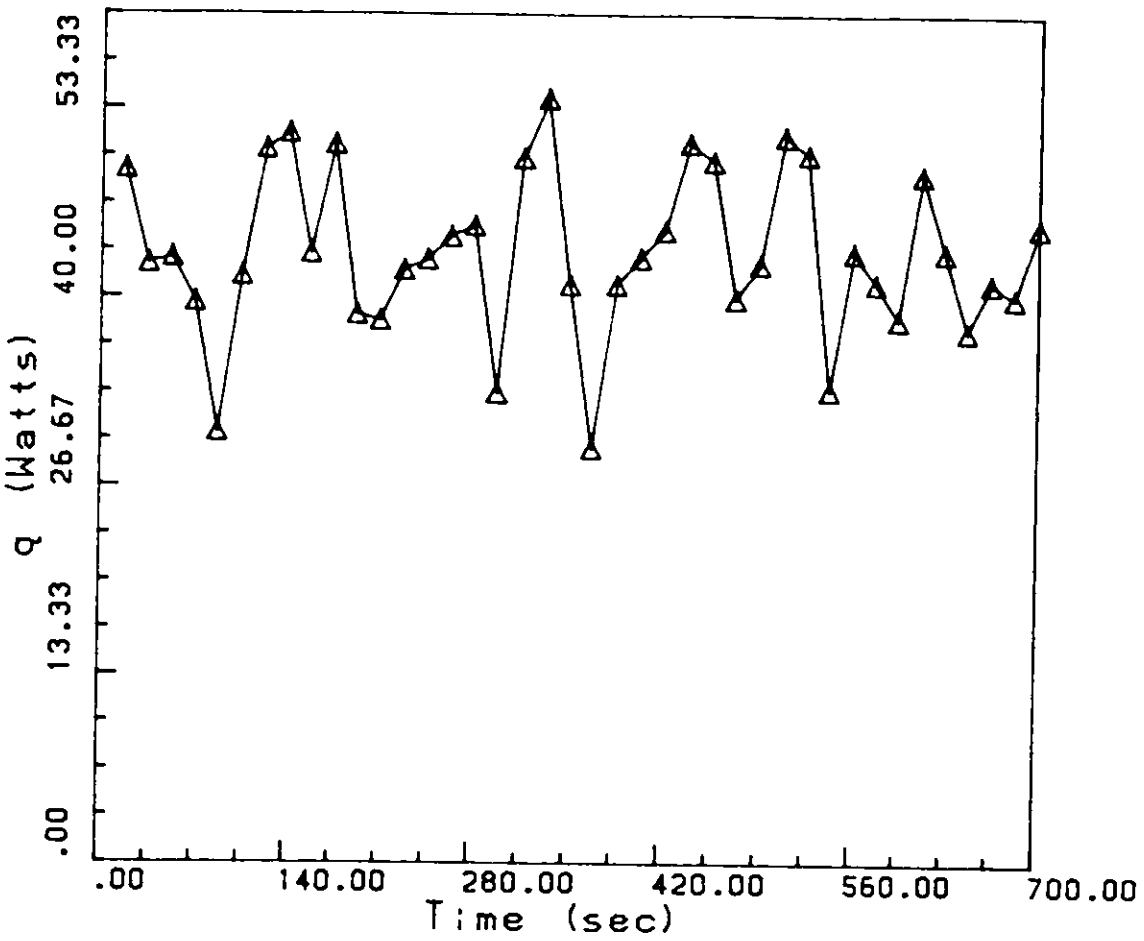

Figure 41. Time record of energy loss. Single jet impingement $\frac{D}{d} = 24$ Re = 42,400

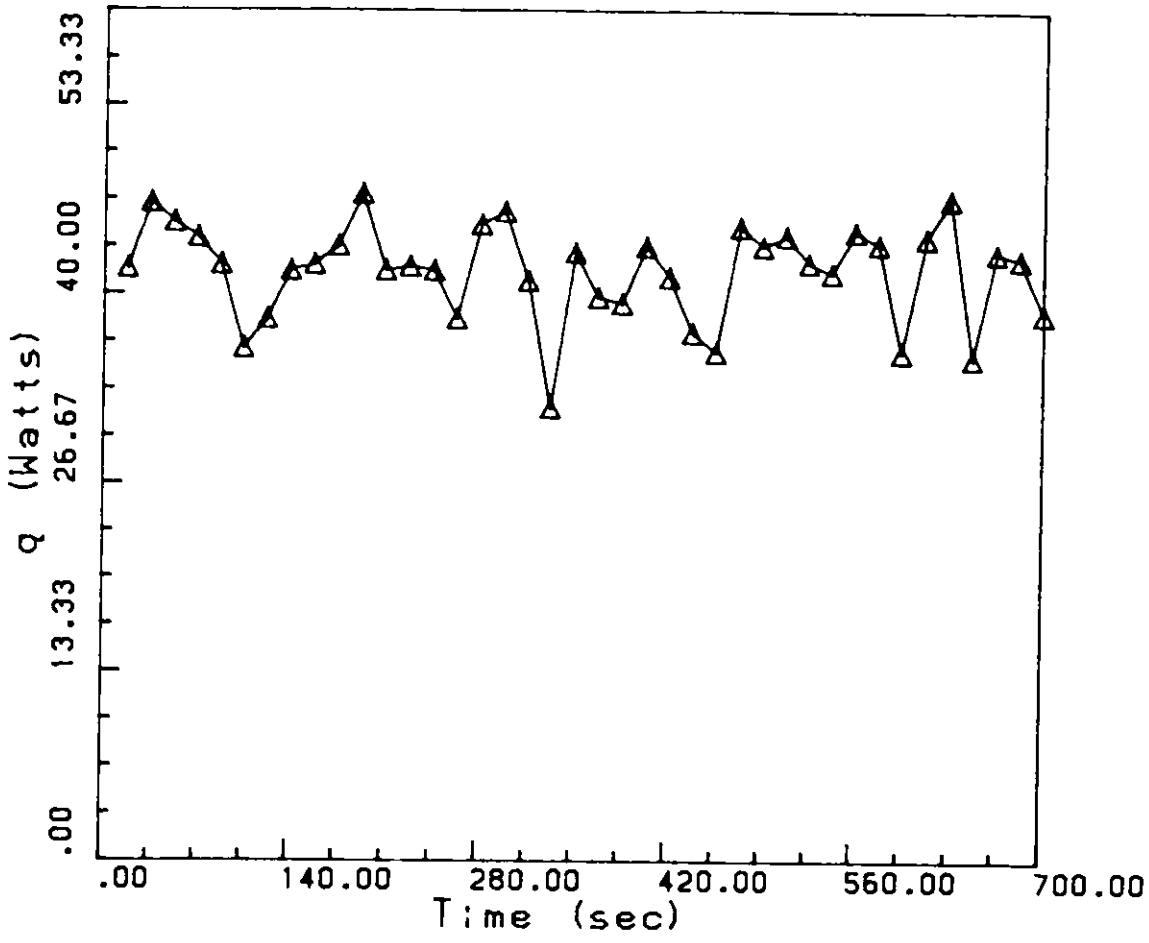

Figure 42. Time record of energy loss. Single jet impingement $\frac{D}{d}=24$ Re = 40,900.

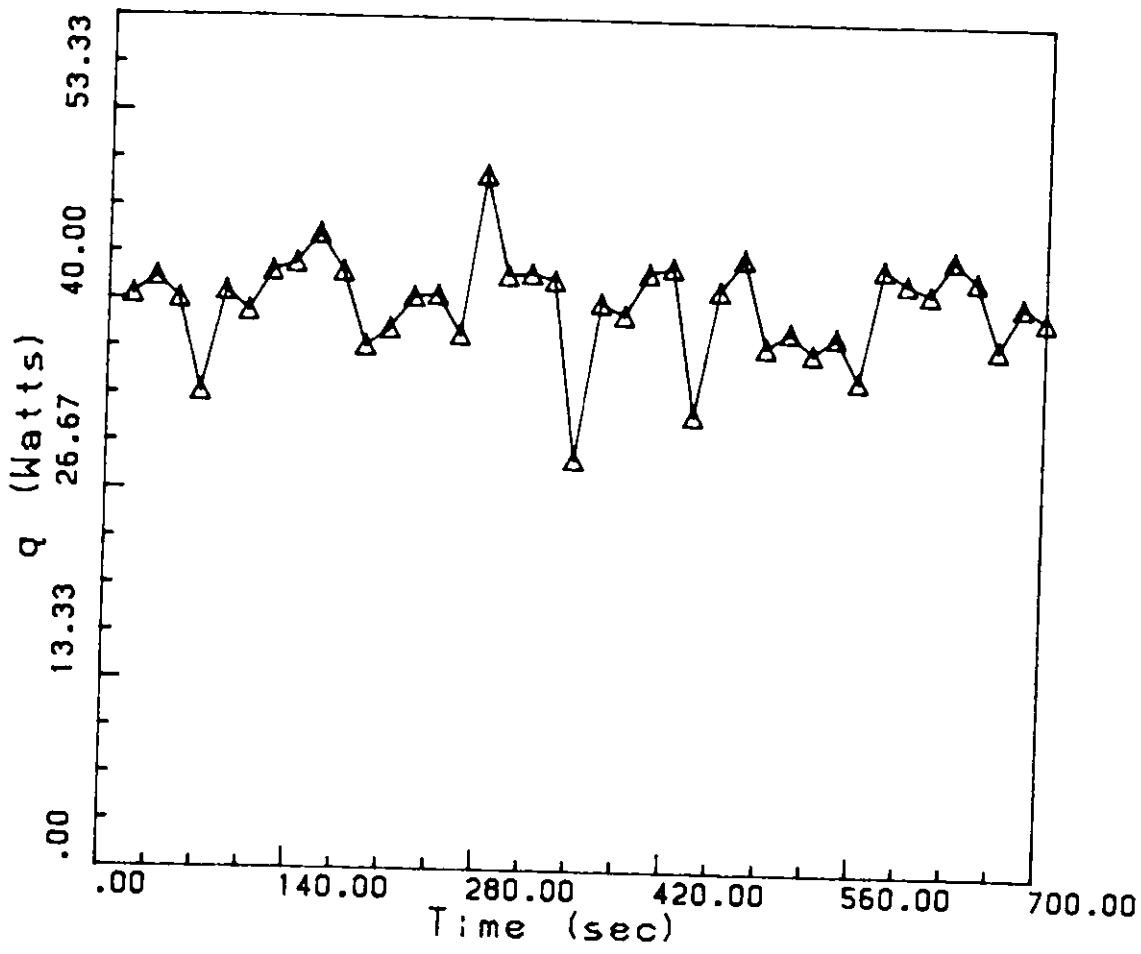

Figure 43. Time record of energy loss. Single jet impingement $\frac{D}{d}=24$ Re = 39,300.

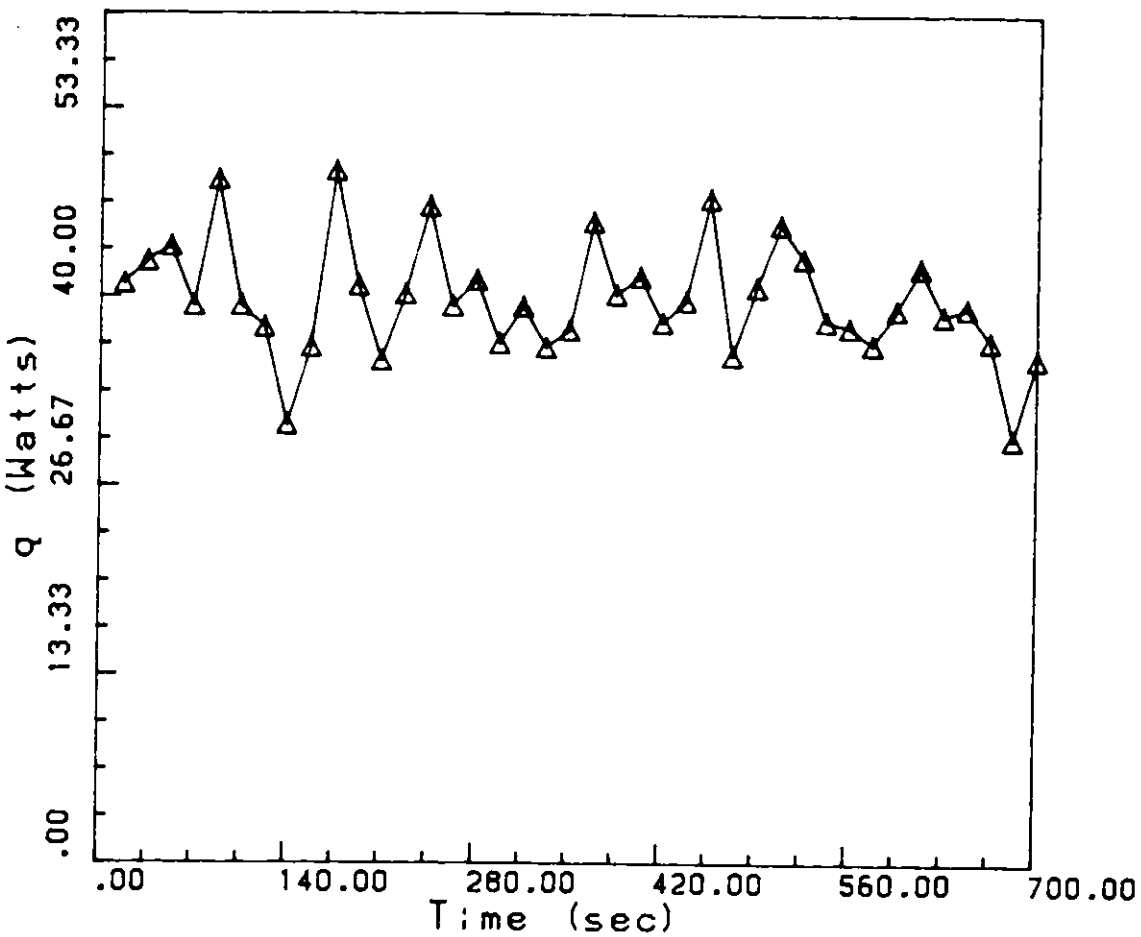

Figure 44. Time record of energy loss. Single jet impingement $\frac{D}{d} = 24$ Re = 37,600.

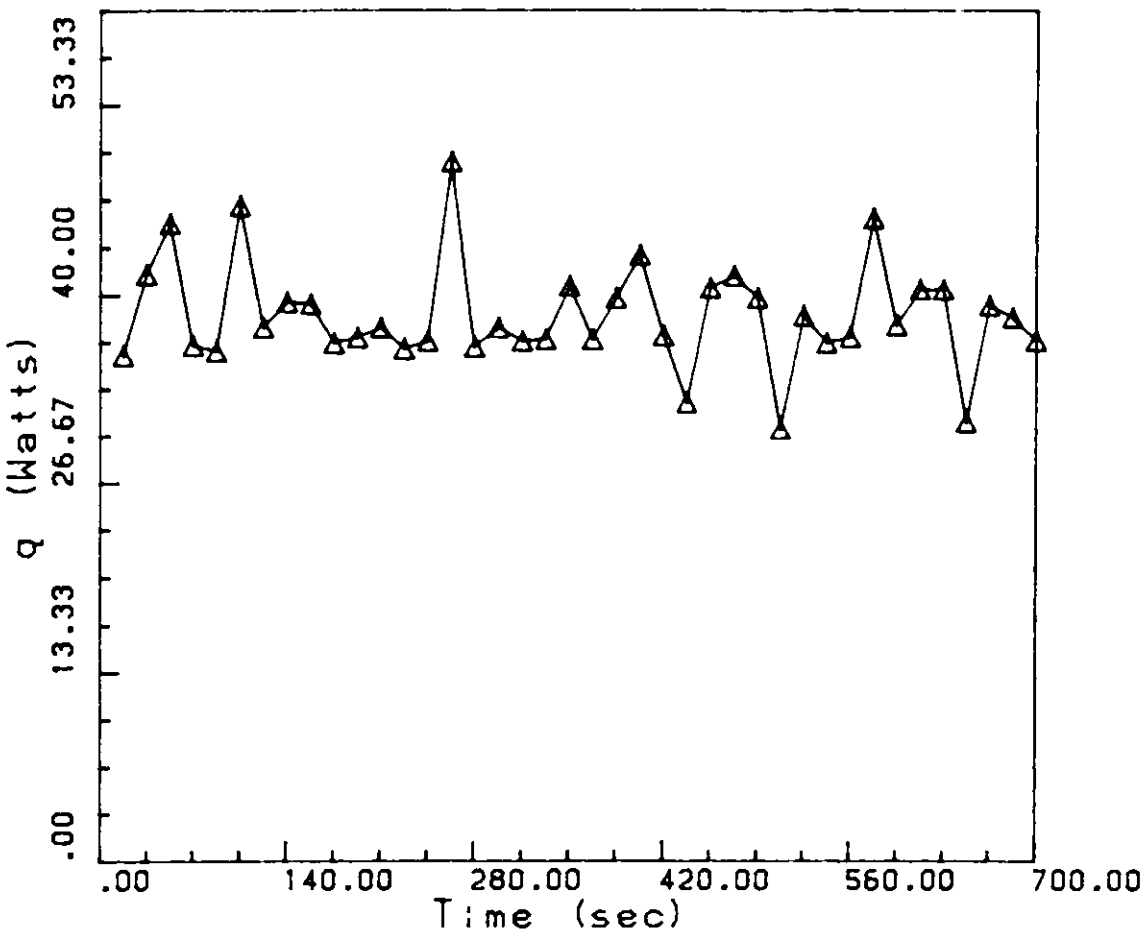

Figure 45. Time record of energy loss. Single jet impingement $\frac{D}{d} = 24$ Re = 35,800.

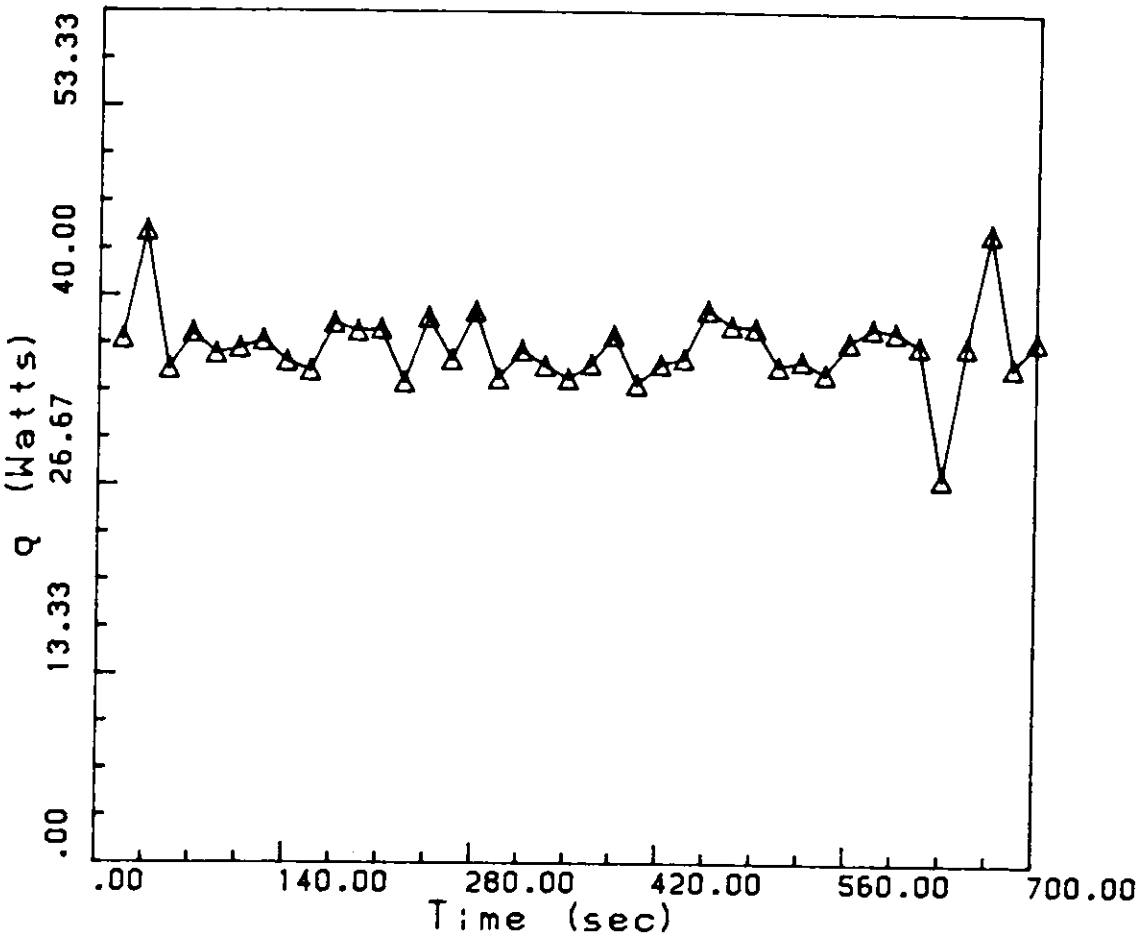

Figure 46. Time record of energy loss. Single jet impingement $\frac{D}{d}=24$ Re = 34,000.

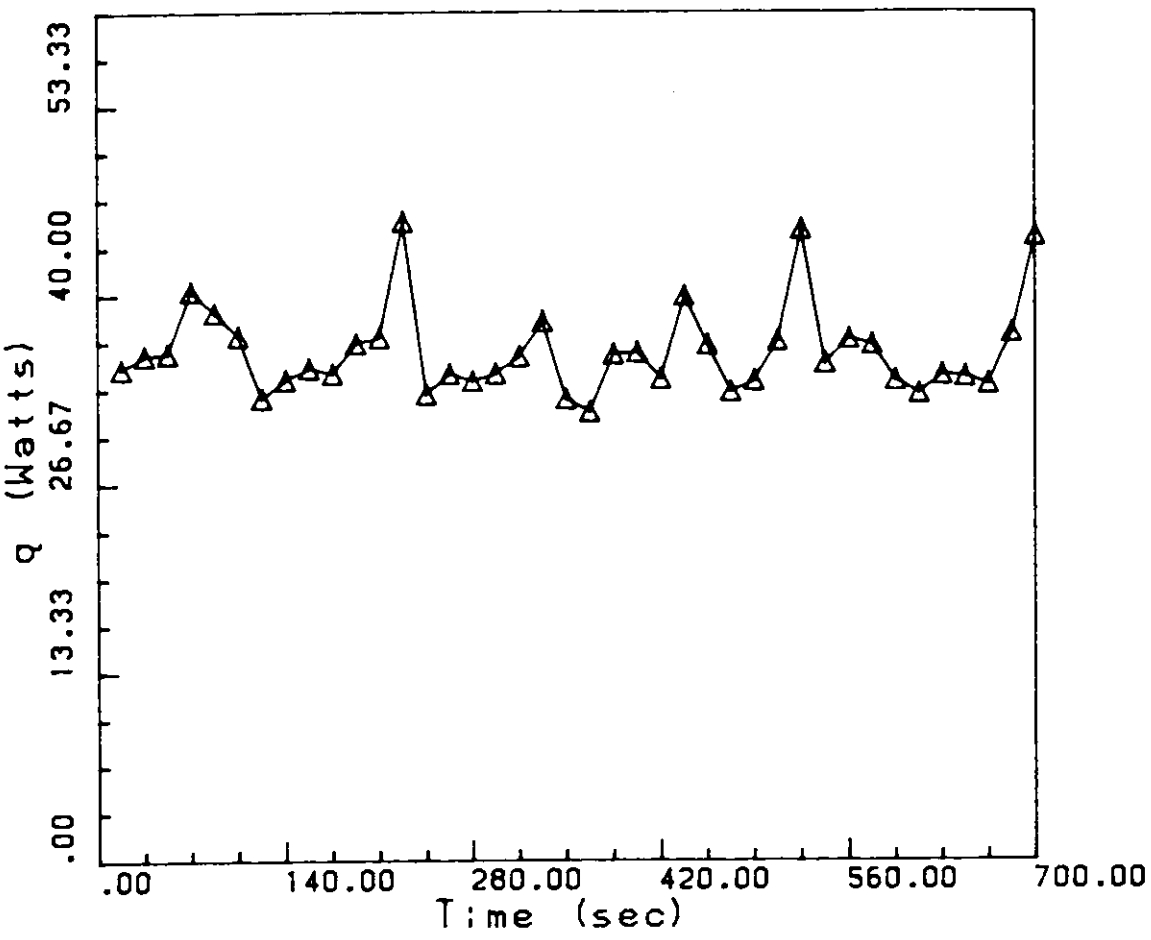

Figure 47. Time record of energy loss. Single jet impingement $\frac{D}{d}=24$ Re = 32,000.

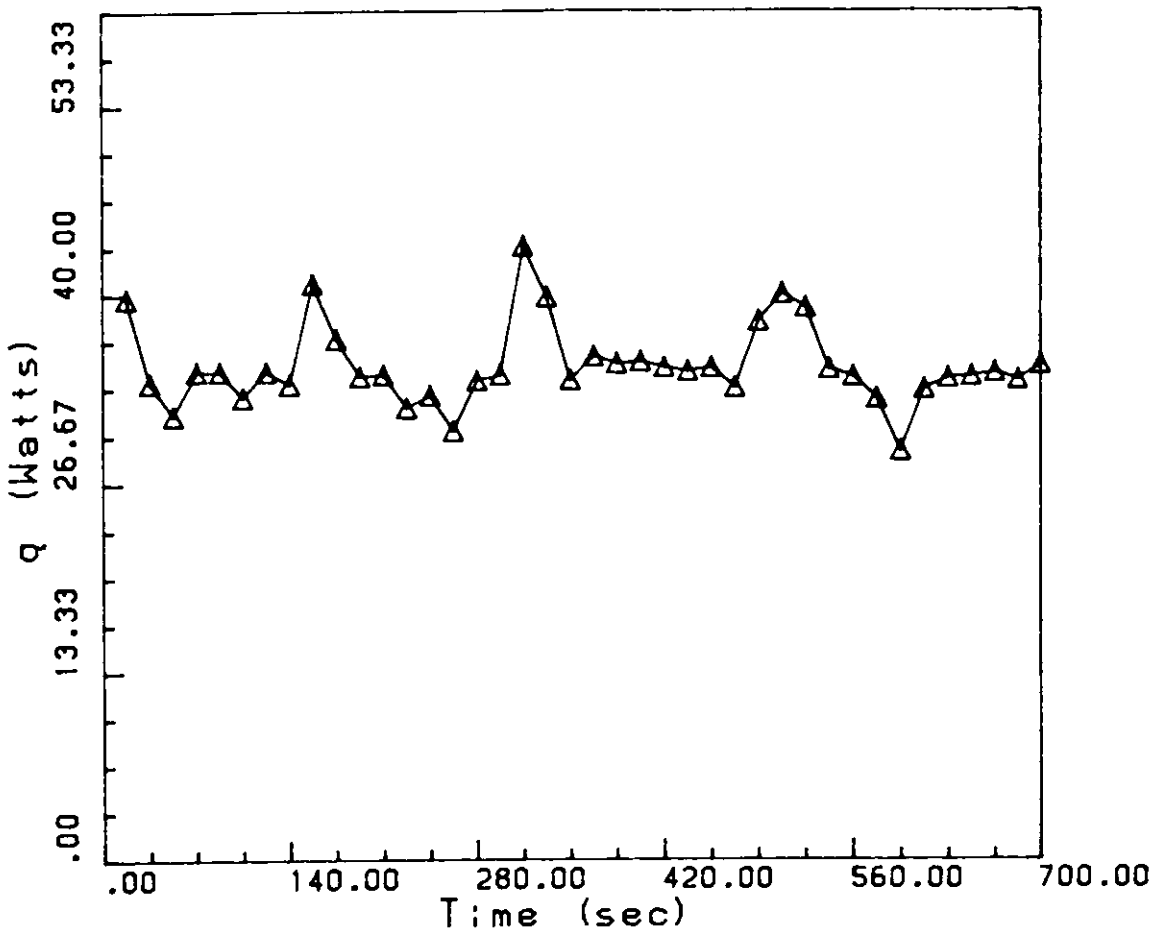

Figure 48. Time record of energy loss. Single jet impingement $\frac{D}{d} = 24$ Re = 30,000.

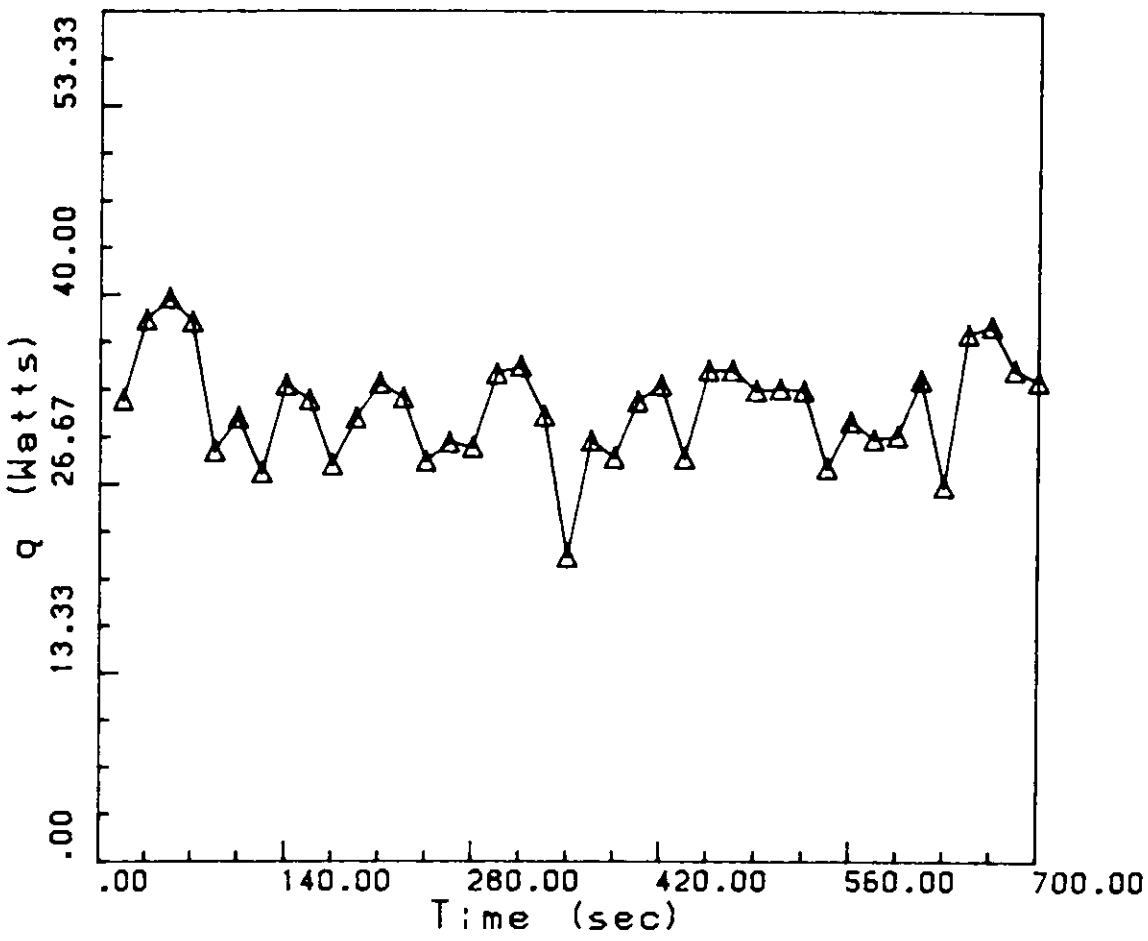

Figure 49. Time record of energy loss. Single jet impingement $\frac{D}{d}=24$ Re = 27,800.

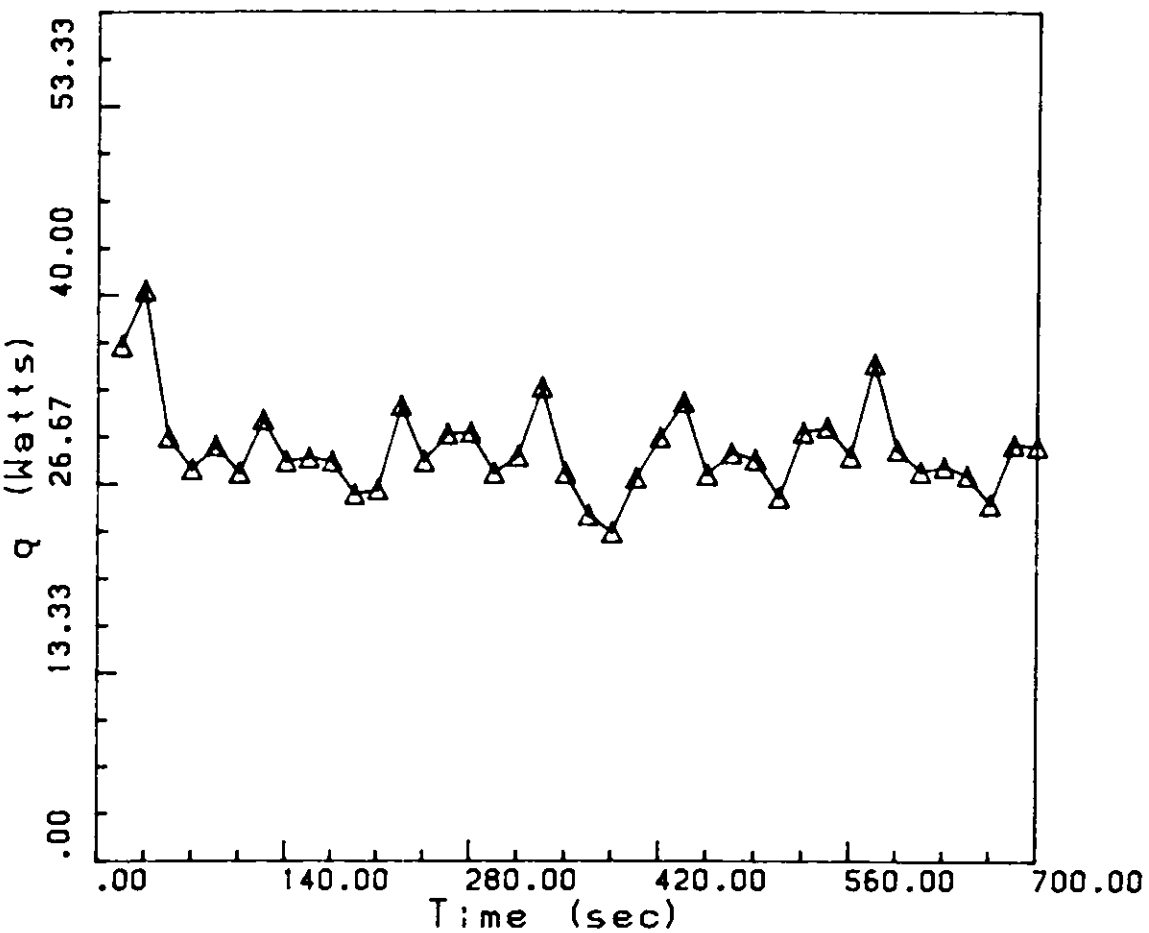

Figure 50. Time record of energy loss. Single jet impingement $\frac{D}{d} = 24$ Re = 24,000.

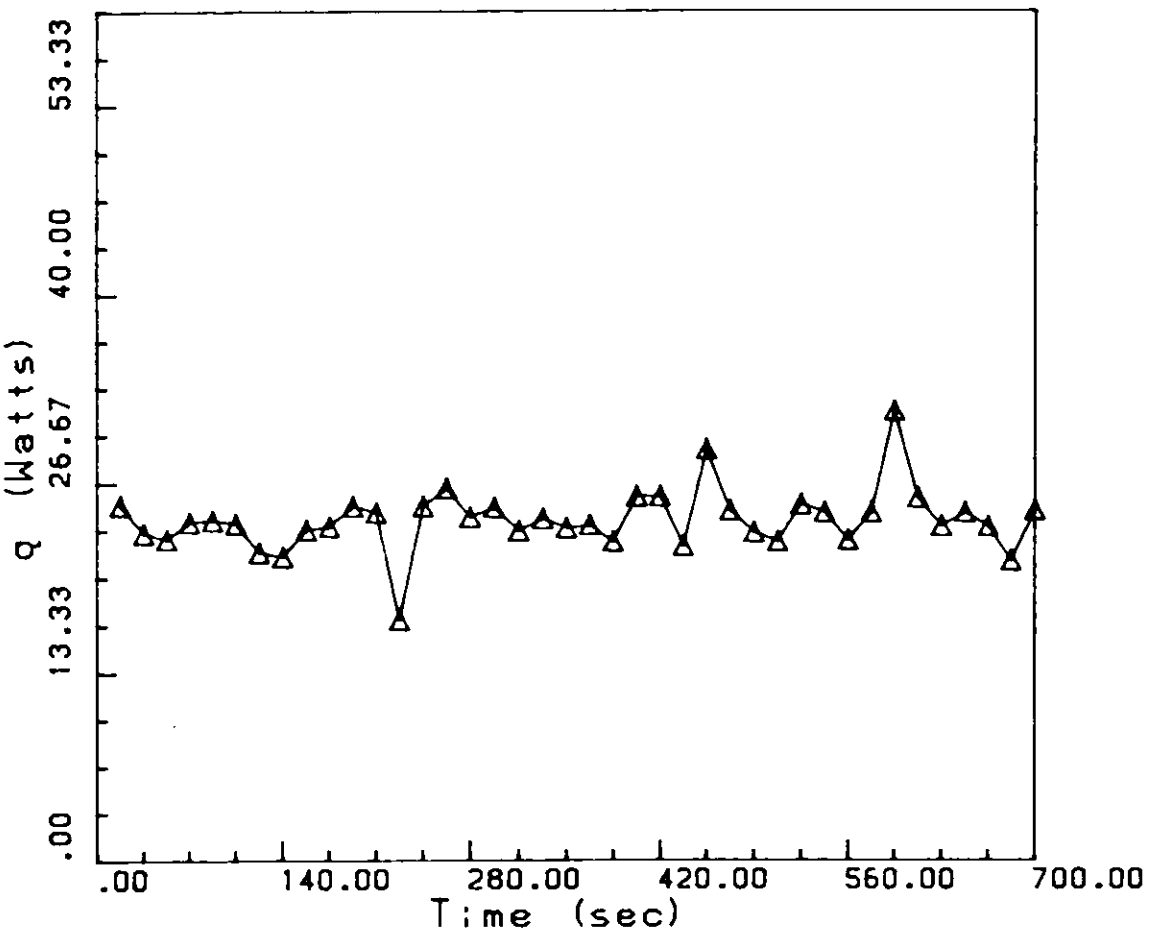

Figure 51. Time record of energy loss. Single jet impingement $\frac{D}{d}=24$ Re=19,600.

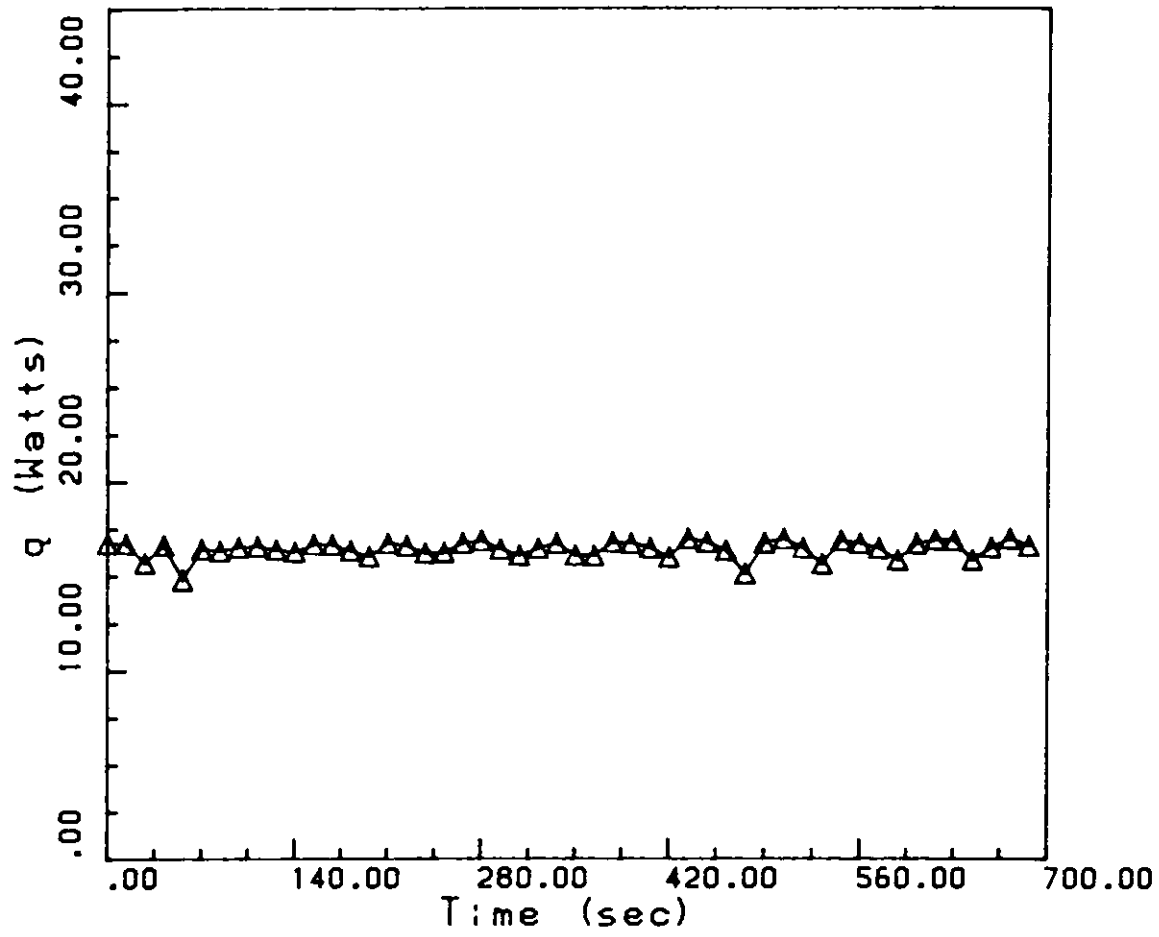

Figure 52. Time record of energy loss. Single jet impingement $\frac{D}{d} = 32$ Re = 4,900.

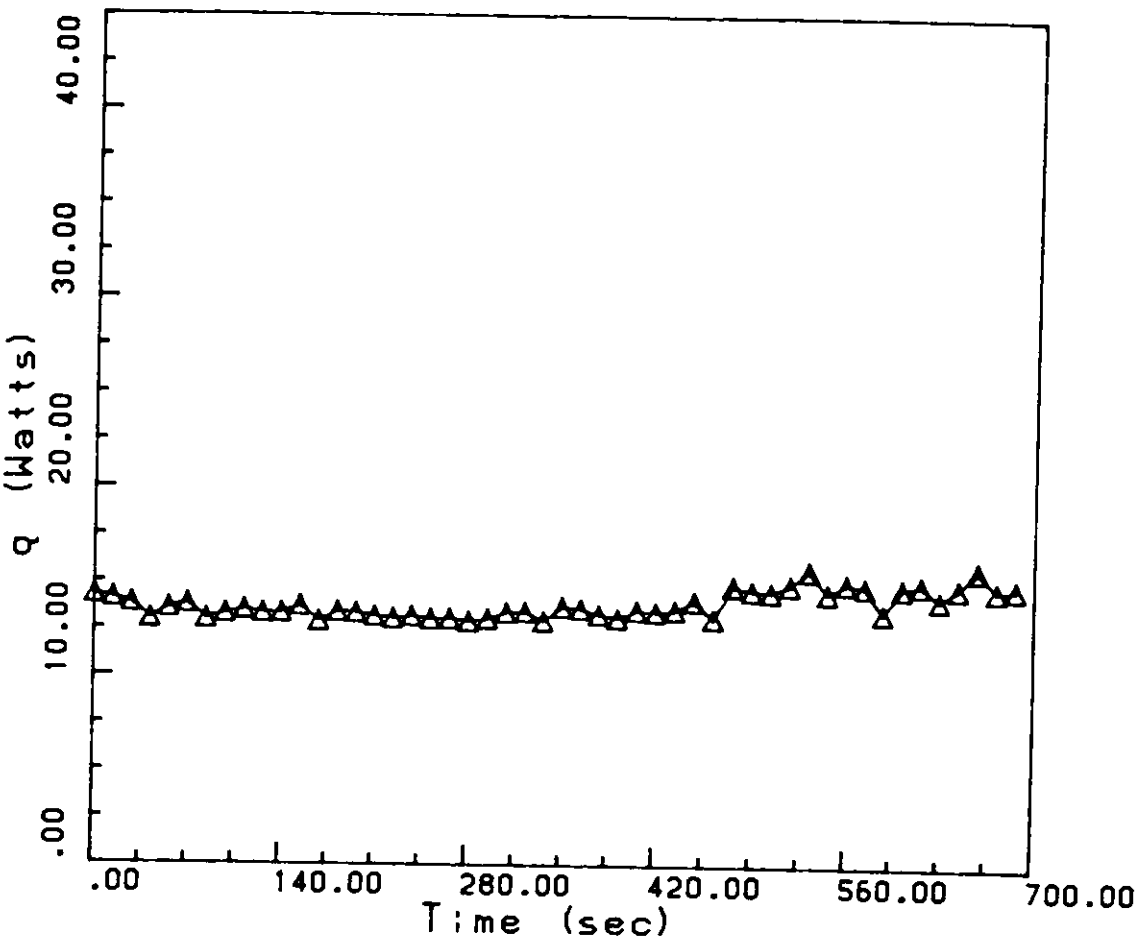

Figure 53. Time record of energy loss. Single jet impingement $\frac{D}{d}=32$ Re = 6,000.

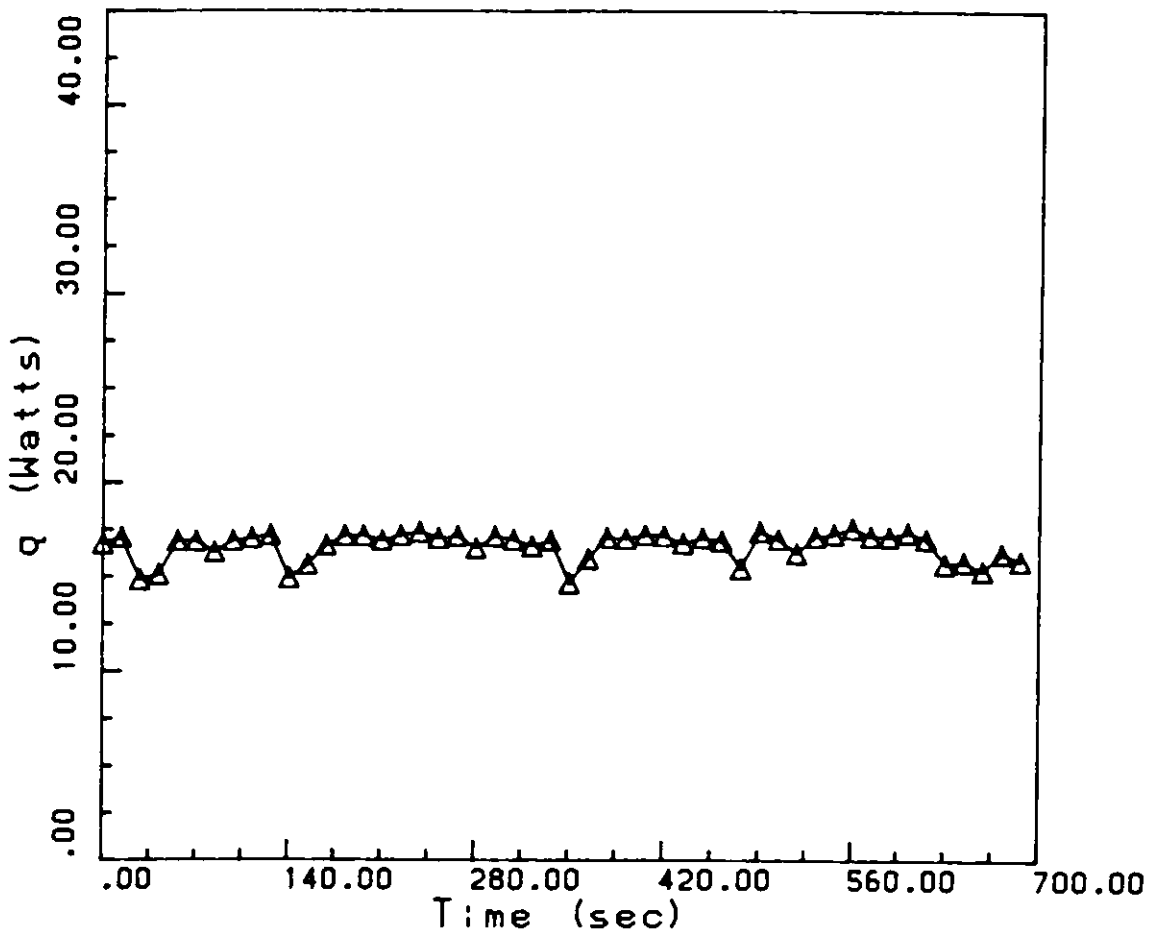

Figure 54. Time record of energy loss. Single jet impingement $\frac{D}{d}=32$ Re = 6,700.

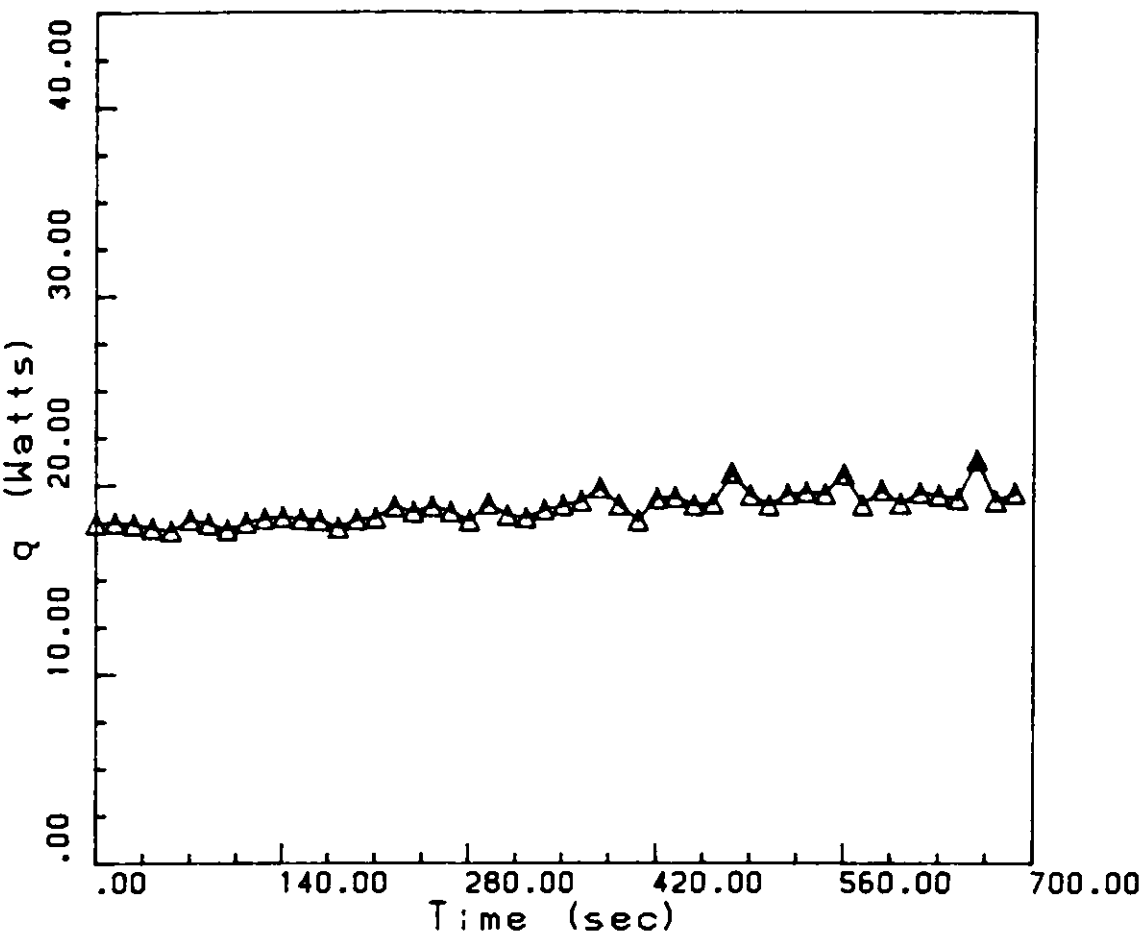

Figure 55. Time record of energy loss. Single jet impingement $\frac{D}{d}=32$ Re=10,000.

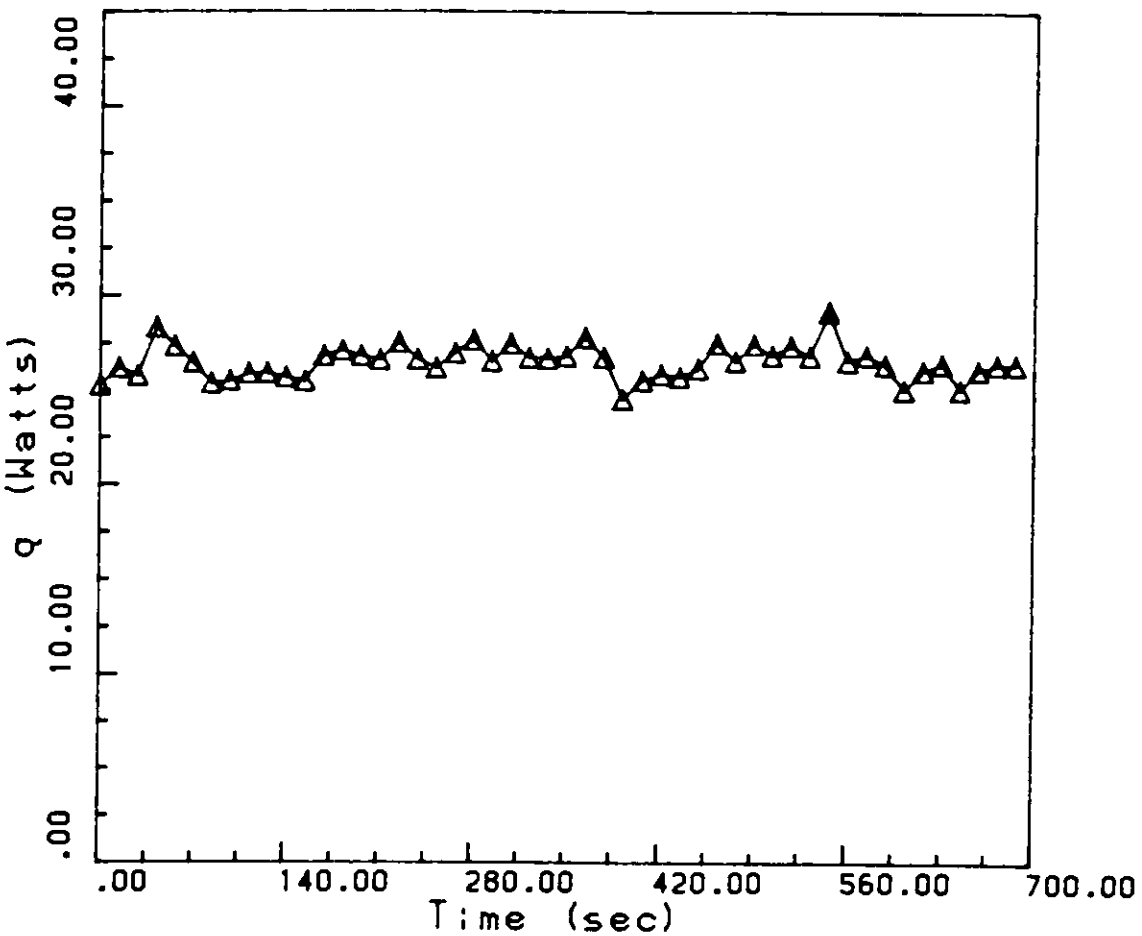

Figure 56. Time record of energy loss. Single jet impingement $\frac{D}{d}=32$ Re = 14,000.

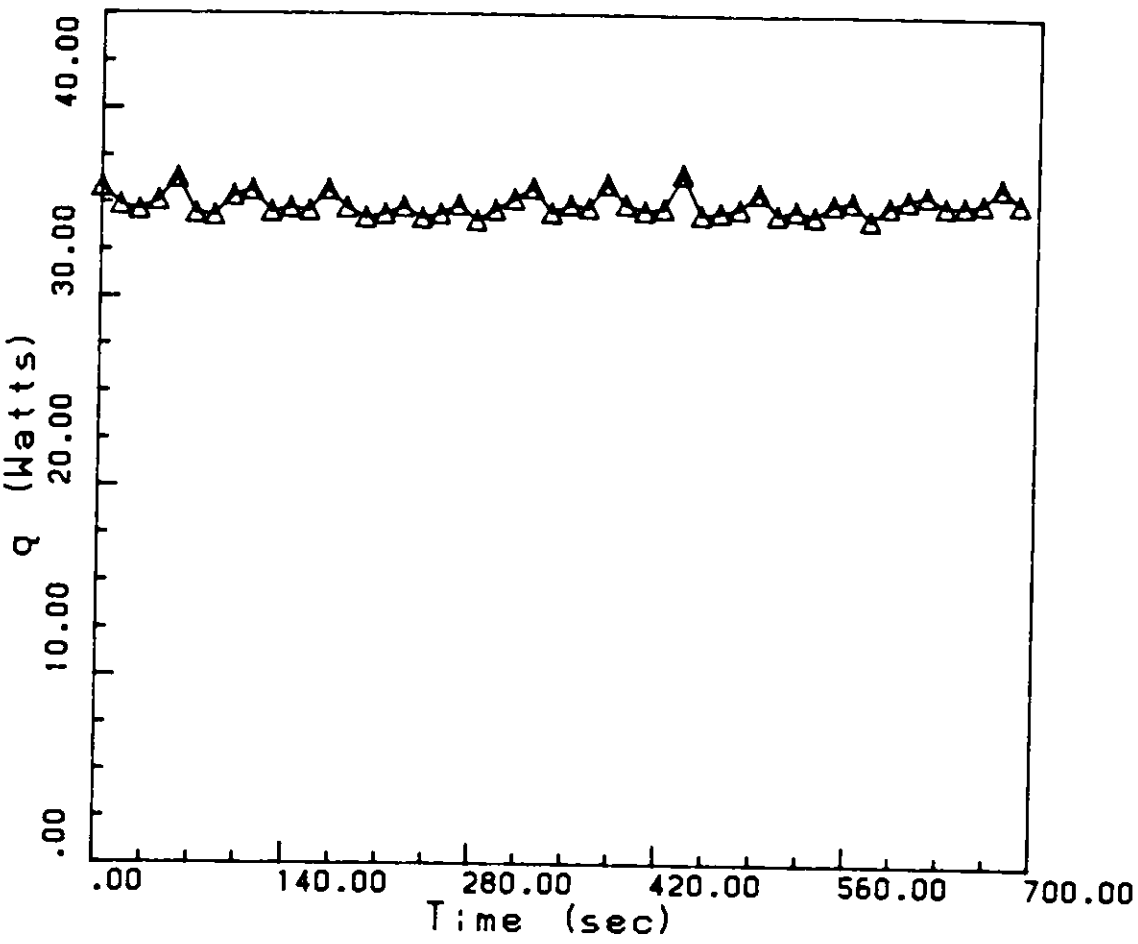

Figure 57. Time record of energy loss. Single jet impingement $\frac{D}{d} = 32$ Re = 16,200.

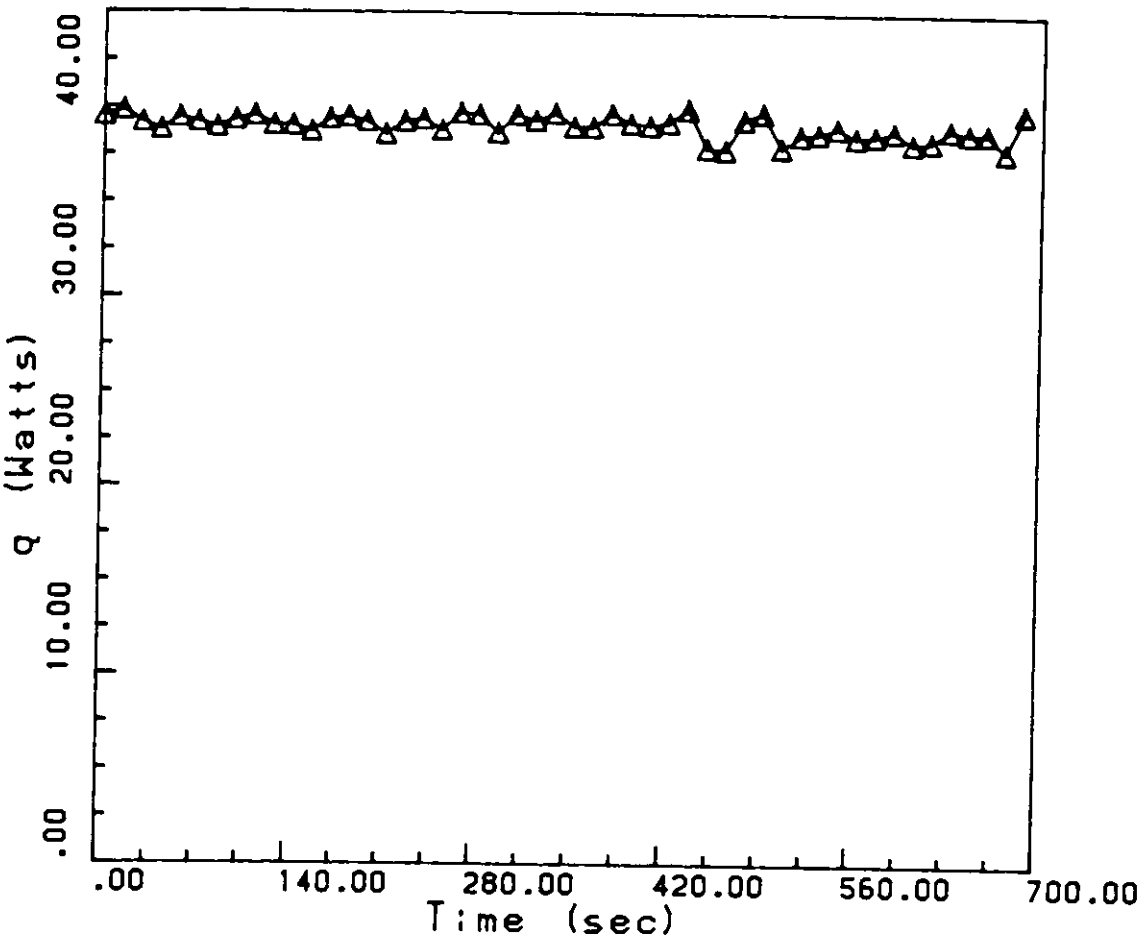

Figure 58. Time record of energy loss. Single jet impingement $\frac{D}{d}=32$ Re = 18,000.

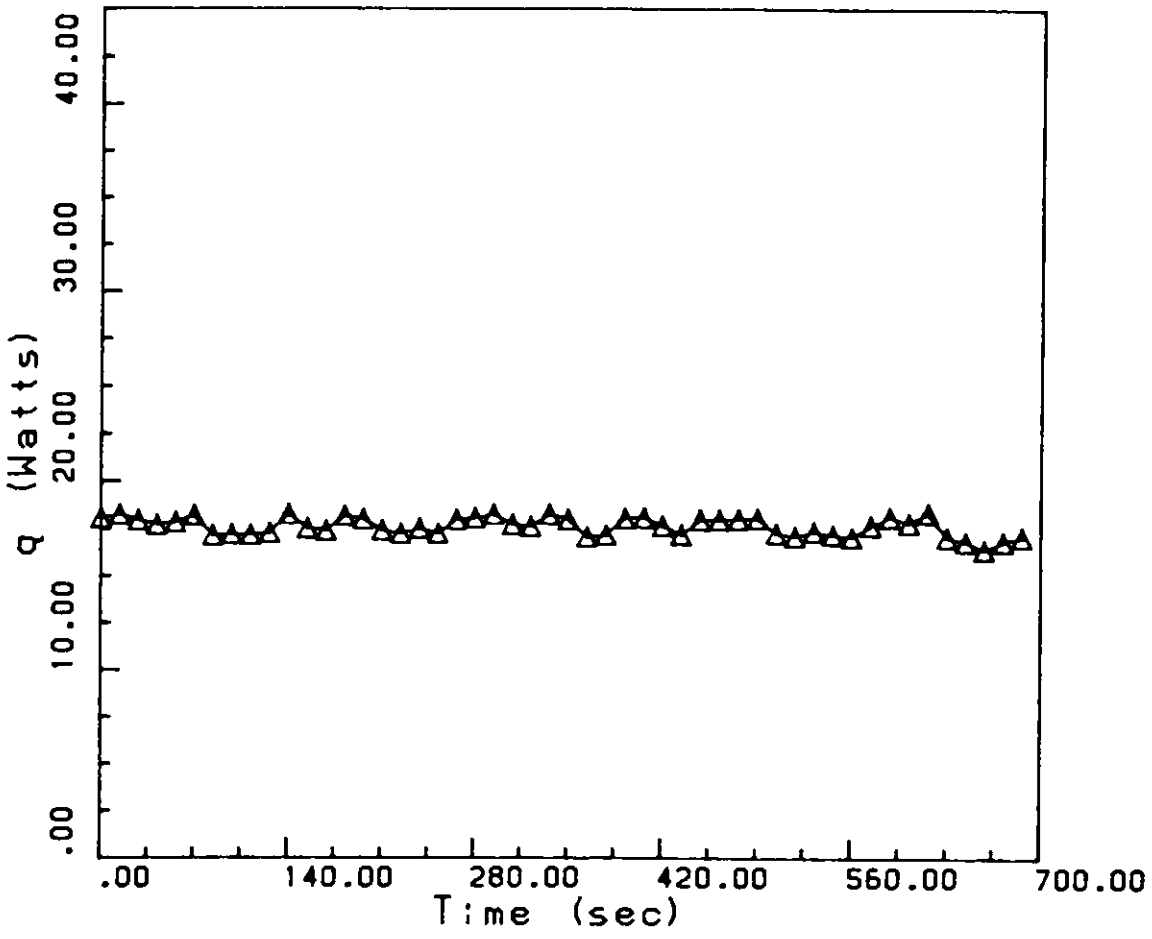

Figure 59. Time record of energy loss. Wind Tunnel Test Re = 19,800.

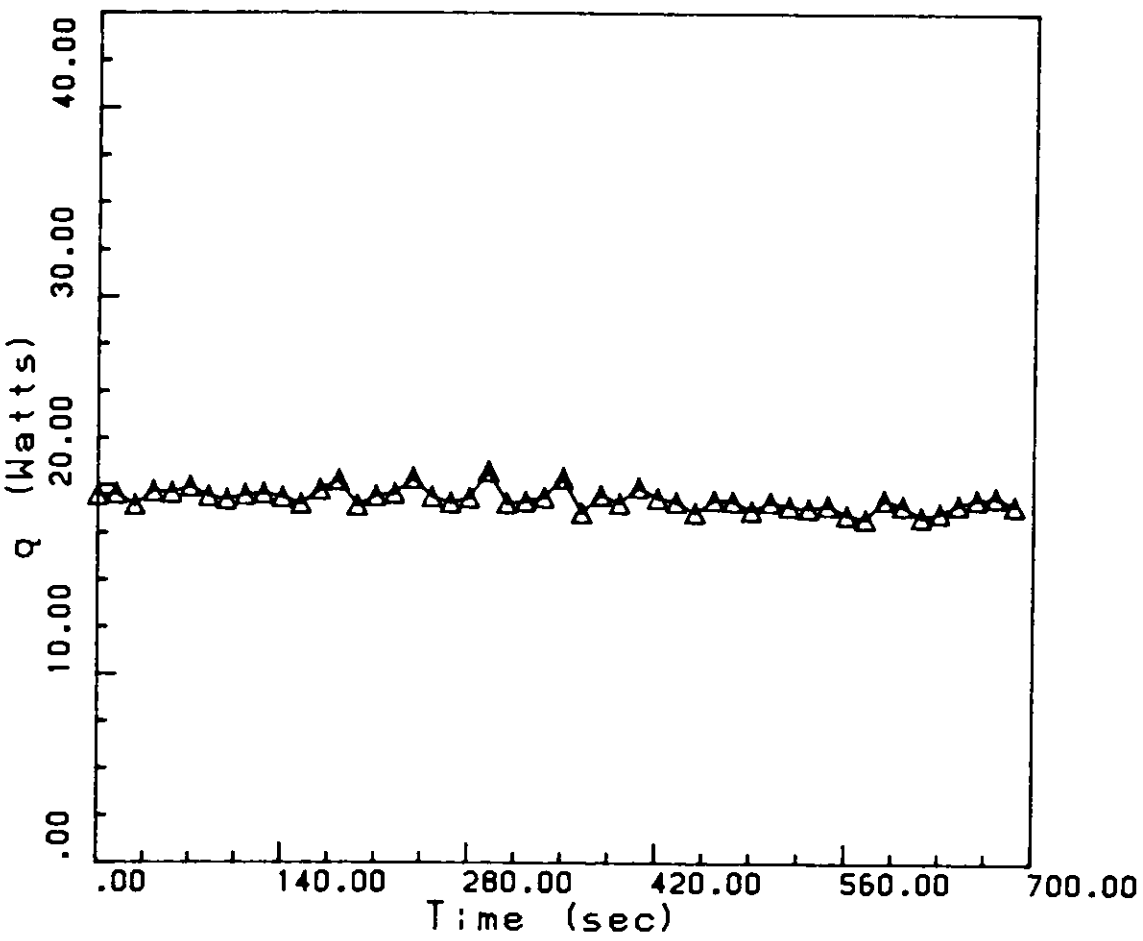

Figure 60. Time record of energy loss. Wind Tunnel Test Re = 21,700.

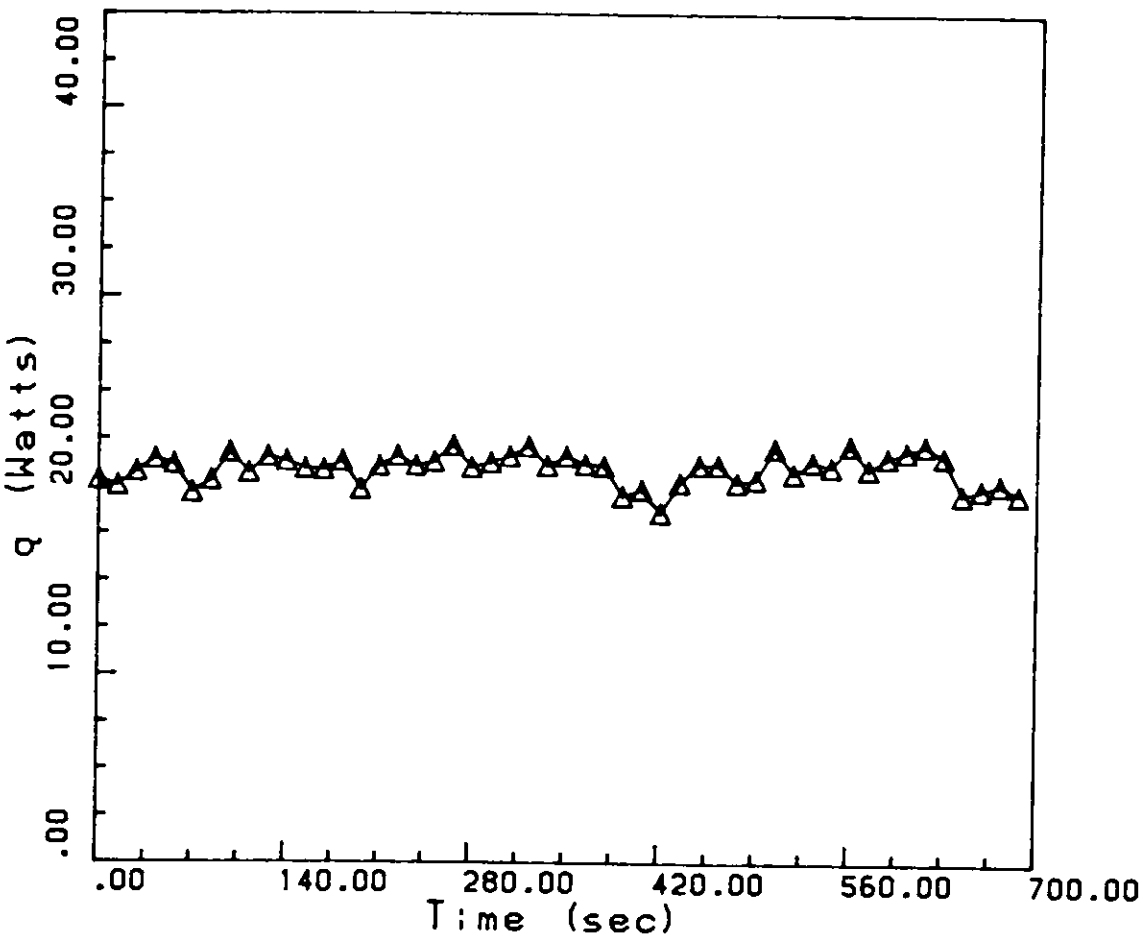

Figure 61. Time record of energy loss. Wind Tunnel Test Re = 26,600.

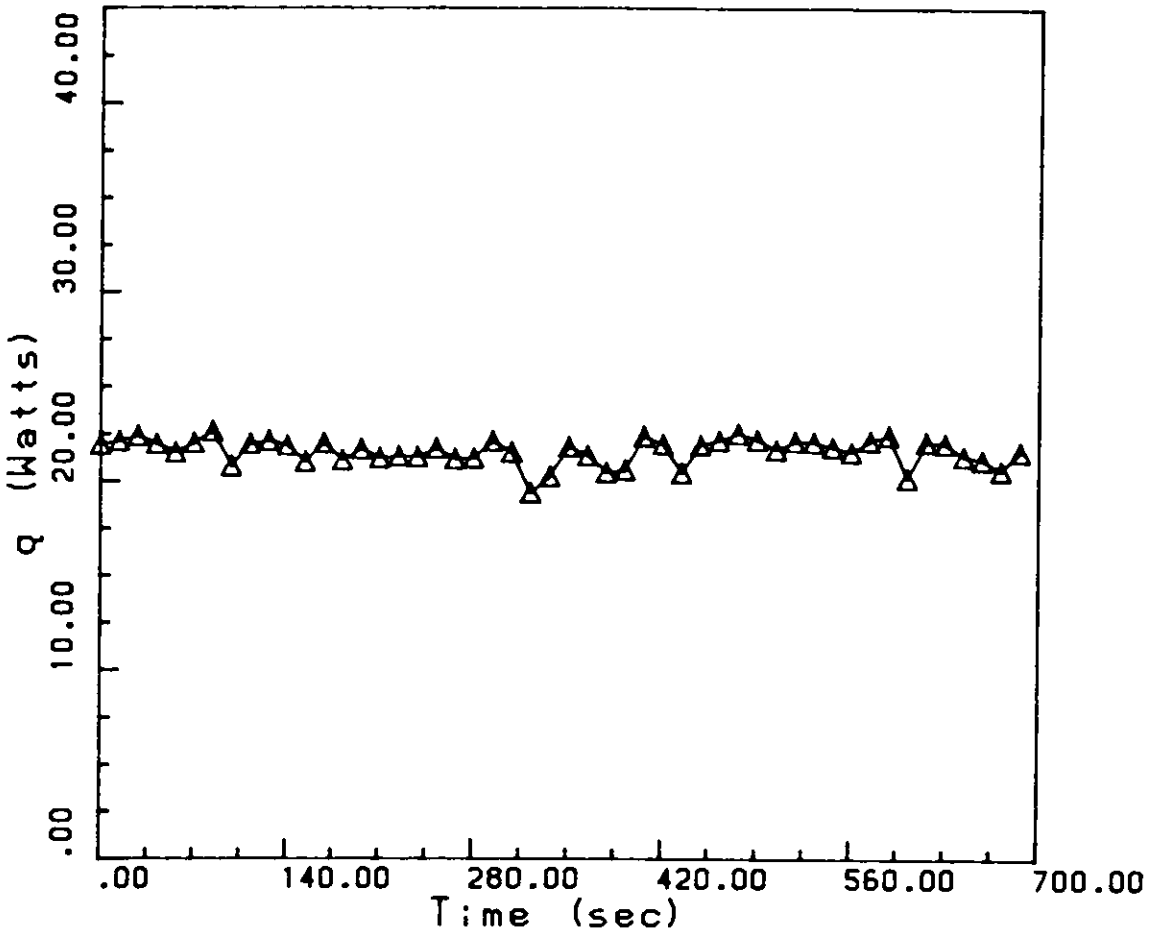

Figure 62. Time record of energy loss. Wind Tunnel Test Re = 30,700.

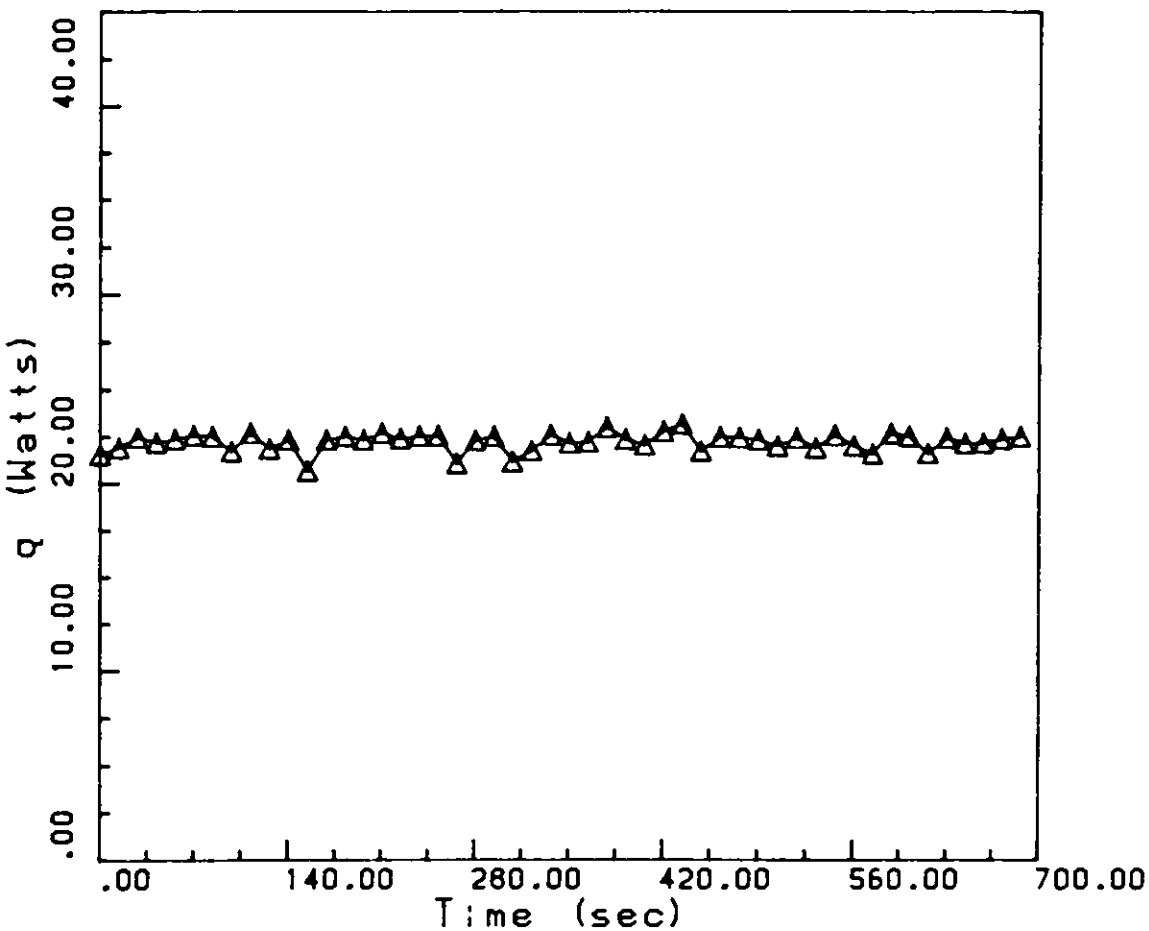

Figure 63. Time record of energy loss. Wind Tunnel Test Re = 32,500.

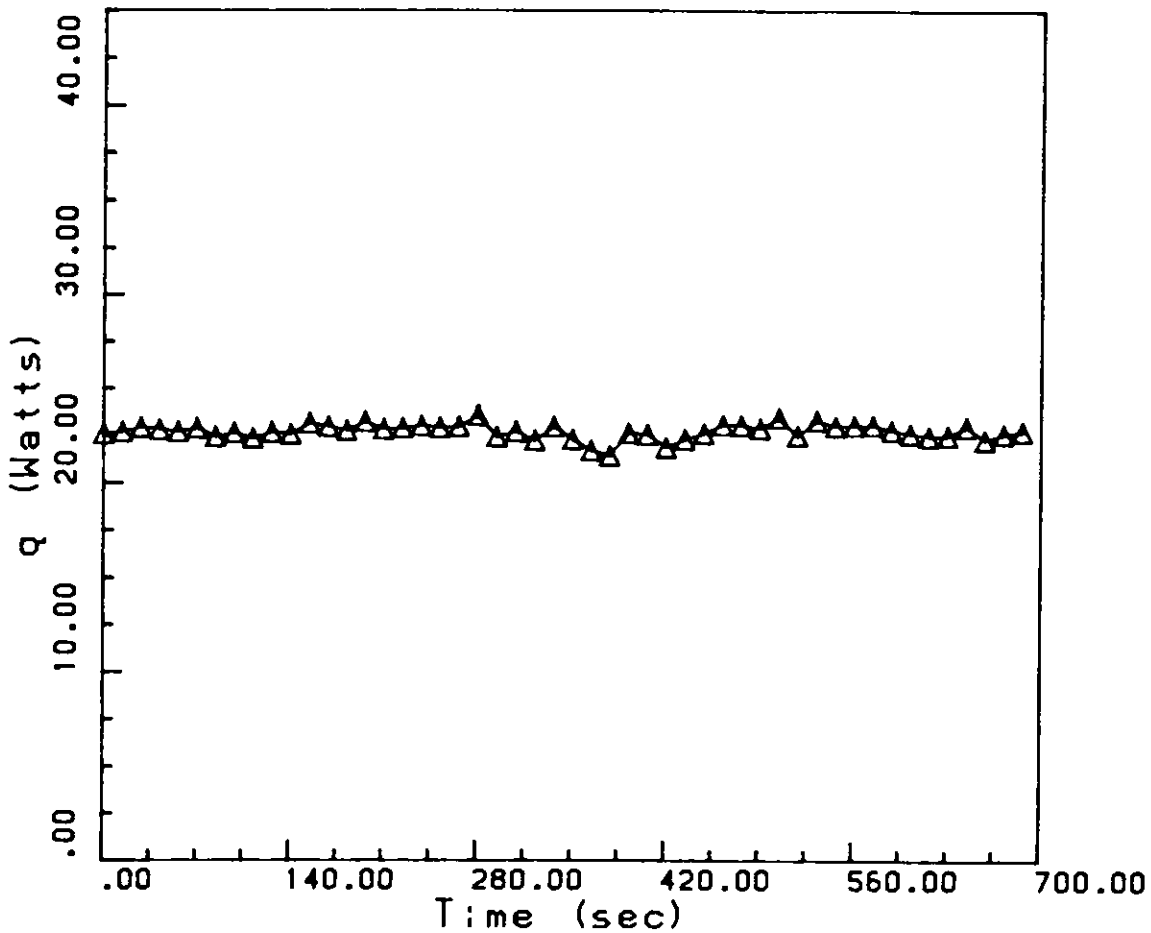

Figure 64. Time record of energy loss. Wind Tunnel Test Re = 34,300.

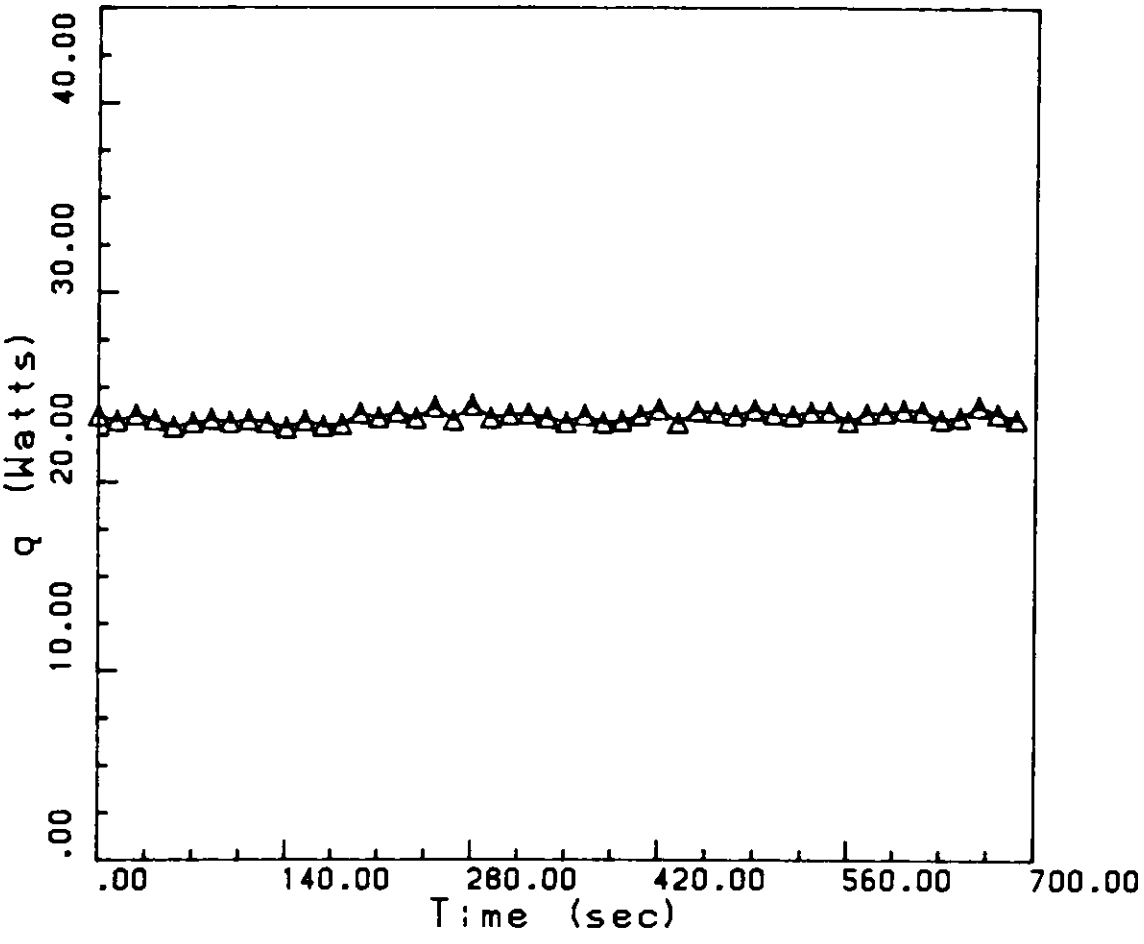

Figure 65. Time record of energy loss. Wind Tunnel Test Re = 36,000.

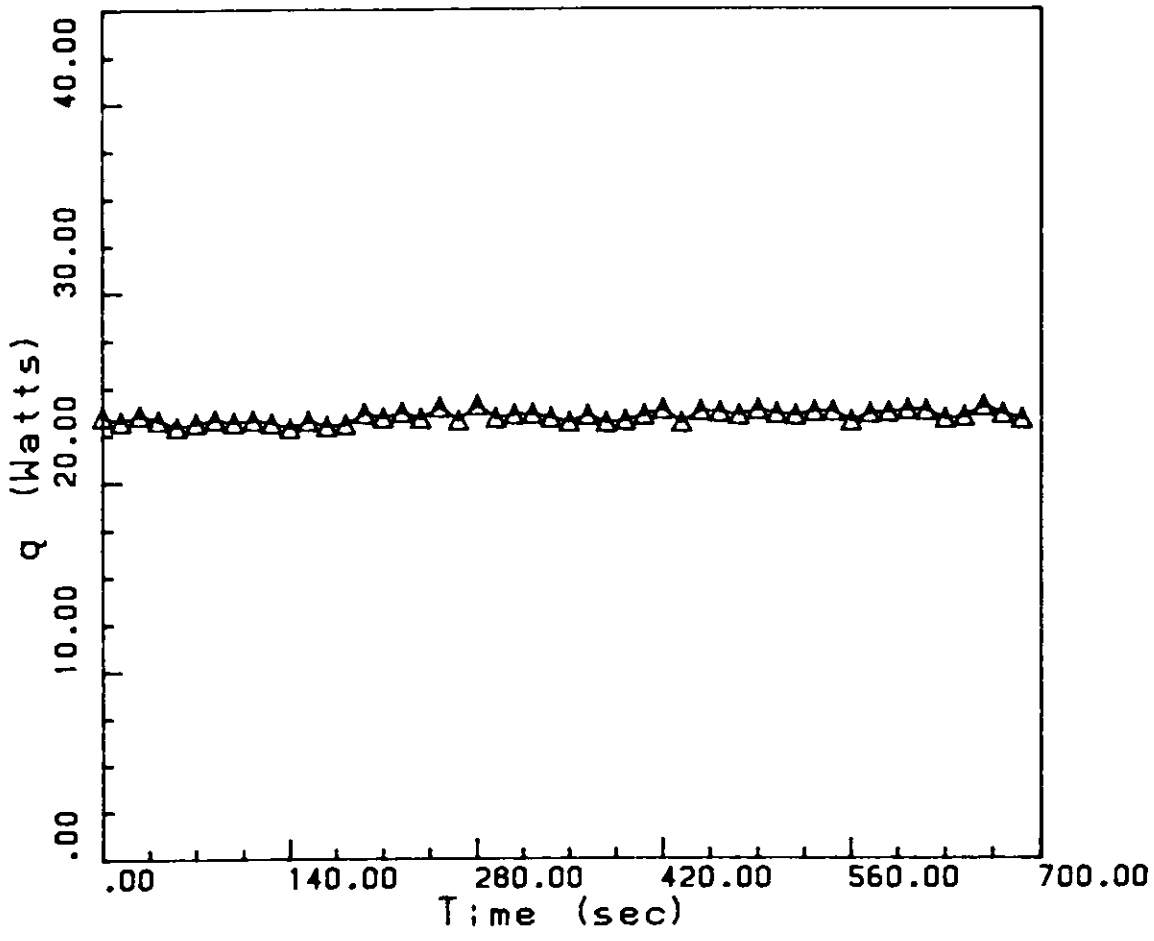

Figure 66. Time record of energy loss. Wind Tunnel Test Re = 37,500.

The vita has been removed from the scanned document